The Astrophysical Journal, 837:95 (37pp), 2017 March 1 https://doi.org/10.3847/1538-4357/aa5df0

A Search for L/T Transition Dwarfs with Pan-STARRS1 and *WISE*. III. Young L Dwarf Discoveries and Proper Motion Catalogs in Taurus and Scorpius–Centaurus

William M. J. Best[1,6], Michael C. Liu[1,6], Eugene A. Magnier[1], Brendan P. Bowler[2,7], Kimberly M. Aller[1,6], Zhoujian Zhang[1], Michael C. Kotson[3], W. S. Burgett[4], K. C. Chambers[1], P. W. Draper[5], H. Flewelling[1], K. W. Hodapp[1], N. Kaiser[1], N. Metcalfe[5], R. J. Wainscoat[1], and C. Waters[1]

[1] Institute for Astronomy, University of Hawaii, 2680 Woodlawn Drive, Honolulu, HI 96822, USA; wbest@ifa.hawaii.edu
[2] McDonald Observatory and the University of Texas at Austin, Department of Astronomy, 2515 Speedway C1400, Austin, TX 78712, USA
[3] Lincoln Laboratory, Massachusetts Institute of Technology, 244 Wood Street, Lexington, MA 02420, USA
[4] GMTO Corporation, 251 S. Lake Ave., Suite 300, Pasadena, CA 91101, USA
[5] Department of Physics, Durham University, South Road, Durham, DH1 3LE, UK
Received 2016 May 8; revised 2017 January 27; accepted 2017 January 31; published 2017 March 7

Abstract

We present the discovery of eight young M7–L2 dwarfs in the Taurus star-forming region and the Scorpius–Centaurus OB Association, serendipitously found during a wide-field search for L/T transition dwarfs using Pan-STARRS1 (optical) and *WISE* (mid-infrared) photometry. We identify PSO J060.3200+25.9644 (near-infrared spectral type L1) and PSO J077.1033+24.3809 (L2) as new members of Taurus based on their VL-G gravity classifications, the consistency of their photometry and proper motions with previously known Taurus objects, and the low probability of contamination by field objects. PSO J077.1033+24.3809 is the coolest substellar member of Taurus found to date. Both Taurus objects are among the lowest-mass free-floating objects ever discovered, with estimated masses ≈6 $M_{\rm Jup}$, and provide further evidence that isolated planetary-mass objects can form as part of normal star formation processes. PSO J060.3200+25.9644 (a.k.a. DANCe J040116.80+255752.2) was previously identified as a likely member of the Pleiades (age ≈ 125 Myr) based on photometry and astrometry, but its VL-G gravity classification and near-infrared photometry imply a much younger age and thus point to Taurus membership. We have also discovered six M7–L1 dwarfs in outlying regions of Scorpius–Centaurus with photometry, proper motions, and low-gravity spectral signatures consistent with membership. These objects have estimated masses ≈15–36 $M_{\rm Jup}$. The M7 dwarf, PSO J237.1470−23.1489, shows excess mid-infrared flux implying the presence of a circumstellar disk. Finally, we present catalogs of Pan-STARRS1 proper motions for low-mass members of Taurus and Upper Scorpius with median precisions of ≈3 mas yr^{-1}, including 67 objects with no previous proper motion and 359 measurements that improve on literature values.

Key words: brown dwarfs – proper motions – stars: formation – stars: individual (PSO J060.3200+25.9644, PSO J077.1033+24.3809, PSO J237.1470−23.1489)

1. Introduction

Brown dwarfs with ages ≲100 Myr are valuable laboratories for testing both the youngest substellar evolutionary models and the lowest-gravity (therefore lowest-mass) atmospheric models. For instance, brown dwarfs with $T_{\rm eff} \lesssim 1400$ K and ages ≲20 Myr will have masses ≲10 $M_{\rm Jup}$ (e.g., Chabrier et al. 2000), firmly in the planetary regime (≲13 $M_{\rm Jup}$). These young, very low-mass brown dwarfs therefore serve as vital templates for understanding directly imaged planets.

Star-forming regions and young open clusters offer the opportunity to identify multiple young brown dwarfs in small areas of the sky, at the age when these objects are brightest. Planetary-mass objects in star-forming regions have been discovered both as companions to stars (e.g., Luhman et al. 2006; Lafreniere et al. 2008) and as free-floating objects (e.g., Luhman et al. 2009; Weights et al. 2009). Wide-field, red-sensitive surveys such as the Pan-STARRS1 3π Survey (PS1; Kaiser et al. 2010; K. Chambers et al. 2017, in preparation), the Two Micron All-Sky Survey (2MASS; Skrutskie et al. 2006), the UKIRT Infrared Deep Sky Survey (UKIDSS; Lawrence et al. 2007), and the *Wide-Field Infrared Survey Explorer* (*WISE*; Wright et al. 2010) have the ability to detect free-floating very low-mass brown dwarfs in nearby star-forming regions (e.g., Lodieu 2013; Esplin et al. 2014), although interstellar reddening at optical and near-infrared wavelengths can make brown dwarfs difficult to distinguish from background giant stars. More discoveries of these objects would improve our understanding of the early evolution of low-mass brown dwarfs and giant planets.

At a distance of ≈145 pc and an age of ≈1–2 Myr (Kraus & Hillenbrand 2009), the Taurus–Auriga molecular cloud (hereinafter Taurus) is one of the closest star-forming regions to the Sun. A comprehensive review of Taurus and its observational history can be found in Kenyon et al. (2008). Taurus has been searched extensively for substellar members from optical to mid-infrared wavelengths (e.g., Guieu et al. 2006; Luhman 2006; Slesnick et al. 2006; Luhman et al. 2009; Quanz et al. 2010; Rebull et al. 2010). Esplin et al. (2014) cataloged 74 members with spectral types M6–L0, which, at the young age of Taurus, span the full brown dwarf mass regime from the stellar/substellar boundary down to planetary masses (≲13 $M_{\rm Jup}$). The coolest known substellar objects in Taurus to date are the free-floating ≈4–7 $M_{\rm Jup}$ 2MASS J04373705+2331080 (hereinafter 2MASS J0437+2331), discovered and classified as L0 by

[6] Visiting Astronomer at the Infrared Telescope Facility, which is operated by the University of Hawaii under Cooperative Agreement no. NNX-08AE38A with the National Aeronautics and Space Administration, Science Mission Directorate, Planetary Astronomy Program.
[7] McDonald Fellow.

Luhman et al. (2009), and the planetary-mass companion 2MASS J04414489+2301513 Bb (Todorov et al. 2010), with a near-IR spectral type of L1 ± 1 on the Allers & Liu (2013a) system and an estimated mass of $\approx 10 \pm 2$ $M_{\rm Jup}$ Bowler & Hillenbrand (2015).

The Scorpius–Centaurus Association (hereinafter Sco–Cen) is the nearest OB association to the Sun. The Sco–Cen complex, reviewed in detail by Preibisch & Mamajek (2008), has a distance similar to Taurus but an older age (≈10–20 Myr). With no significant ongoing star formation, Sco–Cen is much less affected by interstellar reddening, but any planetary-mass objects will also have cooled and become fainter than equivalent-mass objects in Taurus. The Upper Scorpius subgroup in particular has been the target of many searches for ultracool dwarfs (e.g., Martín et al. 2004; Lodieu et al. 2006, 2011; Slesnick et al. 2006, 2008; Dawson et al. 2014). Lodieu et al. (2008) probed the deepest into the substellar regime, spectroscopically confirming over 20 M8–L2 dwarfs in Upper Scorpius with masses down to ≈ 15 $M_{\rm Jup}$.

Here, we present the discovery of two early-L dwarfs in Taurus and six M7–L1 dwarfs in Sco–Cen, serendipitously identified in a wide-field search for L/T transition dwarfs in the Pan-STARRS1 and *WISE* catalogs. In Section 2, we explain how these objects were initially identified and we describe follow-up observations in Section 3. We detail the observed features of our discoveries in Section 4. We discuss their membership in Taurus (Section 5) or Sco–Cen (Section 6), and provide estimated masses and comparisons with model spectra. We summarize our discoveries in Section 7.

2. Photometric Selection

We conducted a search over ≈28,000 deg^2 for L/T transition dwarfs in the field using a merged catalog of PS1 and *WISE* photometry. The search is described in detail in Best et al. (2013, hereinafter Paper I), and the full spectroscopic follow-up results are presented in Best et al. (2015, hereinafter Paper II), including our discovery of 130 ultracool dwarfs. Among these discoveries were 23 late-M and L dwarfs with spectroscopic signs of low gravity, implying youth. This was a surprisingly large number given that we were searching for objects with field ages and cooler spectral types (≈L6–T5) and that objects with ages $\lesssim$200 Myr should comprise at most a few percent of the local population in a galaxy $\gtrsim$10 Gyr old. In Paper II, we determined that our search could find late-M and L dwarfs with $W1 - W2$ colors redder than average for their spectral types, bringing younger objects into our sample.

Our search also specifically avoided the heavily reddened areas of the sky defined in Cruz et al. (2003), which include Taurus and Sco–Cen. The eight discoveries described in this paper lie just outside these reddened regions, with one exception: PSO J060.3200+25.9644 (hereinafter PSO J060.3+25), which lies ≈2° inside the Cruz et al. (2003) Taurus boundaries, but we pursued follow-up observations because its spectral energy distribution (SED) from $z_{\rm P1}$ through $W2$ (0.9–4.6 μm) strongly suggested an unreddened ultracool object.

The PS1 $z_{\rm P1}$ and $y_{\rm P1}$, *WISE*, 2MASS, and MKO photometry for our discoveries were originally presented in Paper II. In Table 1, we update the earlier version of PS1 photometry from Paper II with photometry from the PS1 Data Release 1 (DR1; K. Chambers et al. 2017, in preparation; E. Magnier et al. 2017, in preparation) and include $i_{\rm P1}$ magnitudes. The photometry used in Paper II and in this work is the mean PSF photometry from individually calibrated images; the DR1 photometry in this work includes many more epochs. We also replace the *WISE* All-Sky photometry (Cutri et al. 2012) used in Paper II with AllWISE magnitudes (Cutri et al. 2014). For reference, we reproduce the 2MASS and MKO photometry here in Table 2. We also include photometry for the previously identified Taurus L dwarf 2MASS J0437+2331.

3. Near-infrared Spectroscopy

We obtained near-infrared spectra for our candidates between 2013 January and 2015 May using the NASA Infrared Telescope Facility (IRTF). We used the facility spectrograph SpeX (Rayner et al. 2003) in prism mode with the 0$''$.5 ($R \approx 120$) and 0$''$.8 ($R \approx 75$) slits. Details of our observations are listed in Table 3. For each science target we observed a nearby A0V star contemporaneously for telluric calibration. All spectra were reduced in standard fashion using versions 3.4 and 4.0 of the Spextool software package (Vacca et al. 2003; Cushing et al. 2004). These observations were part of a large program (Paper II) in which our desired S/N was $\gtrsim$30, sufficient for accurate spectral typing based on overall spectral morphology but not necessarily for robust analysis of specific features. We therefore observed PSO J060.3+25 and PSO J077.1033+24.3809 (hereinafter PSO J077.1+24) a second time to achieve higher S/N, and for each object we combined the first and second epochs using the Spextool *xcombspec* routine to obtain a single higher S/N spectrum, which we present in this paper.

While comparing the spectra of our discoveries to spectral standards, we noticed a small wavelength offset in the spectrum of the field L0 standard 2MASS J03454316+2540233 (hereinafter 2MASS J0345+2540) from Burgasser & McElwain (2006). The offset is large enough to affect calculations of the Allers & Liu (2013a) gravity-sensitive spectral indices that we used to analyze our discoveries (Section 4.2). We therefore used IRTF/SpeX to obtain a new spectrum of 2MASS J0345+2540 with more accurate wavelength calibration, which we used for our analysis. Appendix C presents this new spectrum and provides details of the observations.

4. Results

4.1. Ultracool Discoveries

The SpeX prism spectra for our eight young ultracool discoveries are presented in Figure 1 and their spectral types are listed in Table 4. We show their locations in the sky in Figure 2. PSO J060.3+25 was previously identified by Sarro et al. (2014) and Bouy et al. (2015) as a likely very low-mass member of the Pleiades cluster, based on photometry and astrometry. PSO J237.1471−23.1489 (hereinafter PSO J237.1−23) was identified by Lodieu (2013) as a photometric and astrometric candidate member of Upper Sco. We independently discovered these objects and present here spectral confirmation of their ultracool nature. We also find that PSO J060.3+25 is more likely to be a Taurus member than a Pleiad (Section 5.1.3). The other six objects are new discoveries.

In Figures 3 and 4 we compare the colors of our discoveries with those of previously known late-M and early-L dwarfs. Our discoveries in Taurus and Sco–Cen have red $W1 - W2$ colors compared with field objects of similar spectral types, which led to the fortuitous discovery of these young M7–L2 dwarfs even though our search was designed to find L/T transition dwarfs (spectral types ≈L6–T4). The $y_{\rm P1} - W1$, $y_{\rm P1} - J_{\rm MKO}$, and

Table 1
Pan-STARRS1 and AllWISE Photometry

Name	i_{P1} (mag)	z_{P1} (mag)	y_{P1} (mag)	AllWISE Name	$W1$ (mag)	$W2$ (mag)	$W3$ (mag)	$W4$ (mag)
Taurus Discoveries								
PSO J060.3200+25.9644	21.61 ± 0.04	20.06 ± 0.02	19.02 ± 0.02	J040116.80+255752.0	14.99 ± 0.04	14.32 ± 0.05	>11.98	8.58 ± 0.39
PSO J077.1033+24.3809	21.62 ± 0.10	20.18 ± 0.05	19.21 ± 0.06	J050824.81+242251.3	15.15 ± 0.05	14.49 ± 0.07	>11.78	>8.61
Taurus (previously known)								
2MASS J04373705+2331080[a]	⋯	20.75 ± 0.03	19.67 ± 0.10	J043737.06+233107.3	14.45 ± 0.03	13.90 ± 0.05	>11.68	>9.10
Scorpius–Centaurus Discoveries								
PSO J228.6773−29.7088	21.41 ± 0.04	19.87 ± 0.05	18.74 ± 0.03	J151442.59−294231.9	14.82 ± 0.03	14.22 ± 0.05	>11.83	>8.90
PSO J229.2353−26.6737	21.36 ± 0.05	20.14 ± 0.04	18.97 ± 0.02	J151656.49−264025.3	14.73 ± 0.04	14.37 ± 0.06	>12.34	>8.98
PSO J231.7899−26.4494	20.73 ± 0.04	19.10 ± 0.02	18.06 ± 0.02	J152709.57−262658.0	14.18 ± 0.03	13.79 ± 0.04	>12.55	>8.99
PSO J231.8942−29.0600	20.40 ± 0.06	18.81 ± 0.02	17.71 ± 0.01	J152734.62−290335.8	13.88 ± 0.03	13.43 ± 0.03	>11.79	>8.35
PSO J237.1470−23.1489	18.69 ± 0.01	17.41 ± 0.01	16.61 ± 0.01	J154835.30−230855.5	12.92 ± 0.03	12.40 ± 0.03	10.93 ± 0.15	8.75 ± 0.45
PSO J239.7015−23.2665	20.88 ± 0.05	19.26 ± 0.01	18.24 ± 0.02	J155848.37−231559.1	14.43 ± 0.03	13.94 ± 0.05	>12.26	>8.41

Notes. Pan-STARRS1 photometry is the mean PSF magnitudes from the Pan-STARRS1 Data Release 1.
[a] Discovered by Luhman et al. (2009). Also known as PSO J069.4044+23.5186.

Table 2
Near-infrared Photometry

Name	2MASS Photometry				MKO Photometry		
	2MASS Name	J_{2MASS} (mag)	H_{2MASS} (mag)	$K_{S,2MASS}$ (mag)	J_{MKO} (mag)	H_{MKO} (mag)	K_{MKO} (mag)
Taurus Discoveries							
PSO J060.3+25	J04011678+2557527	16.81 ± 0.17	15.73 ± 0.14	15.36 ± 0.17	16.93 ± 0.04	16.10 ± 0.03	[15.53 ± 0.07]
PSO J077.1+24	J05082480+2422518	16.93 ± 0.14	16.47 ± 0.25	15.82 ± 0.22	17.06 ± 0.04	16.31 ± 0.04	15.59 ± 0.03
Taurus (previously known)							
2MASS J0437 +2331	J04373705+2331080	17.38 ± 0.19	16.13 ± 0.15	15.44 ± 0.15	17.24 ± 0.02[a]	16.16 ± 0.01[a]	15.20 ± 0.02[b]
Scorpius–Centaurus Discoveries							
PSO J228.6−29	J15144258−2942315	16.79 ± 0.19	15.95 ± 0.15	15.31 ± 0.16	16.72 ± 0.05	16.18 ± 0.05	[15.37 ± 0.11]
PSO J229.2−26	J15165651−2640251	16.46 ± 0.13	15.98 ± 0.18	15.18 ± 0.15	16.76 ± 0.03	15.85 ± 0.02	[15.14 ± 0.08]
PSO J231.7−26	J15270961−2626574	15.96 ± 0.08	15.21 ± 0.11	14.62 ± 0.10	15.98 ± 0.02	15.25 ± 0.03	[14.64 ± 0.05]
PSO J231.8−29	J15273464−2903354	15.77 ± 0.09	14.83 ± 0.07	14.33 ± 0.08	[[15.72 ± 0.09]]	[[14.91 ± 0.08]]	[[14.29 ± 0.08]]
PSO J237.1−23	J15483530−2308557	14.79 ± 0.05	14.13 ± 0.07	13.60 ± 0.05	[[14.73 ± 0.06]]	[[14.19 ± 0.07]]	[[13.57 ± 0.06]]
PSO J239.7−23	J15584839−2315589	16.30 ± 0.11	15.35 ± 0.11	15.00 ± 0.13	16.25 ± 0.02	15.54 ± 0.02	[15.02 ± 0.07]

Notes. All 2MASS photometry is from the 2MASS Point Source Catalog (Cutri et al. 2003). MKO photometry was obtained using UKIRT/WFCAM (Best et al. 2015) unless enclosed in brackets or otherwise indicated. H_{MKO} and K_{MKO} magnitudes enclosed in single brackets were synthesized using our observed J_{MKO} magnitudes and our low-resolution spectra (Section 3). MKO magnitudes enclosed in double brackets were synthesized using the 2MASS magnitudes for the corresponding filters and our low-resolution spectra.
[a] From the UKIDSS Galactic Plane Survey (DR6; Lucas et al. 2012).
[b] From the UKIDSS Galactic Clusters Survey (DR9; Lawrence et al. 2013).

Table 3
IRTF/SpeX Observations

Object	Date (UT)	Slit (″)	R ($\lambda/\Delta\lambda$)	t_{int} (s)	S/N[a]	A0V Standard
PSO J060.3+25[b]	2013 Jan 25	0.8	75	1920	37	HD 27761
	2013 Nov 23	0.8	75	960		HD 31069
PSO J077.1+24[b]	2013 Jan 26	0.8	75	840	34	HD 34977
	2013 Nov 23	0.8	75	1320		HD 38245
PSO J228.6−29	2013 Apr 18	0.8	75	720	24	HD 146880
PSO J229.2−26	2013 Apr 17	0.8	75	2880	26	HD 143822
PSO J231.7−26	2015 May 18	0.5	120	1440	49	HD 133466
PSO J231.8−29	2015 May 29	0.5	120	3600	84	HD 146606
PSO J237.1−23	2015 May 18	0.5	120	720	79	HD 133466
PSO J239.7−23	2013 Apr 18	0.8	75	720	33	HD 147013

Notes.
[a] Mean J-band (1.20–1.31 μm) S/N per resolution element.
[b] We present a combined spectrum and S/N from the two observations (Section 3).

$(J - H)_{MKO}$ colors of our discoveries are normal compared with field objects of similar spectral types.

4.2. Spectral Indices and Spectral Types

We used three methods to assign spectral types for our discoveries: visual comparison with low-gravity field standards and two index-based methods. Table 4 gives the spectral types calculated from the index-based system of Allers & Liu (2013a, hereinafter AL13). The AL13 indices were designed to assign near-infrared spectral types consistent with optical spectral types, independent of surface gravity. Since all of our discoveries show clear spectral signs of low gravity (Section 4.3), we adopted the AL13 index-based types as our final spectral types, rounded to the nearest subtype and assigned an uncertainty of 1 subtype (following AL13). For confirmation, we visually compared our spectra to the VL-G standards of AL13. All of our visually determined types are within 1 subtype of the adopted index-based types.

In Table 5, we list the spectral types determined using the index-based system of Burgasser et al. (2006, hereinafter B06), compared with our adopted AL13 spectral types. The B06 and

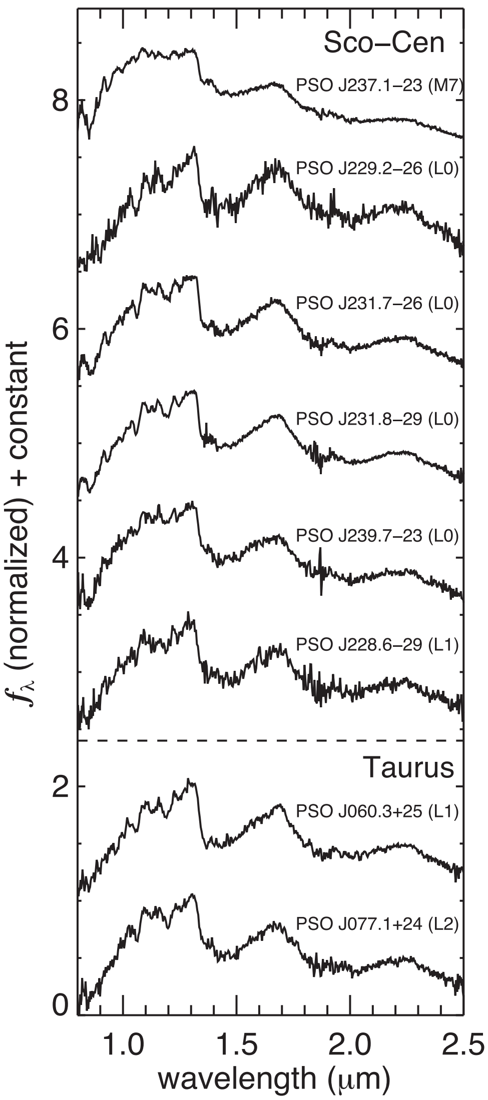

Figure 1. SpeX prism spectra for our eight discoveries, normalized at the J-band peak (1.27 μm), arranged from earliest to latest spectral type, and offset by a constant. Our two Taurus discoveries are at the bottom.

AL13 spectral types are consistent within their 2σ uncertainties, although the B06 types are mostly 1–3 subtypes later. This is probably a consequence of the fact that the B06 indices are not defined for spectral types earlier than L0, so the B06 spectral types are averages only of L types.

4.3. Low-gravity Signatures

Low-gravity signatures in ultracool dwarf spectra are a well-established indication of ages $\lesssim$200 Myr (e.g., Kirkpatrick et al. 2008; Allers & Liu 2013a). We used the AL13 system based on gravity-sensitive near-IR spectral indices to assess whether our spectra display signs of low gravity. In this system, an object is assigned a score of 0 for field gravity (FLD-G, ages $\gtrsim$200 Myr), 1 for intermediate gravity (INT-G, ages $\approx$50–200 Myr), or 2 for very low gravity (VL-G, ages $\approx$10–30 Myr). We calculated indices and gravity scores for our discoveries following Aller et al. (2016), who adapted AL13 to incorporate Monte Carlo assessment of the uncertainties in the indices and gravity classes. We also visually examined the gravity-sensitive features in our spectra as a check on the gravity scores.

We classify six of our discoveries as VL-G: PSO J060.3+25, PSO J077.1+24, PSO J231.7899−26.4494 (hereinafter PSO J231.7−26), PSO J231.8942−29.0600 (hereinafter PSO J231.8−29), PSO J237.1−23, and PSO J239.7016−23.2664 (hereinafter PSO J239.7−23). Table 6 lists their indices and gravity scores. Figure 5 compares the spectra of these six VL-G objects with field standards from Kirkpatrick et al. (2010) and VL-G standards from AL13 having the same spectral types. For the L0 field standard 2MASS J0345+2540, we use our new SpeX prism spectrum (Appendix C). All six of our spectra display weak 0.99 μm FeH and 1.25 μm K I absorption, and a triangular H band shape, all signs of youth. PSO J060.3+25, PSO J077.1+24, PSO J231.7−26, and PSO J231.8−29 also show strong 1.06 μm VO absorption, which AL13 identified as an additional sign of youth for L0–L4 dwarfs.

For the other two objects, PSO J228.6773−29.7088 (hereinafter PSO J228.6−29) and PSO J229.2354−26.6738 (hereinafter PSO J229.2−26), the S/N of our spectra was too low ($\lesssim$30) to yield robust gravity scores from the AL13 indices. Figure 6 shows these spectra, again compared with the appropriate field and VL-G standards. In spite of the measurement uncertainties, visual inspection confirms that both objects have weak 0.99 μm FeH and 1.25 μm K I absorption, strong 1.06 μm VO absorption, and triangular H band shapes, so we regard them as strong candidate VL-G objects.

4.4. Proper Motions

Proper motions are key to establishing membership in star-forming regions and clusters whose bulk motion through space is well defined. We use proper motions from PS1 Processing Version 3.2 (PV3.2), the version used for the photometry and mean positions in PS1 DR1. (PS1 proper motions will be part of a future public release.) PV3.2 astrometry is calibrated to the *Gaia* DR1 (Gaia Collaboration et al. 2016) astrometric reference frame. We present the proper motions for our discoveries in Table 7 and we discuss their consistency with members of Taurus and Sco–Cen in Sections 5 and 6. We present catalogs of proper motions for low-mass members of Taurus and Upper Sco in Appendices A and B, along with a brief summary of the method used to calculate PS1 proper motions.

4.5. No Candidate Binaries

As in Paper II, we used the spectral index criteria of Bardalez Gagliuffi et al. (2014, hereinafter BG14) and visual inspection to search for spectral features indicating that our discoveries may be unresolved binaries. PSO J228.6−29 satisfies only 1 of the 12 BG14 criteria, and our other seven discoveries meet none of the BG14 criteria. Similarly, we found no evidence of spectral blends via visual inspection. None of these objects appear to be candidate unresolved binaries.

In addition, we investigated whether any of our discoveries could be members of wide binary or multiple systems. We searched for nearby known members of the star-forming regions in which our discoveries reside, using the catalogs of Esplin et al. (2014) for Taurus and Luhman & Mamajek (2012) for Upper Scorpius. As several of our Sco–Cen discoveries lie outside the classical boundaries of Upper Scorpius (Section 6), we also searched across all catalogs in *Vizier*[8] for objects near

[8] http://vizier.u-strasbg.fr/viz-bin/VizieR

Table 4
Index-based Spectral Types from Allers & Liu (2013a)

Name	Index-derived Spectral Types H_2O	H_2OD	H_2O-1	H_2O-2	Avg. SpT[a]	Visual SpT[b]	Adopted SpT[c]
Taurus Discoveries							
PSO J060.3+25	$L1.3^{+1.4}_{-1.4}$	⋯	$L0.8^{+1.2}_{-1.2}$	$L0.5^{+1.1}_{-1.2}$	$L0.9^{+0.9}_{-0.9}$	L0.5	L1
PSO J077.1+24	$L2.0^{+1.2}_{-1.2}$	⋯	$L0.1^{+1.2}_{-1.2}$	$L1.5^{+0.8}_{-1.0}$	$L1.7^{+0.9}_{-0.9}$	L1	L2
Taurus (previously known)							
2MASS J0437+2331[d]	$L1.5^{+1.3}_{-1.4}$	⋯	$L0.1^{+1.3}_{-1.3}$	$L0.0^{+1.2}_{-1.2}$	$L0.9^{+0.9}_{-0.9}$	L1.5	L1
Scorpius–Centaurus Discoveries							
PSO J228.6−29	$L1.4^{+1.9}_{-2.2}$	$L1.7^{+1.4}_{-1.4}$	$L1.1^{+1.4}_{-1.4}$	$M9.5^{+1.7}_{-1.9}$	$L0.8^{+1.1}_{-1.3}$	L0.5	L1
PSO J229.2−26	⋯	⋯	$M9.8^{+1.3}_{-1.3}$	⋯	$M9.8^{+1.3}_{-1.3}$	L0	L0
PSO J231.7−26	$M9.9^{+0.9}_{-0.9}$	⋯	$M9.6^{+1.1}_{-1.2}$	$L0.0^{+0.9}_{-0.9}$	$M9.9^{+0.6}_{-0.6}$	L0	L0
PSO J231.8−29	$L0.3^{+0.6}_{-0.6}$	⋯	$L1.0^{+1.1}_{-1.1}$	$M9.9^{+0.6}_{-0.6}$	$L0.2^{+0.4}_{-0.4}$	L0	L0
PSO J237.1−23	$M7.1^{+0.5}_{-0.6}$	⋯	$M7.3^{+1.2}_{-1.2}$	$M7.1^{+0.6}_{-0.6}$	$M7.1^{+0.4}_{-0.4}$	M7.5	M7
PSO J239.7−23	$L0.1^{+1.2}_{-1.2}$	⋯	$M9.5^{+1.3}_{-1.3}$	$L0.1^{+1.3}_{-1.4}$	$L0.0^{+0.9}_{-0.9}$	M9	L0

Notes.
[a] Calculated as the weighted average of the spectral types from Monte Carlo trials for all indices, excluding those that fell outside the valid range for each index.
[b] Spectral types determined by visual comparison with the VL-G spectral standards proposed by Allers & Liu (2013a). Uncertainties for these visual spectral types are ±1 subtype for all objects.
[c] The index-based average spectral types rounded to the nearest subtype, which we adopt as the final spectral types for our discoveries with uncertainties of ±1 subtype.
[d] Classified as L0 by Luhman et al. (2009) using an optical spectrum.

these discoveries. We found no known members of Taurus or Sco–Cen within 70″ (corresponding to a projected separation ≈10,000 au) of our discoveries. At wider separations, it is still possible for a pair of low-mass stars and/or brown dwarfs to be physically bound (Dhital et al. 2010; Deacon et al. 2014). However, such a binary is likely to have formed through capture in the natal cluster rather than as an initially bound system (Kouwenhoven et al. 2010). Thus, we conclude that all of our discoveries are likely to be free-floating brown dwarfs that formed as single objects.

5. Taurus Discoveries

Two of our discoveries, PSO J060.3+25 (L1) and PSO J077.1+24 (L2), reside at the projected outer edges of the nearby Taurus star-forming region. Figure 2 shows their sky locations in Taurus. In Section 5.1, we present confirmation that they are bona fide members of Taurus. We also estimate their masses (Section 5.2) and assess whether they have circumstellar disks (Section 5.3).

We first explore why these objects were not identified in previous studies of Taurus, a region that has been repeatedly searched for ultracool dwarfs. Our objects lie ≈8° (≈20 pc) from the projected center of Taurus, on opposite sides from each other. Many searches surveyed smaller and/or more central regions of Taurus that did not include our objects (e.g., Guieu et al. 2006; Luhman et al. 2009; Quanz et al. 2010; Rebull et al. 2010). Our objects also lie just outside the footprint of *Spitzer* images analyzed by Esplin et al. (2014). Our objects are very faint, especially at optical wavelengths, so previous searches using *i*-band photometry (e.g., Slesnick et al. 2006) were not able to detect them. Similarly, both objects lie within the area searched by Esplin et al. (2014) using *WISE* photometry, but are fainter than the $W1 \leqslant 14$ mag limit used in that search. Luhman (2006) would have detected PSO J077.1+24 in 2MASS photometry, but its $(J-H)_{2MASS} = 0.46 \pm 0.28$ mag color is bluer than the $(J-H)_{2MASS} \geqslant 0.6$ mag cut used in that search.[9] PSO J060.3+25 lies just outside the Luhman (2006) search area but would also have been excluded due to its relatively blue $(H-K_S)_{2MASS}$ color (also having a large error). We note also that Luhman (2006) used previously known low-mass members of Taurus as templates to define color cuts, and many of those members are reddened by local extinction. Our discoveries do not appear to be reddened, as discussed in Sections 5.1.2 and 5.1.5.

5.1. Evidence for Membership

5.1.1. Youth

Both PSO J060.3+25 and PSO J077.1+24 have VL-G gravity classes (Section 4.3). While more work is needed to calibrate the ages of VL-G objects (Allers & Liu 2013a), the classification suggests an age ≲30 Myr, much younger than the field population.

5.1.2. Photometry

Figure 7 compares the photometry of PSO J060.3+25 and PSO J077.1+24 to that of known Taurus members from Esplin et al. (2014). The J versus $J-K_S$ (2MASS) and y_{P1} versus $y_{P1}-W1$ color–magnitude diagrams for Taurus make evident the significant reddening in this region of the sky. We calculated reddening vectors for these color–magnitude diagrams using the y_{P1} coefficient from Schlafly & Finkbeiner

[9] We note the large error on this color is due to this object being near the detection limit of 2MASS. Our deeper MKO photometry (Table 2) shows this object has $(J-H)_{MKO} = 0.75 \pm 0.06$ mag.

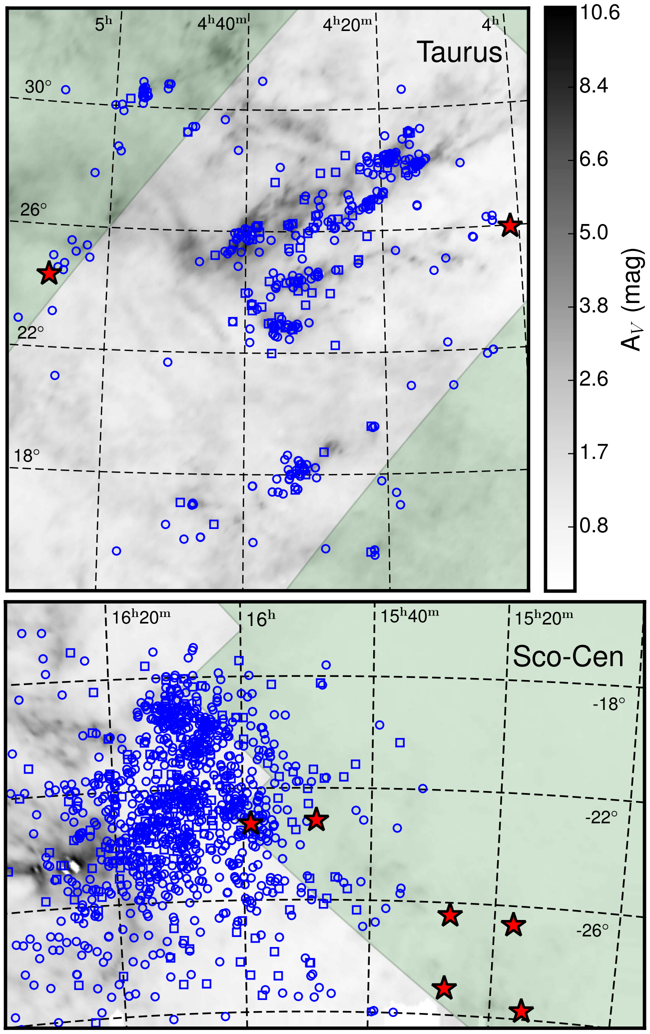

Figure 2. Top: locations in Taurus of our discoveries (red stars) and known stars (blue circles) and ultracool dwarfs (SpT $\geqslant$ M6, blue squares) from Esplin et al. (2014). The grayscale background shows visual extinction (scale at right) from the reddening map of Schlafly et al. (2014). The green shading marks the regions included in our search (Paper II), i.e., outside of reddened regions identified by Cruz et al. (2003). Our two discoveries lie on the outskirts of Taurus in regions of low extinction. Bottom: portion of Sco–Cen surveyed by PS1 (north of $-30°$) shown in the same format, with known members of Upper Sco from Luhman & Mamajek (2012); Dawson et al. (2014), and Rizzuto et al. (2015). The two leftmost discoveries are in Upper Sco, while the other four appear to be members of Upper Centaurus–Lupus. The knot of high extinction near (16^h30^m, $-24°$) is the ρ Ophiuchi star-forming region.

(2011, their Table 6, $R_V = 3.1$) and the $J/K_S/W1$ coefficients from Davenport et al. (2014, their Table 3). We include these reddening vectors, scaled to an extinction of $A_V = 5$ mag, in Figure 7. Our two discoveries sit at the faint end of the unreddened cluster sequence, consistent with their projected locations on the unobscured outskirts of the region. While some young early-L dwarfs have unusually red $(J - K_S)_{2MASS}$ colors for their spectral types (e.g., Gagné et al. 2015b), we note that the $(J - K_S)_{2MASS}$ colors of our Taurus discoveries (1.45 ± 0.24 mag for PSO J060.3+25, 1.11 ± 0.26 mag for PSO J077.1+24) are consistent with those of older field dwarfs with the same spectral types (Schmidt et al. 2010; Faherty et al. 2013). However, both PSO J060.3+25 and PSO J077.1+24 have $W1 - W2$ colors (Figure 3) that are 3σ redder than those of field early-L dwarfs, a common sign of low gravity (Gizis et al. 2012).

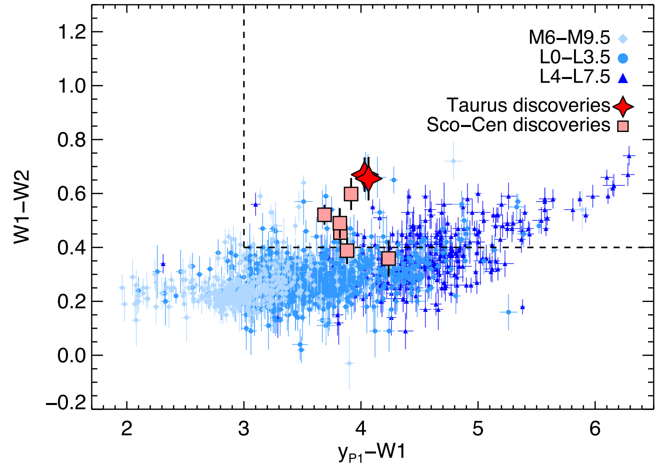

Figure 3. $W1 - W2$ vs. $y_{P1} - W1$ (AllWISE) diagram featuring our discoveries in Taurus (red stars) and Sco–Cen (pink triangles), plotted over previously known ultracool dwarfs in shades of blue (cooler spectral types have darker shades). The black dashed lines represent the color cuts we used in our search (Paper II), for which we used *WISE* All-Sky photometry. We chose objects above and to the right of the dashed lines. (The two Sco–Cen discoveries with AllWISE $W1 - W2 < 0.4$ mag were included in our search because they have *WISE* All-Sky $W1 - W2 > 0.4$ mag.) Our young M7–L2 discoveries have somewhat redder $W1 - W2$ colors than field objects of the same spectral types, which explains why our search for L/T transition dwarfs found these earlier-type objects.

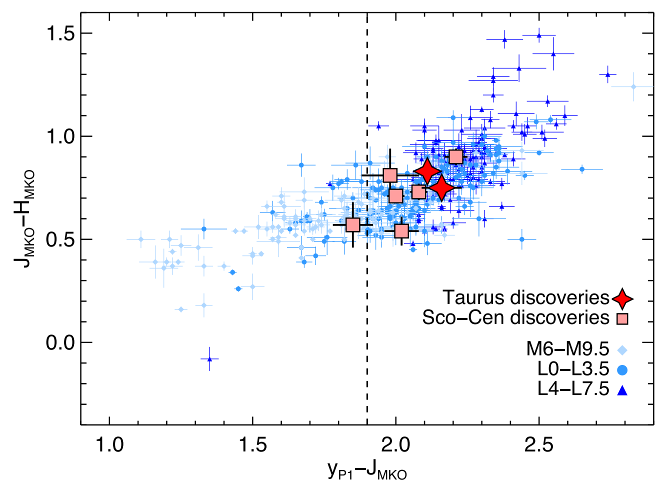

Figure 4. $(J - H)_{MKO}$ vs. $y_{P1} - J_{MKO}$ diagram for our discoveries, using the same format as Figure 3. We chose objects in our search to the right of the dashed line (using an earlier, preliminary version of y_{P1} photometry); $J - H$ was not used to select objects. Our discoveries have normal $y_{P1} - J_{MKO}$ and $(J - H)_{MKO}$ colors compared with field objects of the same spectral types.

5.1.3. Proper Motions

To assess the kinematic consistency of our discoveries with previously known members of Taurus, we created a list of proper motions for the Taurus stars and brown dwarfs from Esplin et al. (2014) that are not saturated in PS1. We obtained the proper motions from PS1 Processing Version 3.2 (PV3.2), the same source as the proper motions of our discoveries (Section 4.4). We discuss our complete list of proper motions in detail in Appendix A. Figure 8 compares the proper motions of PSO J060.3+25 and PSO J077.1+24 with all reliable PS1 Taurus proper motions. We calculated a weighted mean proper motion for the known Taurus members of ($\mu_\alpha \cos\delta = 7.6 \pm 0.2$, $\mu_\delta = -17.4 \pm 0.2$ mas yr^{-1}), with a weighted rms of 4.9 mas yr^{-1} in R.A. and 6.4 mas yr^{-1} in decl.

Table 5
Index-based Spectral Types from Burgasser et al. (2006) for L Dwarfs

Name	Index Values (Derived Spectral Types)[a]						
	H_2O-J	CH_4-J	H_2O-H	CH_4-H	CH_4-K	Avg. SpT	Adopted SpT[b]
Taurus Discoveries							
PSO J060.3+25	0.867 (L2.3)	0.933 (<T0)	0.780 (L3.4)	1.118 (<T1)	1.122 (<L0)	L2.8 ± 0.8	L1
PSO J077.1+24	0.946 (L0.4)	0.924 (<T0)	0.803 (L2.5)	1.167 (<T1)	1.137 (<L0)	L1.5 ± 1.4	L2
Taurus (previously known)							
2MASS J0437+2331[d]	0.810 (L3.9)	0.942 (<T0)	0.788 (L3.1)	1.190 (<T1)	1.147 (<L0)	L3.5 ± 0.6	L1
Scorpius–Centaurus Discoveries							
PSO J228.6−29	0.852 (L2.7)	0.837 (<T0)	0.735 (L5.2)	1.126 (<T1)	1.146 (<L0)	L3.9 ± 1.8	L1
PSO J229.2−26	0.918 (L1.0)	0.969 (<T0)	0.755 (L4.4)	1.119 (<T1)	1.111 (<L0)	L2.7 ± 2.4	L0
PSO J231.7−26	0.920 (L1.0)	0.927 (<T0)	0.841 (L1.0)	1.167 (<T1)	1.135 (<L0)	L1.0 ± 0.5[c]	L0
PSO J231.8−29	0.923 (L0.9)	0.905 (<T0)	0.821 (L1.7)	1.150 (<T1)	1.136 (<L0)	L1.3 ± 0.6	L0
PSO J237.1−23	0.978 (<L0)	0.918 (<T0)	0.929 (<L0)	1.053 (<T1)	1.026 (<L0)	⋯	M7
PSO J239.7−23	0.971 (L0.0)	0.913 (<T0)	0.810 (L2.2)	1.071 (<T1)	1.106 (<L0)	L1.1 ± 1.5	L0

Notes.
[a] Spectral types calculated using the polynomials defined in Burgasser (2007).
[b] For a description, see Section 4.2 and Table 4.
[c] The two contributing index-based spectral types are both L1.0, so we adopt an uncertainty of 0.5 subtypes.
[d] Classified as L0 by Luhman et al. (2009) using an optical spectrum.

PSO J077.1+24 has a proper motion of (14.1 ± 12.5, −27.1 ± 12.1 mas yr^{-1}), consistent with the mean Taurus proper motion. Because the Taurus region has a number of distinct subgroups, we also compared the proper motion of PSO J077.1+24 to that of the closest subgroup on the sky identified by Luhman et al. (2009), L1544. This subgroup has a median proper motion of (0.9 ± 1, −17.6 ± 1 mas yr^{-1}; Luhman et al. 2009), consistent with PSO J077.1+24.

For PSO J060.3+25, we adopt the proper motion (14.3 ± 3.1, −26.4 ± 3.2 mas yr^{-1}) from Bouy et al. (2015). Our PS1 proper motion of (19.0 ± 8.2, −38.1 ± 8.2 mas yr^{-1}) is consistent, but the Bouy et al. (2015) measurement is more precise. The adopted proper motion is very similar to PSO J077.1+24 and consistent with our mean Taurus proper motion. The closest Taurus subgroup on the sky to PSO J060.3+25 identified by Luhman et al. (2009), B209 (≈4° away), has a mean proper motion of (6.9 ± 1, −22.3 ± 1 mas yr^{-1}; Luhman et al. 2009), consistent within 1.8σ in R.A. and 1.0σ in decl.

PSO J060.3+25 (a.k.a. DANCe J040116.80+255752.2) was also previously identified by Sarro et al. (2014) and Bouy et al. (2015) as a high-probability (93%) member of the Pleiades cluster, based on $zYJHK_S$ photometry and astrometry. The Pleiades lie at a mean distance of 136.2 ± 1.2 pc (Melis et al. 2014), commensurate with the ≈145 pc distance to Taurus. The projected center of the Pleiades lies ≈3°.5 away from PSO J060.3+25, or ≈8 pc at the distance of the Pleiades, so it is possible that PSO J060.3+25 falls within the 9.5 ± 0.5 pc tidal radius of the Pleiades (Danilov & Loktin 2015). The mean proper motion for low-mass brown dwarfs ($0.012-0.025\,M_\odot$) in the Pleiades is (21.6, −47.6 mas yr^{-1}) with a dispersion of $\sigma_\mu = 7.5 \pm 6.1$ mas yr^{-1} (Zapatero Osorio et al. 2014b), so the proper motion of PSO J060.3+25 is intermediate between the bulk motions of Taurus and the Pleiades, and consistent within 2σ with both groups. Our VL-G classification for PSO J060.3+25 suggests a younger age (≲30 Myr) than for the Pleiades (≈125 Myr; Stauffer et al. 1998b), although the age range of VL-G objects has not been firmly established (e.g., Liu et al. 2016). We note that Allers & Liu (2013b) classified several Pleiades members as VL-G, but they used spectra with mostly lower resolution ($R \approx 50$) and S/N (≲20) than the prism spectra we present here for our discoveries, so we regard those classifications as provisional. In Figure 9, we also compare the J- and K-band photometry of known Taurus members and our discoveries, as a function of spectral type, to known VLM members of the Pleiades. The published spectral types for the Pleiades members are derived from multiple sources and methods and are therefore heterogenous, but classification of these objects using the AL13 system shows a consistent result (Allers & Liu 2013b). Figure 9 shows that our discoveries have J magnitudes more consistent with the younger, brighter members of Taurus. We therefore find it more likely that PSO J060.3+25 is a member of the 1–2 Myr old Taurus region. A radial velocity measurement would help to further assess the Taurus membership of PSO J060.3+25.

5.1.4. Likelihood of Field Contamination

We investigated the possibility that PSO J060.3+25 or PSO J077.1+24 could be a foreground or background field object in the direction of Taurus by estimating the number of such contaminating field objects from our search. For this estimate, we generously defined the boundaries of the Taurus region to be $4^h00^m \leqslant \alpha \leqslant 5^h15^m$ and $14° \leqslant \delta \leqslant 32°$ (see Figure 2), covering 309.4 deg^2. Our search covered the entire sky between declinations −30° and +70° except for locations within 3° of the Galactic plane (Paper II), an area totaling 28,070 deg^2. (We noted in Section 2 that our search also avoided reddened regions identified by Cruz et al. 2003, but PSO J060.3+25 actually lies within one of these reddened regions, so we include those regions in this estimate.)

Table 6
Low-resolution Gravity Indices from Allers & Liu (2013a)

Name	FeH_z	VO_z	KI_J	H-cont	Index Scores[a]	Gravity Score[b]	Gravity Class	Adopted SpT
Taurus Discoveries								
PSO J060.3+25	$1.006^{+0.035}_{-0.036}$	$1.203^{+0.032}_{-0.034}$	$1.038^{+0.016}_{-0.016}$	$0.971^{+0.022}_{-0.023}$	2122 (2122)	$2.0^{+0.0}_{-0.5}$	VL-G	L1
PSO J077.1+24	$1.043^{+0.039}_{-0.042}$	$1.196^{+0.029}_{-0.030}$	$0.994^{+0.017}_{-0.017}$	$0.977^{+0.025}_{-0.026}$	2122 (2122)	$2.0^{+0.0}_{-0.5}$	VL-G	L2
Scorpius–Centaurus Discoveries								
PSO J231.7−26	$1.075^{+0.020}_{-0.021}$	$1.214^{+0.015}_{-0.015}$	$1.032^{+0.011}_{-0.011}$	$0.993^{+0.015}_{-0.015}$	2n22 (2n22)	$2.0^{+0.0}_{-0.0}$	VL-G	L0
PSO J231.8−29	$1.075^{+0.011}_{-0.011}$	$1.239^{+0.009}_{-0.009}$	$1.061^{+0.006}_{-0.006}$	$0.995^{+0.008}_{-0.008}$	2122 (2122)	$2.0^{+0.0}_{-0.0}$	VL-G	L0
PSO J237.1−23	$1.056^{+0.019}_{-0.019}$	$1.045^{+0.014}_{-0.014}$	$1.026^{+0.009}_{-0.009}$	$0.999^{+0.007}_{-0.007}$	2n22 (2n22)	$2.0^{+0.0}_{-0.0}$	VL-G	M7
PSO J239.7−23	$1.032^{+0.034}_{-0.035}$	$1.101^{+0.025}_{-0.025}$	$1.065^{+0.019}_{-0.019}$	$0.974^{+0.025}_{-0.026}$	2n12 (2n12)	$2.0^{+0.0}_{-1.0}$	VL-G	L0

Notes. This table includes the discoveries for which our spectrum has high enough S/N to extract reliable measurements of the AL13 gravity indices, corroborated by visual inspection. Our spectra for PSO J228.6−29 and PSO J229.2−26 and the 2MASS J0437+2331 spectrum from Bowler et al. (2014) did not yield reliable gravity scores, but do show visual indications of low gravity (Sections 4.3 and 5.1.5).
[a] Scores in parentheses were determined using the original AL13 classification scheme, in which objects with index values corresponding to INT-G but within 1σ of the FLD-G value are classified with a score of "?."
[b] The overall gravity score and the 68% confidence limits were calculated as described in Aller et al. (2016).

We found a total of 14 VL-G L0–L2 dwarfs in our search, including two previously known objects and three discoveries that we consider to be strong VL-G candidates. We would therefore expect our search to find 0.15 VL-G L0–L2 dwarfs in an arbitrary Taurus-sized area of sky.

In addition, we assessed the likelihood that an early-L dwarf observed in the direction of Taurus would have a proper motion consistent with members of Taurus (as do PSO J060.3+25 and PSO J077.1+24). We used the Besançon Galactic model[10] (Robin et al. 2003) to generate a synthetic population of field M dwarfs in a volume spanning our Taurus boundaries between 50 and 240 pc. We assigned uncertainties to the synthetic proper motions using an astrometric error versus K_S relationship derived from our Taurus proper motions (Section 5.1.3). Assuming that early-L dwarfs have the same kinematics as M dwarfs in the field, we used Monte Carlo trials to determine that 20.3 ± 0.2% of early-L dwarfs in the direction of Taurus will have proper motions within 3σ of the mean Taurus $\mu_\alpha \cos\delta$ and μ_δ.

We would therefore expect our search to find $(3.13 \pm 0.03) \times 10^{-2}$ VL-G dwarfs within our Taurus boundaries having proper motions consistent with Taurus membership. Poisson statistics give us a probability of 96.9% that neither PSO J060.3+25 nor PSO J077.1+24 is an interloping field object in the direction of Taurus, and a negligible 5×10^{-4} probability that both objects are contaminants.

5.1.5. Comparison with 2MASS J04373705+2331080

Prior to our discoveries, 2MASS J0437+2331 was the only known free-floating L dwarf member of Taurus, discovered and classified as L0 by Luhman et al. (2009). We used the SpeX Prism spectrum for 2MASS J0437+2331 from Bowler et al. (2014) to assign a near-infrared spectral type of L1 ± 1, based on a calculated type of L0.9 ± 0.9 using the AL13 indices (Section 4.2).

Luhman et al. (2009) claimed membership in Taurus for 2MASS J0437+2331 based on weaker Na I and K I absorption features in its red-optical spectrum, which are recognized signs of youth (Kirkpatrick et al. 2006), along with its central projected location in Taurus. Similarly to two of our Sco–Cen discoveries, the spectrum for 2MASS J0437+2331 does not have a high enough S/N for us to confidently assign a gravity class, but Figure 12 shows that it more closely resembles the L1 VL-G standard than the field standard, confirming its young age. Figure 7 shows that the y_{P1} JK_SW1 photometry of 2MASS J0437+2331 is also similar to that of PSO J060.3+25 and PSO J077.1+24, and consistent with being a slightly reddened member of Taurus. 2MASS J0437+2331 has a proper motion of (15.9 ± 13.5, −54.8 ± 13.4 mas yr^{-1}), consistent with our mean motion of Taurus in R.A. but nearly 2σ different in decl. We note that 2MASS J0437+2331 satisfies all the criteria for our search (Section 2), except that it lies well within the excluded reddened region of Cruz et al. (2003).

We compare the spectrum of 2MASS J0437+2331 to those of PSO J060.3+25 and PSO J077.1+24 in Figures 10 and 11, along with the appropriate field (Kirkpatrick et al. 2010) and VL-G (AL13) standards. Interestingly, the near-IR spectrum of 2MASS J0437+2331 is notably redder than those of our discoveries and its position in the color–magnitude diagrams in Figure 7 is consistent with an extinction of $A_V \approx 2$–4 mag. This redness was also noted by Alves de Oliveira et al. (2013), who calculated an extinction of $A_V = 2.1$–3.3 mag for 2MASS J0437+2331 based on 2MASS photometry and comparison to the near-IR spectra of other young M and L dwarfs. However, Luhman et al. (2009) found an extinction of $A_J = 0$ mag for 2MASS J0437+2331 using an optical spectrum, which is more sensitive to dust-induced reddening than longer near-IR wavelengths. Our near-IR spectrum also closely resembles the L2 VL-G standard in color. It therefore appears that the red near-IR colors of 2MASS J0437+2331 are photospheric in nature.

Overall, we find supporting evidence that 2MASS J0437+2331 is a member of Taurus and we find the photometric and spectral qualities of PSO J060.3+25 and PSO J077.1+24 to be very similar to those of 2MASS J0437+2331. The only notable difference is the redder overall near-infrared spectral

[10] http://model.obs-besancon.fr

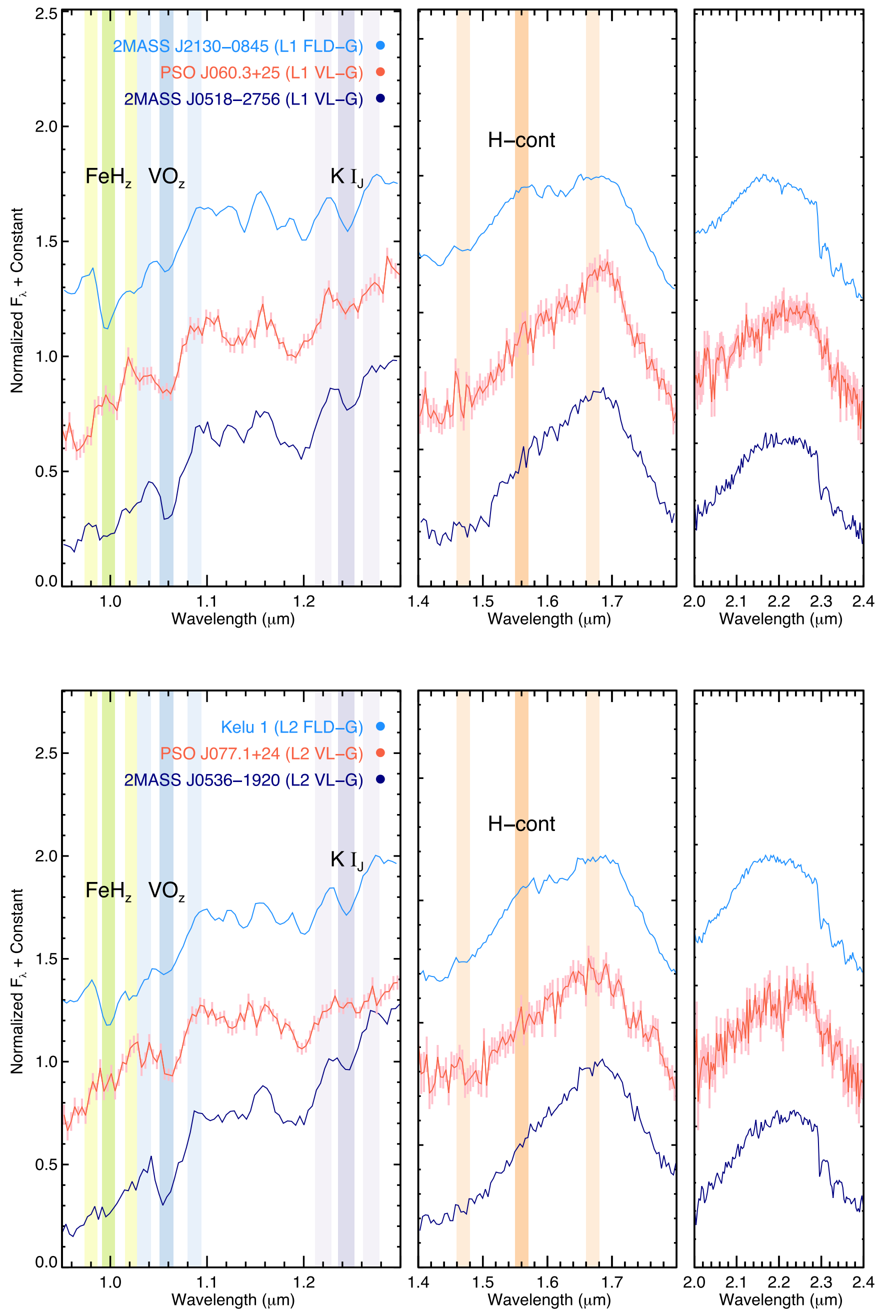

Figure 5. Our six VL-G discoveries (middle/red, with error bars), compared with field standards (top/light blue) from Kirkpatrick et al. (2010) and VL-G standards (bottom/dark blue) from AL13 of the same spectral type. The vertical colored bands show the wavelength intervals used to calculate the labeled spectral indices. For all six objects, the FeH_z, K I_J, and H-cont features are more similar to the VL-G standards, and the VO_z absorption also indicates VL-G for the L dwarfs. (VO_z is not a valid gravity indicator for M dwarfs.)

slope of 2MASS J0437+2331, which does not appear to be due to interstellar extinction (Luhman et al. 2009).

5.1.6. Membership in Taurus

Because of the locations of PSO J060.3+25 and PSO J077.1+24 on Taurus color–magnitude diagrams, their plausibly consistent proper motions, their VL-G gravity classifications, their photometric and spectral similarity to the known Taurus L1 dwarf 2MASS J0437+2331, and the low probability of contamination by field objects, we consider PSO J060.3+25 and PSO J077.1+24 to be bona fide members of Taurus. Their near-infrared colors, consistent with those of field early-L dwarfs but bluer than 2MASS J0437+2331, confirm that the near-infrared redness observed in some low-gravity early-L dwarfs (e.g., Gizis et al. 2012; Faherty et al. 2013; see also Aller et al. 2016) is not a universal feature even for very young (1–2 Myr) L1 and L2 dwarfs.

5.2. Luminosities and Masses

To estimate the masses of our Taurus discoveries, we assumed a distance of 145 ± 15 pc and an age of 1–2 Myr (Kraus & Hillenbrand 2009). We first calculated bolometric luminosities for each object using our spectral types, the K_{MKO} bolometric corrections of Liu et al. (2010, their Table 6), and the distance to

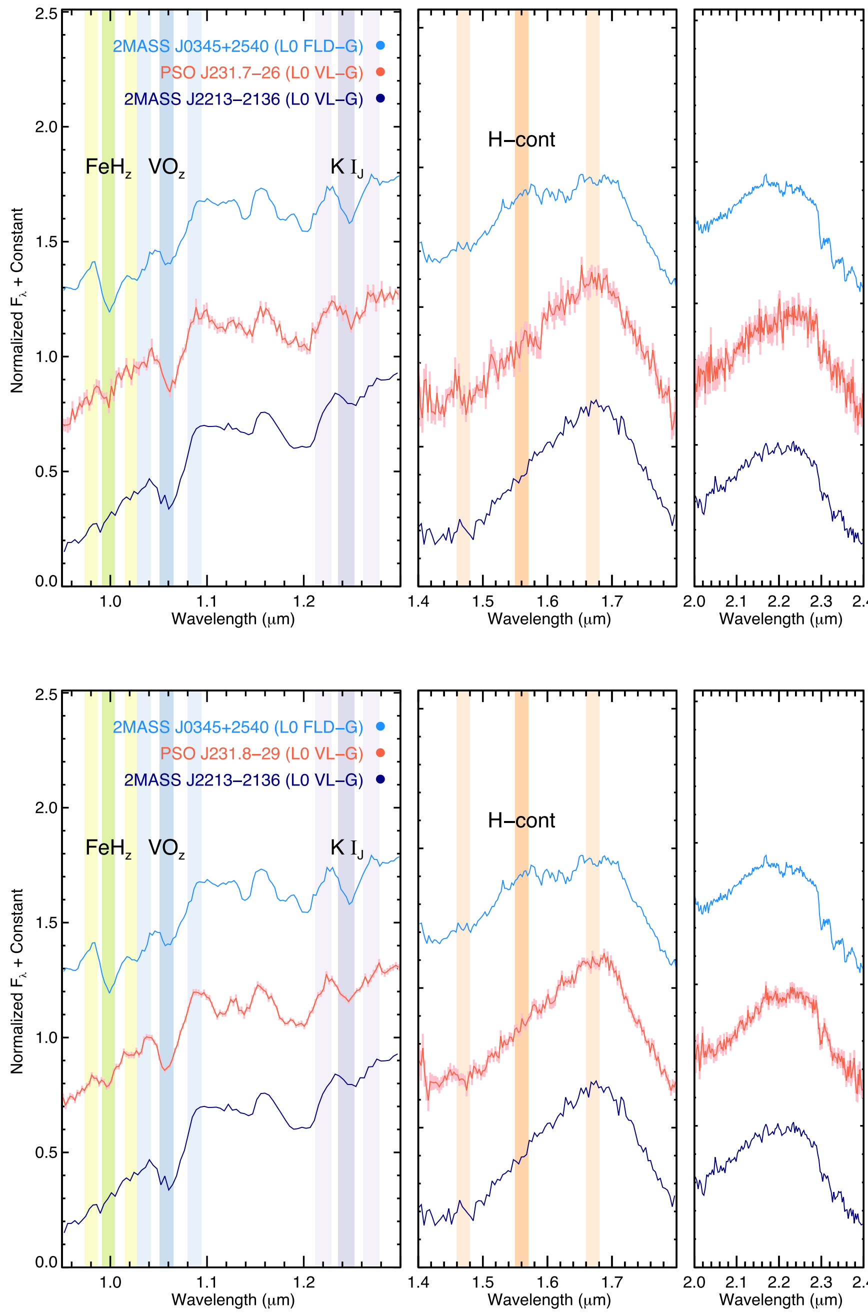

Figure 5. (Continued.)

Taurus. We then used the Lyon/DUSTY evolutionary models[11] (Chabrier et al. 2000) and our $L_{\rm bol}$ values to interpolate masses at the age of Taurus. We propagated the uncertainties on our spectral types (±1 subtype), $K_{\rm MKO}$ magnitudes, bolometric correction, distance, and age into our mass determinations using Monte Carlo simulations, and we quote 68% confidence limits. We used normal distributions for each uncertainty except for age, for which we used a uniform distribution spanning 1–2 Myr to avoid unreasonably young ages. We estimate masses of $6.0^{+0.9}_{-0.8}$ $M_{\rm Jup}$ for PSO J060.3+25 and $5.9^{+0.9}_{-0.8}$ $M_{\rm Jup}$ for PSO J077.1+24 (Table 7). We also applied this method to 2MASS J0437+2331 using $K_{\rm MKO} = 15.20 \pm 0.02$ mag from the UKIDSS Galactic Clusters Survey (GCS; Lawrence et al. 2007, 2013). We estimate log $(L_{\rm bol}/L_\odot) = -3.17^{+0.9}_{-1.0}$ dex and a mass of $7.1^{+1.1}_{-1.0}$ $M_{\rm Jup}$ for 2MASS J0437+2331, consistent with the masses of our discoveries and the 4–7 $M_{\rm Jup}$ estimate of Luhman et al. (2009).

With no evidence of companionship to any nearby star or of unresolved binarity (Section 4.5), our discoveries are among the lowest-mass free-floating substellar objects ever discovered, similar to 2MASS J0437+2331, the young β Pictoris Moving Group L dwarf PSO J318.5338−22.8603 ($8.3 \pm 0.5\,M_{\rm Jup}$; Liu et al. 2013; Allers et al. 2016), the young TW Hydrae Associaton L dwarfs 2MASS J11193254−1137466 (4.3–7.6 $M_{\rm Jup}$; Kellogg et al. 2016) and WISEA J114724.10−204021.3 (5–13 $M_{\rm Jup}$; Schneider et al. 2016), the AB Doradus Moving Group T dwarf SDSS J111010.01+011613.1 (≈10–12 $M_{\rm Jup}$; Gagné et al. 2015a), and the field Y dwarf WISE J085510.83−071442.5 (3–10 $M_{\rm Jup}$;

[11] The more recent BHAC15 models (Baraffe et al. 2015) do not extend to masses below 0.01 $M_\odot$ (≈10 M_{Jup})

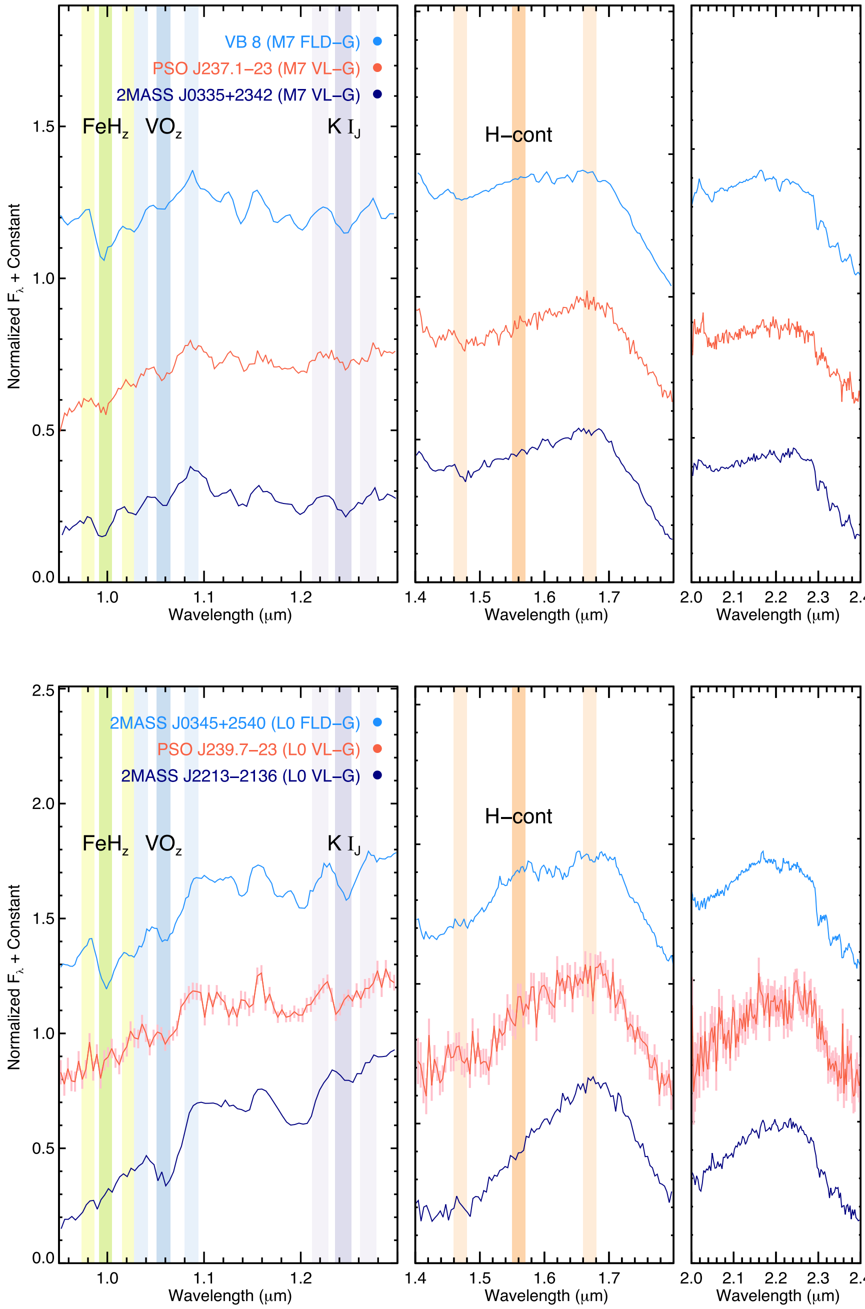

Figure 5. (Continued.)

Luhman 2014; Leggett et al. 2015). They provide significant evidence that free-floating planetary-mass objects can form as part of normal star formation processes.

For comparison, we also converted spectral types into effective temperatures and then used the DUSTY models and our $T_{\rm eff}$ values to estimate masses. No empirically calibrated conversion of spectral type to $T_{\rm eff}$ has been determined for very young L dwarfs, so we extrapolated the scale of Luhman et al. (2003, 2008), arriving at 2000 K for the L1 dwarf and 1800 K for the L2 dwarf. We assumed an error of ± 100 K for each object. With this distance-independent approach, we estimate masses of $7.1^{+1.4}_{-1.1}$ $M_{\rm Jup}$ for PSO J060.3+25 and $5.2^{+0.9}_{-0.8}$ $M_{\rm Jup}$ for PSO J077.1+24. If instead we use the field dwarf (i.e., not young) SpT-to-$T_{\rm eff}$ conversion of Stephens et al. (2009, Equation (3)), we find temperatures of 2112 ± 100 K for the L1 dwarf and 1971 ± 100 K for the L2 dwarf, resulting in masses of $8.6^{+2.0}_{-1.6}$ $M_{\rm Jup}$ for PSO J060.3+25 and $6.8^{+1.3}_{-1.1}$ $M_{\rm Jup}$ for PSO J077.1+24.

We note also that a recent study by Daemgen et al. (2015) identified evidence suggesting an older sub-population of Taurus with an age of ≈20 Myr. If confirmed and our discoveries are in fact members of this sub-population, the older age would lead to a factor of ≈3 increase in our mass estimates.

5.3. Evidence for Circumstellar Disks

Many low-mass stellar members of Taurus are known to host circumstellar disks (e.g., Andrews et al. 2013; Esplin et al. 2014). We searched for evidence of elevated fluxes at mid-infrared wavelengths that would indicate the presence of circumstellar

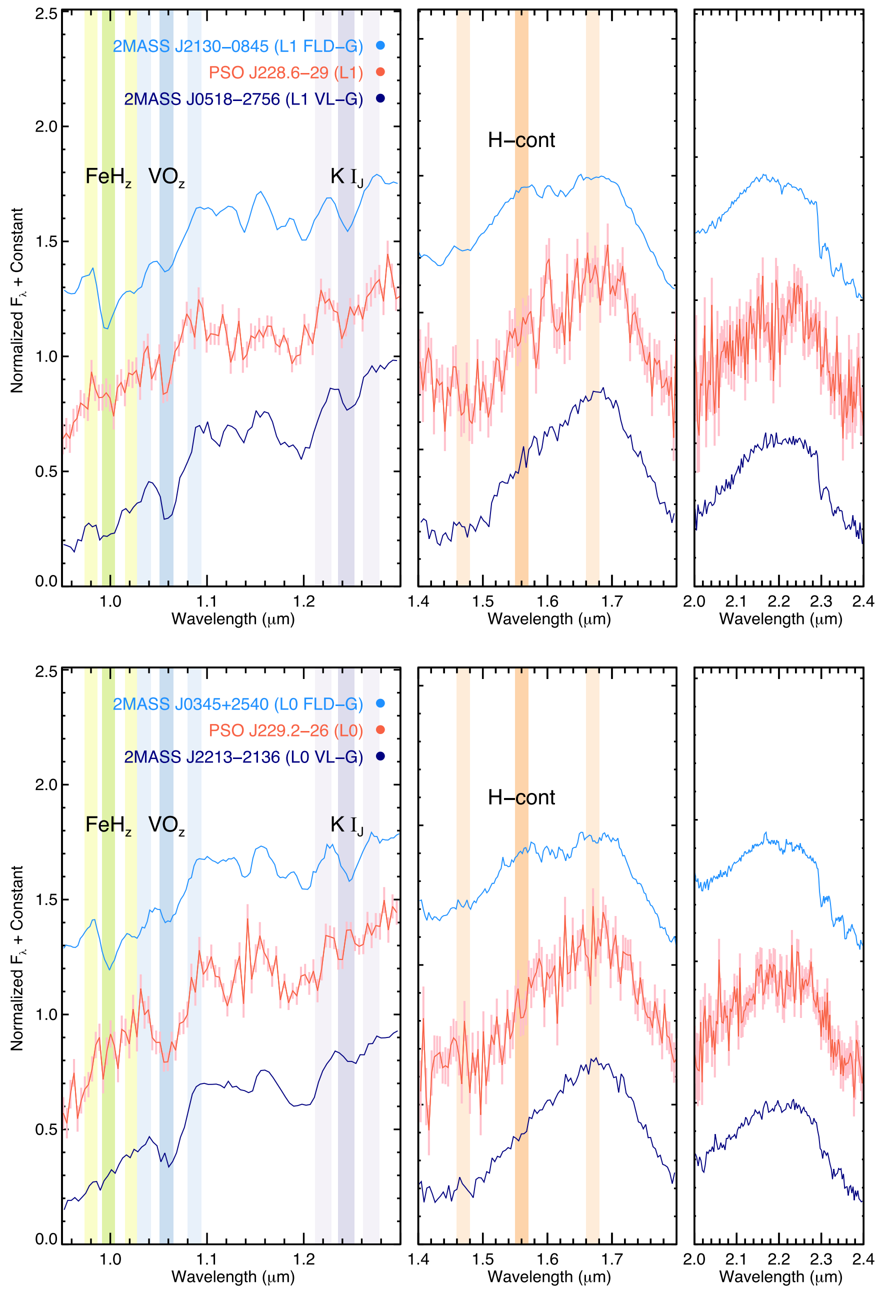

Figure 6. Same as Figure 5, but showing the two objects (PSO J228.6−29 and PSO J229.2−26) for which we did not calculate gravity classes due to low S/N. These two spectra nevertheless show FeH$_z$, VO$_z$, K I$_J$, and H-cont features resembling those of the VL-G standards.

disks around our Taurus discoveries. We fit the BT-Settl grid of synthetic spectra from Baraffe et al. (2015) to our 0.85–2.45 μm prism spectra of PSO J060.3+25, PSO J077.1+24, and 2MASS J0437+2331 following the method of Bowler et al. (2011). In summary, the models are smoothed to the resolving power of the data and resampled to the same wavelength grid. The 1.60–1.65 μm and 1.8–1.95 μm regions are ignored to avoid incomplete methane line lists and low S/N portions of our spectra. The spectra are flux-calibrated to each object's J-band photometry. A scale factor, equal to the square of the object's radius divided by its distance, is calculated by minimizing the χ^2 value following Cushing et al. (2008). Assuming a distance of 145 ± 15 pc to Taurus allows us to simultaneously infer the radius at each grid point.

The results of the fits are shown in Figure 13. The best-fit synthetic spectra ($T_{\rm eff} = 1800$ K, $\log g = 5.5$ dex [cgs] for both of our discoveries and $T_{\rm eff} = 1600$ K, $\log g = 5.5$ dex for 2MASS J0437+2331) offer relatively poor fits to the data, largely failing to reproduce the observed H- and K-band spectral shapes. The best-fit models have field-age surface gravities, contrary to the VL-G classes indicated by the observed spectra, so we include synthetic spectra with the same $T_{\rm eff}$ as the best-fit models but with $\log g = 3.5$ dex (roughly the gravity expected for VL-G objects) in Figure 13 for comparison. The inferred radii for our discoveries are all $\geqslant 2\ R_{\rm Jup}$, consistent with expectations for very young objects still undergoing gravitational contraction (e.g., Burrows et al. 1997). Synthetic photometry of the best fitting models is generally consistent

Table 7
Proper Motions, Luminosities, and Masses

Name	SpT	$\mu_\alpha \cos\delta$[a] (mas yr^{-1})	μ_δ[a] (mas yr^{-1})	χ^2_ν	N_{ep}	Δt (years)	$\log(L_{bol}/L_\odot)$ (dex)	Mass[b] (M_{Jup})
Taurus (age = 1.5 ± 0.5 Myr, distance = 145 ± 15 pc)								
PSO J060.3+25	L1	19.0 ± 8.2	−38.1 ± 8.2	0.8	43	17.2	$-3.32^{+0.09}_{-0.10}$	$6.0^{+0.9}_{-0.8}$
		14.3 ± 3.1[c]	−26.4 ± 3.2[c]		29[c]	12.9[c]		
PSO J077.1+24	L2	14.1 ± 12.5	−27.1 ± 12.1	0.6	27	16.0	$-3.34^{+0.09}_{-0.10}$	$5.9^{+0.9}_{-0.8}$
2MASS J0437+2331	L1	15.9 ± 13.5	−54.8 ± 13.4	0.5	16	15.0	$-3.17^{+0.09}_{-0.10}$	$7.1^{+1.1}_{-1.0}$
Upper Centaurus–Lupus (age = 16 ± 1 Myr, distance = 140 ± 15 pc)								
PSO J228.6−29	L1	−18.4 ± 11.5	−25.6 ± 11.0	1.3	18	15.4	$-3.29^{+0.10}_{-0.10}$	$15.1^{+0.6}_{-0.6}$
PSO J229.2−26	L0	−30.8 ± 10.9	−38.4 ± 10.3	0.9	29	15.3	$-3.18^{+0.09}_{-0.11}$	$15.7^{+1.6}_{-1.5}$
PSO J231.7−26	L0	−25.8 ± 5.5	−28.1 ± 5.4	1.0	35	16.2	$-2.93^{+0.10}_{-0.10}$	20^{+4}_{-4}
PSO J231.8−29	L0	−21.1 ± 2.8	−36.3 ± 2.3	0.5	36	16.5	$-2.82^{+0.10}_{-0.11}$	25^{+8}_{-6}
Upper Scorpius (age = 11 ± 2 Myr, distance = 145 ± 15 pc)								
PSO J237.1−23	M7	−11.4 ± 2.8	−19.7 ± 2.8	2.1	34	16.6	$-2.43^{+0.10}_{-0.11}$	36^{+15}_{-10}
PSO J239.7−23	L0	−0.1 ± 7.2	−23.0 ± 3.5	0.6	38	15.7	$-3.10^{+0.09}_{-0.10}$	$16.2^{+1.4}_{-1.2}$

Notes.
[a] Proper motions from Pan-STARRS1 Processing Version 3.2, calculated using PS1, 2MASS, and *Gaia* DR1 astrometry (Section 4.4).
[b] Masses estimated using L_{bol} and the Lyon/DUSTY evolutionary models (Chabrier et al. 2000) as described in Sections 5 and 6.
[c] From Bouy et al. (2015). We adopt this proper motion for our analysis in Section 5.

with the observed photometry from Pan-STARRS, UKIRT, and the *W1* (3.4 μm) filter from *WISE*, but is significantly lower for the *W2* (4.6 μm) channel at the 7–9σ level. This may represent evidence of thermal excess from a disk around both objects, but we note that the observed *W2* photometry is much more consistent with the $\log g = 3.5$ dex model spectra. The discrepancy at *W2* is therefore likely to be a consequence of the poor model fits, or possibly a result of a systematic error in the model atmospheres, for example from imperfect opacity sources.

The Taurus objects have photometric upper limits in *WISE* for the *W3* (12 μm) and *W4* (22 μm) bands, with one exception. PSO J060.3+25 has a reported 2.6σ detection in *W4* that is significantly brighter than the synthetic model photometry. We visually inspected the *WISE* images of this object and could not confirm that the *W4* detection is distinct from noise. A clear excess at 22 μm would indicate the presence of a disk, but this marginal detection requires confirmation by deeper imaging.

We note that Luhman et al. (2009) also found no excess at mid-IR wavelengths in *Spitzer* photometry that would indicate the presence of a disk around 2MASS J0437+2331.

6. Scorpius–Centaurus Discoveries

The Scorpius–Centaurus Association is the nearest OB association to the Sun. We have discovered six new late-M and early-L members of Sco–Cen. Using the boundaries defined by de Zeeuw et al. (1999), PSO J237.1−23 (M7) and PSO J239.7−23 (L0) lie within the Upper Scorpius subgroup (hereinafter Upper Sco), while PSO J228.6−29 (L1), PSO J229.2−26 (L0), PSO J231.7−26 (L0), and PSO J231.8−29 (L0) sit on the northern outskirts of the Upper Centaurus–Lupus subgroup (hereinafter UCL). Figure 2 shows the sky locations of our discoveries. Upper Sco and UCL are among the reddened regions on the sky identified by Cruz et al. (2003) that we excluded from our search, and our discoveries lie just outside the excluded areas.

Like Taurus, the Upper Sco region has been searched multiple times for brown dwarfs. Unlike in Taurus, more than a dozen L0–L2 dwarfs have previously been confirmed in Upper Sco, in particular by Lodieu et al. (2008) using early release data from the UKIDSS GCS. Our discoveries were not found by that search, nor by Lodieu et al. (2006, 2011), because of incomplete coverage of the region by the early version of GCS. They also remained undetected by searches using optical data as part of the selection process (Martín et al. 2004; Slesnick et al. 2006, 2008). The objects were detected in GCS Data Release 8 and later versions, but were only observed in *H* and *K* bands, and so were not included in the search of Dawson et al. (2011, 2013) who required *Z* and *J* photometry in their selection process. PSO J237.1−23 was identified as a candidate member of Upper Sco by Lodieu (2013) as part of their "*HK*-only sample," but PSO J239.7−23 is too faint to qualify for this sample. Searches for young ultracool dwarfs have not focused on UCL, so our four discoveries lie outside regions targeted by previous efforts.

In this section we follow the structure of Section 5, presenting the evidence that our discoveries are members of Sco–Cen (Section 6.1), estimating their masses (Section 6.2), and comparing their SEDs to model atmospheres to look for evidence of circumstellar disks (Section 6.3).

6.1. Evidence for Membership

6.1.1. Youth

Four of our six Sco–Cen discoveries have VL-G gravity classes, suggesting ages $\lesssim$30 Myr. The other two, PSO J228.6−29 and PSO J229.2−26, have lower-S/N spectra that do not permit robust calculation of the AL13 gravity-sensitive indices but nevertheless show clear visual indications of low gravity (Section 4.3).

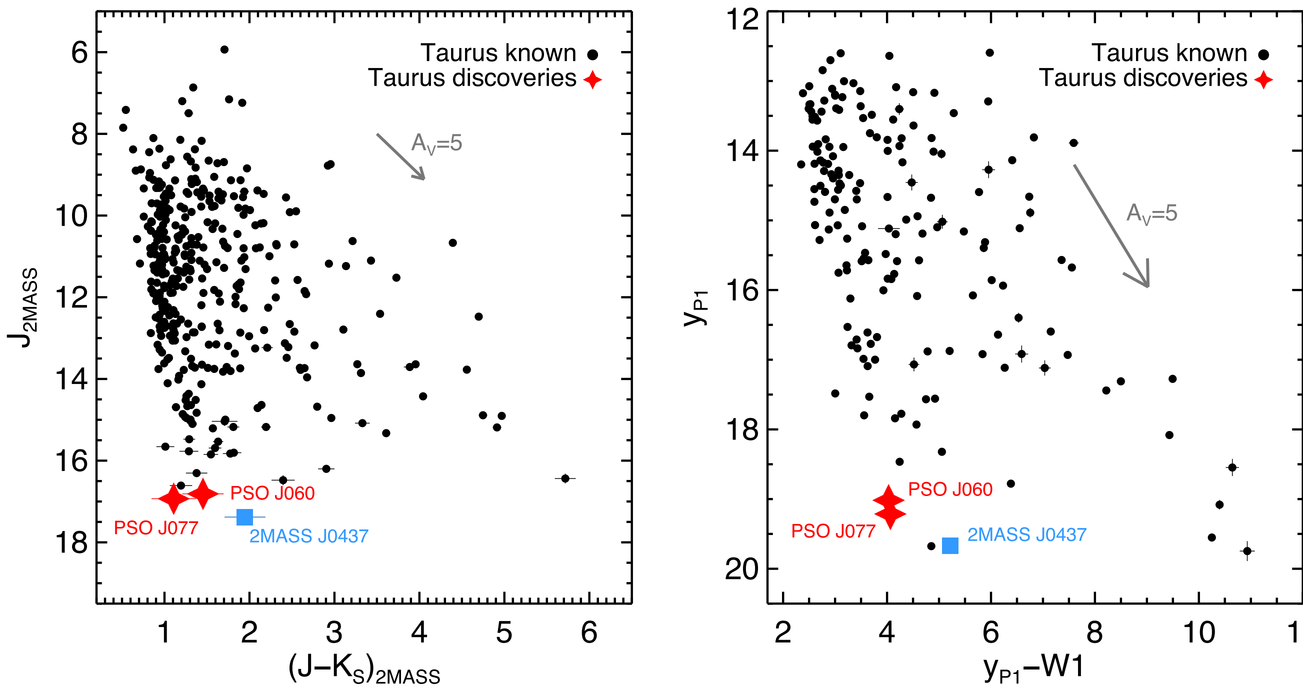

Figure 7. Comparison of the photometry of our discoveries in the Taurus star-forming region (red stars) to known Taurus members from Esplin et al. (2014; black circles). We also highlight the known Taurus L1 dwarf 2MASS J0437+2331 (Section 5.1.5, blue square) and indicate reddening vectors equivalent to an extinction of $A_V = 5$ mag with gray arrows. Left: J vs. $J - K_S$ (2MASS) diagram. Right: y_{P1} vs. $y_{P1} - W1$ diagram for Taurus objects not saturated in PS1. Both plots show an unreddened cluster sequence on the left, with many objects significantly reddened by the Taurus molecular cloud. Our two discoveries lie at the faint end of the cluster sequence and are minimally affected by extinction, consistent with their locations on the outer edges of Taurus.

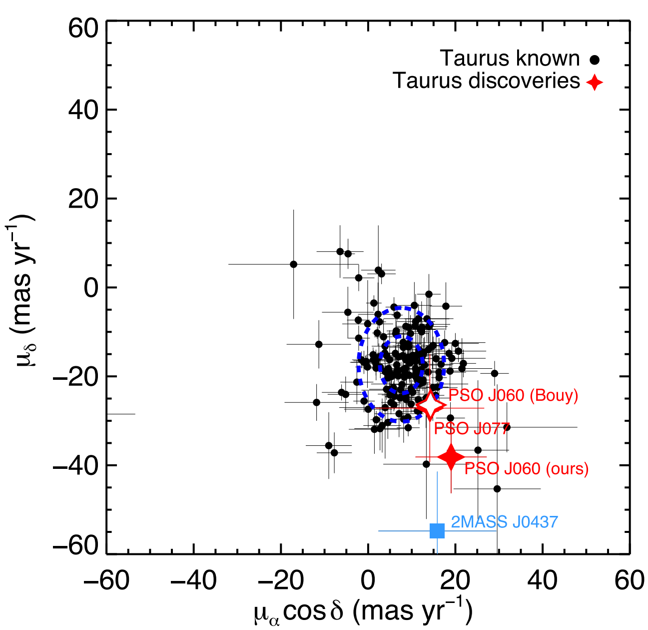

Figure 8. Vector-point diagram showing the proper motions of our discoveries in the Taurus star-forming region (red stars) and those of known Taurus members from Esplin et al. (2014) that are not saturated in PS1 and have reliable PS1 proper motion fits (black circles). We also include the only previously known L dwarf in Taurus, 2MASS J0437+2331 (Luhman et al. 2009), which we classify as L1. We adopt the proper motion for PSO J060.3+25 from Bouy et al. (2015), shown with an open red star. Note that the PS1 proper motion for PSO J077.1+24 and the Bouy et al. (2015) proper motion for PSO J060.3+25 are very similar and their symbols coincide in the figure. Both of these adopted proper motions are consistent with the mean Taurus proper motion, while the PS1 proper motion for 2MASS J0437+2331 is $\approx 2\sigma$ discrepant in μ_δ.

6.1.2. Photometry

Figure 14 demonstrates the consistency of our six discoveries' photometry with that of known Upper Sco members from Luhman & Mamajek (2012, hereinafter LM12), Dawson et al. (2014), and Rizzuto et al. (2015), and with photometric/astrometric candidates from unreddened regions in the UKIDSS GCS Data Release 10 (Lodieu 2013, their Table A1). The LM12 catalog contains a handful of objects that are reddened by interstellar extinction and we include reddening vectors (Section 5.1.2) scaled to an extinction of $A_V = 2$ mag in Figure 14. Most of our discoveries lie along the unreddened cluster sequence of the Upper Sco J versus $J - K$ and y_{P1} versus $y_{P1} - W1$ color–magnitude diagrams, fully consistent with the reddening-free sample of Lodieu (2013). PSO J237.1−23 is redder than the cluster sequence in $y_{P1} - W1$, likely evidence for a circumstellar disk (Section 6.3). As with PSO J060.3+25 and PSO J077.1+24 in Taurus, the Sco–Cen objects have $(J - K_S)_{2MASS}$ colors that are consistent with field L0–L1 dwarfs but have $W1 - W2$ colors that are 1–3σ redder than the field population (Gizis et al. 2012; Faherty et al. 2013).

6.1.3. Proper Motion

We compare the proper motions of our Sco–Cen discoveries to the proper motions of several literature sources in Figure 15. Pecaut et al. (2012) calculated proper motions for F-type stars in Upper Sco and UCL, and Lodieu (2013) calculated proper motions for a list of unreddened photometric/astrometric members and candidates in UKIDSS GCS. LM12 do not quote proper motions for their catalog of Upper Sco members, so we obtained PS1 Processing Version 3.2 (PV3.2) proper motions for these objects as well as those from Dawson et al. (2014) and Rizzuto et al.

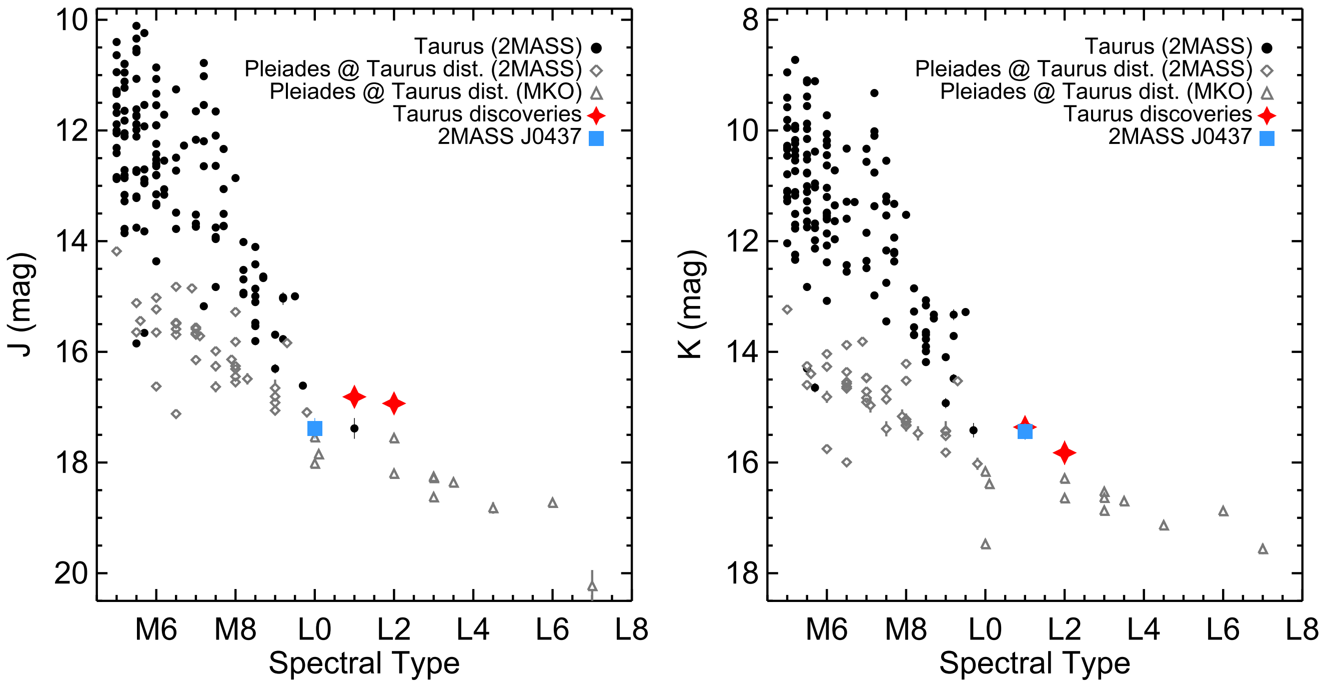

Figure 9. J (left) and K (right) apparent magnitudes as a function of spectral type for our discoveries in the Taurus star-forming region (red stars) compared with known members of Taurus (Esplin et al. 2014, black circles) and the Pleiades (gray open symbols). Pleiades magnitudes have been adjusted by +0.136 mag to place the objects at the distance of Taurus (145 pc). We use 2MASS photometry (Skrutskie et al. 2006, diamonds) for the brighter Pleiades members, and MKO photometry from the UKIDSS Galactic Clusters Survey (Lawrence et al. 2012, triangles) for members too faint to be detected by 2MASS. We also highlight the previously coolest known member of Taurus, 2MASS J0437+2331 (blue square), which we classify as L1 on the AL13 system. Our discoveries lie $\gtrsim$1 mag above the Pleiades sequence but are consistent with an extension of the Taurus sequence, supporting membership in the younger Taurus region. References for Pleiades spectral types: Bihain et al. (2006, 2010), Festin (1998), Martín et al. (1996, 1998a, 1998b, 2000), Pinfield et al. (2003), Stauffer et al. (1998a, 1998b), Steele & Jameson (1995), and Zapatero Osorio et al. (1997, 2014a).

(2015). From these PS1 proper motions we calculated a weighted mean proper motion for known Upper Sco members of ($\mu_\alpha \cos\delta = -8.5 \pm 0.1$, $\mu_\delta = -19.6 \pm 0.1$ mas yr^{-1}), with a weighted rms of 4.3 mas yr^{-1} in R.A. and 5.6 mas yr^{-1} in decl. Our complete list of PS1 proper motions for objects from this combined catalog that are not saturated in PS1 is described in Appendix B. Figure 15 demonstrates the consistency of the proper motions of our discoveries with all literature sources.

6.1.4. Likelihood of Field Contamination

We estimated the likelihood that any of our Sco–Cen discoveries could be interloping foreground or background field objects, using the same approach as in Section 5.1.4. Upper Sco and UCL are distinct regions with different ages and bulk proper motions (Pecaut et al. 2012), so we considered them separately.

We defined the boundaries of Upper Sco to be $343° \leqslant l \leqslant 360°$ and $10° \leqslant b \leqslant 30°$ (Figure 2). The portion of this region surveyed by PS1 (i.e., north of $\delta = -30°$) covers 281.0 deg^2. We found that $28.42 \pm 0.11\%$ of a synthetic population (Besançon Galactic model) of field M dwarfs in the direction of Upper Sco will have proper motions within 3σ of the mean Upper Sco $\mu_\alpha \cos\delta$ and μ_δ (Section 6.1.3). We estimate that our search would find $(3.99 \pm 0.02) \times 10^{-2}$ field VL-G dwarfs within the projected boundaries of Upper Sco having proper motions consistent with Upper Sco membership. We find a probability of 96.1% that both PSO J237.1−23 and PSO J239.7−23 are members of Upper Sco.

For UCL, we used the data for F stars from Pecaut et al. (2012) to calculate a weighted mean proper motion of ($\mu_\alpha \cos\delta = -23.0 \pm 0.1$, $\mu_\delta = -23.8 \pm 0.1$ mas yr^{-1}) with a weighted rms of 5.7 mas yr^{-1} in R.A. and 4.9 mas yr^{-1} in decl. Only 0.51% of our synthetic M dwarf population have proper motions consistent within 3σ with the mean UCL motion. PSO J228.6−29, PSO J229.2−26, PSO J231.7−26, and PSO J231.8−29 all have proper motions consistent with UCL, so the probability that any of them is a field interloper is negligible based on proper motions alone.

6.1.5. Membership in Scorpius–Centaurus

All six of our discoveries in the direction of Sco–Cen have VL-G gravity classifications or clear spectral indications of low gravity. Their positions in color–magnitude diagrams, proper motions, and very low probability of contamination by field objects confirm that they are members of Sco–Cen.

6.2. Luminosities and Masses

We calculated bolometric luminosities and estimated the masses of our Sco–Cen discoveries using the method described in Section 5.2. We adopted a distance of 145 ± 15 pc (de Zeeuw et al. 1999; Preibisch & Zinnecker 1999) and an age of 11 ± 2 Myr (Pecaut et al. 2012) for Upper Sco. The mean distance to UCL is 140 ± 2 pc (de Zeeuw et al. 1999). de Bruijne (1999) found a substantial depth of 50 ± 20 pc for UCL, but all four of our UCL discoveries have photometry consistent with members of Upper Sco (Figure 14), so we used the same distance uncertainty as Upper Sco and adopted a UCL distance of 140 ± 15 pc, along with an age of 16 ± 1 Myr (Pecaut et al. 2012). We used normal distributions for the age and distance uncertainties in our Monte Carlo simulations. Our luminosity and mass estimates for our Sco–Cen discoveries are

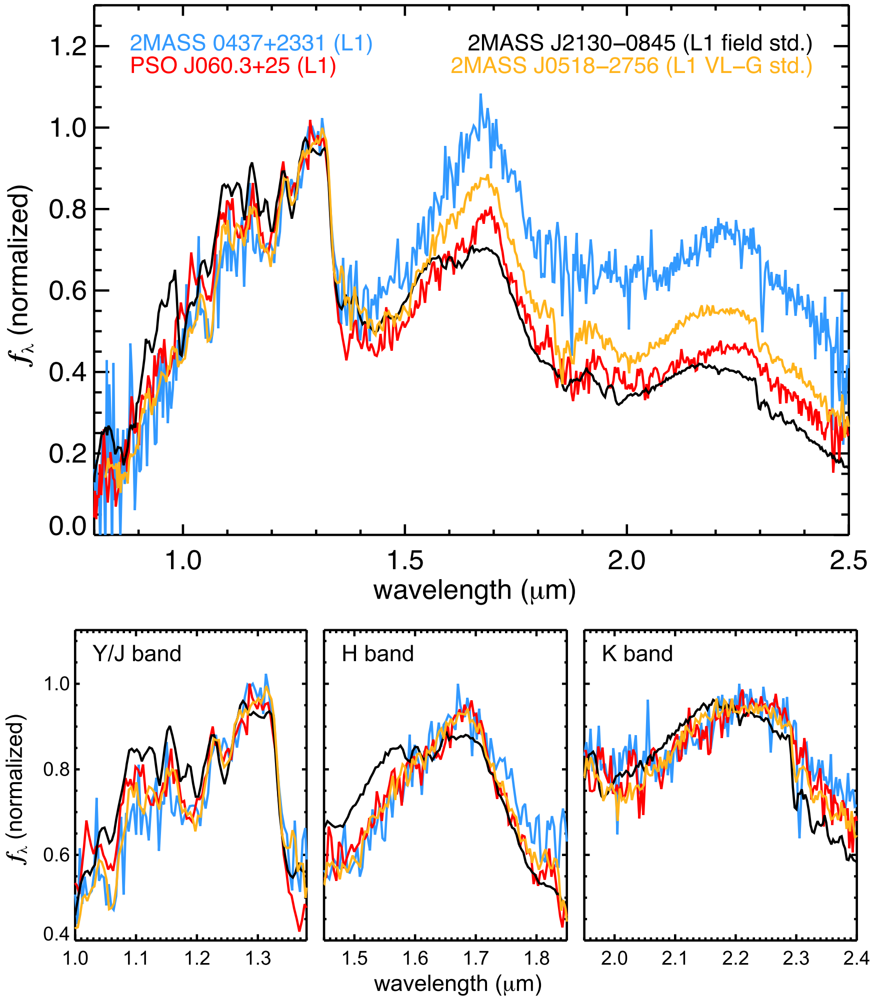

Figure 10. Top: SpeX Prism spectrum of 2MASS J0437+2331 (blue) from Bowler et al. (2014), overplotted with PSO J060.3+25 (red) along with the field (black; Kirkpatrick et al. 2010) and VL-G (orange; Allers & Liu 2013a) standards of the same spectral type (L1) as PSO J060.3+25. All four spectra are normalized at the J-band peak. 2MASS J0437+2331 is notably redder than PSO J060.3+25 as well the L1 VL-G standard, while PSO J060.3+25 has colors similar to those of the field standard. Bottom: the same four spectra plotted separately for Y/J, H, and K bands, normalized separately for each band to compare the spectral shapes in each band. The two young Taurus objects and the L1 VL-G standard have similar shapes in all bands, distinct from the older field standard.

listed in Table 7. The masses span 15–36 $M_{\rm Jup}$, near the low-mass end of the brown dwarf regime and comparable to the lowest-mass members known in these regions (Lodieu et al. 2011; Aller et al. 2013).

6.3. A Candidate Circumstellar Disk

At ages $\gtrsim$10 Myr, our discoveries in Sco–Cen are less likely to harbor circumstellar disks than are the ≈1–2 Myr Taurus objects (e.g., Mathews et al. 2012). However, LM12 have demonstrated that ≈25% of M5–L0 objects in Upper Sco have disks detectable at mid-infrared wavelengths. They developed color versus spectral type relationships to identify stars and brown dwarfs with candidate circumstellar disks, using colors including $K_S - W2$, $K_S - W3$, and $K_S - W4$. Our L dwarf discoveries were not detected in $W3$ or $W4$, and LM12 cautioned that the $K_S - W2$ colors do not reliably discriminate between excess flux from a disk and rapidly reddening photospheres beyond spectral type M8.5. We nevertheless checked the $K_S - W2$ colors of our L dwarfs (including the Taurus discoveries), and none are redder than the typical colors of Upper Sco M9–L1 dwarfs (LM12), so we cannot identify any candidate disk hosts among these objects.

PSO J237.1−23, the lone M dwarf (M7) among our discoveries, has significantly mid-infrared redder colors than those of late-M dwarfs lacking disks, strongly suggesting the presence of a circumstellar disk. The $K_S - W2$ and $K_S - W3$ colors both satisfy the LM12 criteria by $\gtrsim 5\sigma$. PSO J237.1−23 also has a marginal $W4$ detection at 8.75 ± 0.45 mag, which, if real, would give the object a $K_S - W4$ color over 3.5 mag redder than the LM12 limit for disk-hosting M7 dwarfs. We therefore consider PSO J237.1−23 to be a clear candidate circumstellar disk host, joining over a dozen other candidates in Upper Sco with spectral types M7 or later (LM12).

We also looked for evidence of excess mid-infrared fluxes using the method described in Section 5.3, fitting the BT-Settl model spectra (Baraffe et al. 2015) to the prism spectra of our Sco–Cen discoveries. The results are shown in Figure 16. As with our Taurus discoveries, the best-fit synthetic spectra for our Sco–Cen objects have field-age gravities inconsistent with the low-gravity features in the observed spectra, fit the emprical JHK-band morphologies fairly poorly, and have radii $\geqslant 2$ $R_{\rm Jup}$ (consistent with models). Synthetic photometry from the models is generally consistent with the observed photometry. The significantly lower synthetic flux at $W2$ seen in our Taurus discoveries (Figure 13) is present here for two of the six Sco–

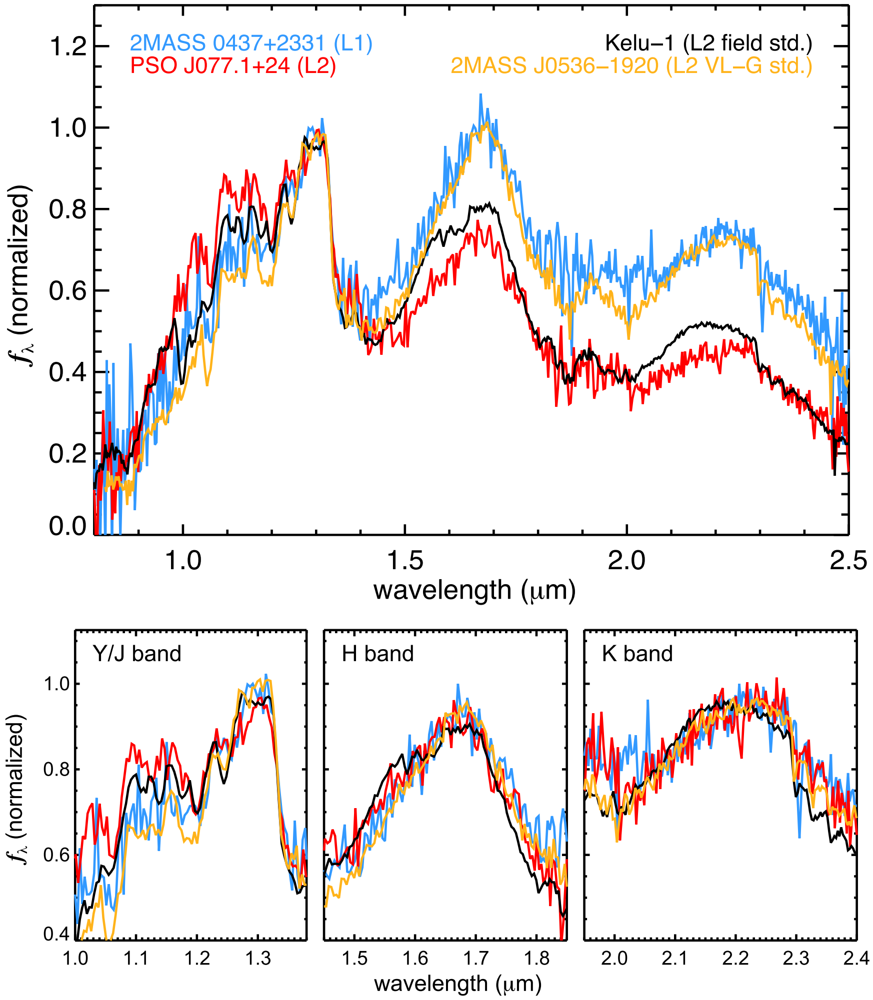

Figure 11. SpeX Prism spectrum of 2MASS J0437+2331 (blue) from Bowler et al. (2014), overplotted with PSO J077.1+24 (red) along with the field (black; Kirkpatrick et al. 2010) and VL-G (orange; Allers & Liu 2013a) standards of the same spectral type (L2) as PSO J077.1+24, using the same format as Figure 10. 2MASS J0437+2331 is significantly redder than PSO J077.1+24 but has similar colors to the L2 VL-G standard, while PSO J077.1+24 has colors more similar to those of the field standard.

Cen objects, although again this is likely to be an consequence of poor model fits. Our disk candidate, PSO J237.1−23, does show an excess in observed flux relative to the best-fit and low-gravity models at all four *WISE* bands, although the model synthetic fluxes are higher than observations in the optical bands, indicating that the fit has failed to correctly capture the observed SED.

7. Summary

As part of a wide-field search for L/T transition dwarfs using the Pan-STARRS1 and *WISE* surveys, we have serendipitously discovered eight young late-M and early-L dwarfs in the nearby Taurus and Scorpius–Centaurus star-forming regions. PSO J060.3+25 (spectral type L1) and PSO J077.1+24 (L2) are members of Taurus. Both have VL-G gravity classifications indicating ages $\lesssim$30 Myr, photometry consistent with previously known ultracool members of Taurus, and proper motions consistent with the Taurus population. We estimate the probability that neither object is a foreground (or background) field dwarf to be 97%. The spectral and photometric properties of our two discoveries are also similar to the only previously known free-floating L dwarf in Taurus, 2MASS J0437+2331 (Luhman et al. 2009). At the young ($\approx$1–2 Myr) age of Taurus, PSO J060.3+25 and PSO J077.1+24 have estimated masses of $\approx$6 $M_{\rm Jup}$, and they join 2MASS J0437+2331 ($\approx$7 $M_{\rm Jup}$, spectral type L1) as the lowest-mass isolated known members of Taurus. PSO J077.1+24 is additionally the coolest known free-floating object discovered in Taurus to date.

PSO J060.3+25 was previously identified by Sarro et al. (2014) and Bouy et al. (2015) as DANCe J040116.80 +255752.2, a likely ultracool member of the Pleiades (age $\approx$ 125 Myr) based on its photometry and astrometry. Our spectrum confirms the late spectral type of PSO J060.3+25, but its VL-G gravity class implies an age ($\lesssim$30 Myr) consistent with the much younger Taurus star-forming region and its near-infrared photometry is more consistent with other VLM members of Taurus.

The other six M7–L1 dwarf discoveries lie on the outskirts of the Upper Scorpius and Upper Centaurus–Lupus associations (ages $\approx$11–16 Myr), with estimated masses $\approx$15–36 $M_{\rm Jup}$. Four have VL-G gravity classifications; our spectra for the other two did not have enough S/N for confident gravity classification, but visual inspection finds they have clear spectral signatures of low gravity. The photometry and proper motions of all six objects are fully consistent with membership in Scorpius–Centaurus. Lodieu (2013) previously identified

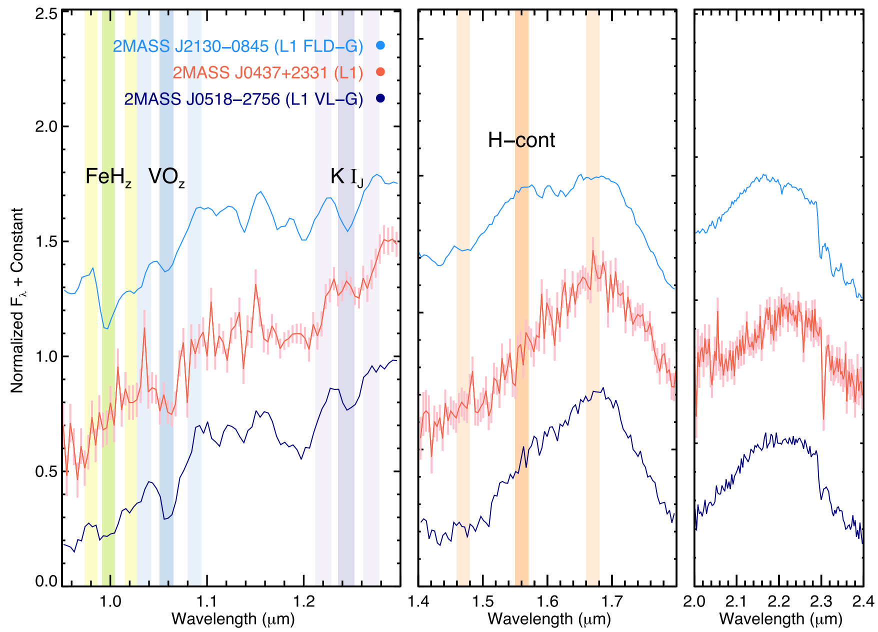

Figure 12. Same as Figure 5, but showing the SpeX Prism spectrum for 2MASS J0437+2331 (Luhman et al. 2009; Bowler et al. 2014). We did not determine a gravity class for 2MASS J0437+2331 due to low spectral S/N, but its FeH$_z$, VO$_z$, K I$_J$, and H-cont features do resemble those of the L1 VL-G standard (Allers & Liu 2013a).

PSO J237.1−23 as an astrometric and photometric candidate member of Upper Sco, which we confirm with our independent discovery and spectroscopy.

We found no spectral indications that any of our discoveries have unresolved companions, nor did we find any comoving objects nearby. The Taurus objects represent strong evidence that normal star formation processes can produce isolated objects with masses as low as ≈6 $M_{\rm Jup}$.

The $J-K$ colors of all seven young L dwarf discoveries are consistent with those of older field L0–L2 dwarfs. This contrasts with the redder $J-K$ colors of some previously discovered young early-L dwarfs and confirms that near-infrared redness is not a universal feature of very young (1–2 Myr) brown dwarfs. Our discoveries do have $W1-W2$ colors that are redder than those of early-L field objects, which we identify as the primary reason we discovered these objects during a search for L/T transition dwarfs.

We fit BT-Settl synthetic spectra (Baraffe et al. 2015) to our observed spectra and found that the best-fit models reproduce our spectra relatively poorly in the near-infrared. At 4.6 μm (*WISE W*2 band), all three Taurus objects and two Sco–Cen objects show a significant observed excess flux over the model predictions. These elevated fluxes are suggestive of the presence of a circumstellar disk but may also indicate a source of systematic error in the model atmospheres. The M7 dwarf PSO J237.1−23 shows strong excess fluxes at *W*2, *W*3, and possibly at *W*4, making it a likely host for a circumstellar disk.

Our discovery of these eight young brown dwarfs in well-searched regions of the sky, while looking for older objects with cooler spectral types, has a few important implications.

1. The combination of PS1 and *WISE* photometry is a powerful tool for identifying young ultracool dwarfs (see also Paper II).
2. Unusually red $W1-W2$ colors in late-M and early-L dwarfs may indicate the objects are young (Figure 3), providing leverage for searches for young *M*/*L* dwarfs.
3. There are likely to be more young planetary-mass brown dwarfs that could be discovered with focused searches in even well-studied star-forming regions.

We thank the anonymous referee for a helpful critique that improved the quality of this paper. We thank Katelyn Allers, Brian Cabreira, Dave Griep, Tony Matulonis, and Eric Volquardsen for assisting with IRTF observations. The Pan-STARRS1 Surveys (PS1) have been made possible through contributions of the Institute for Astronomy, the University of Hawaii, the Pan-STARRS Project Office, the Max-Planck Society and its participating institutes, the Max Planck Institute for Astronomy, Heidelberg and the Max Planck Institute for Extraterrestrial Physics, Garching, The Johns Hopkins University, Durham University, the University of Edinburgh, Queen's University Belfast, the Harvard-Smithsonian Center for Astrophysics, the Las Cumbres Observatory Global Telescope Network Incorporated, the National Central University of Taiwan, the Space Telescope Science Institute, the National Aeronautics and Space Administration under grant No. NNX08AR22G issued through the Planetary Science Division of the NASA Science Mission Directorate, the National Science Foundation under grant No. AST-1238877, the University of Maryland, Eotvos Lorand University (ELTE), and the Los Alamos National Laboratory. This project makes use of data products from the Wide-field Infrared Survey Explorer, which is a joint project of the University of California, Los Angeles, and the Jet Propulsion Laboratory/California Institute of Technology, funded by the National Aeronautics and Space Administration. This work has made use of data from the European Space Agency (ESA) mission *Gaia* (http://www.cosmos.esa.int/gaia), processed by the *Gaia* Data Processing and Analysis Consortium (DPAC, http://www.cosmos.esa.int/web/gaia/dpac/consortium). Funding for the DPAC has been provided by national institutions, in particular the institutions participating in the *Gaia* Multilateral Agreement. This research has made use of the 2MASS data products; the UKIDSS data products; the VISTA data products; NASA's

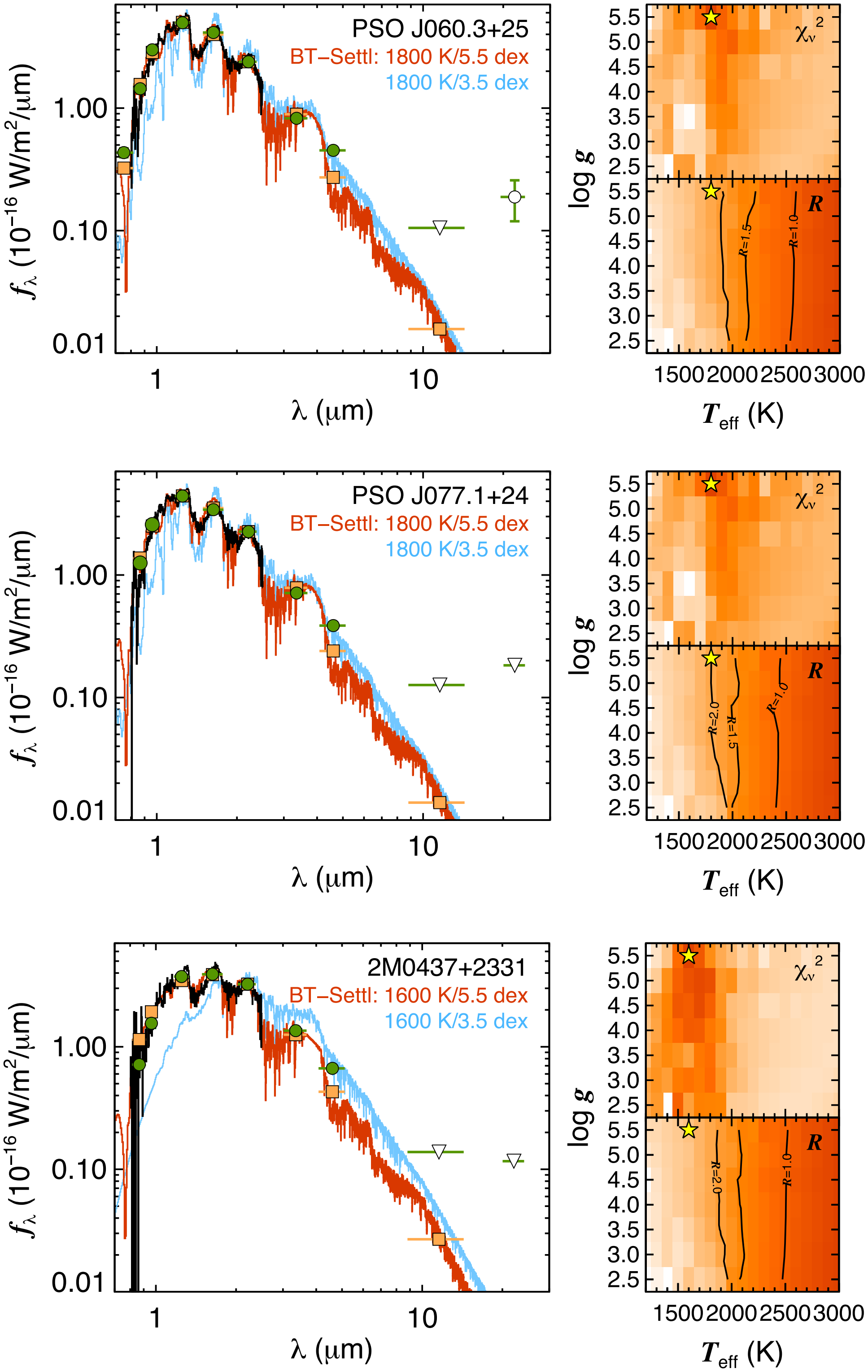

Figure 13. Best-fit BT-Settl model spectra (Baraffe et al. 2015) for our two Taurus discoveries and 2MASS J0437+2331. For each object, the left-hand plot includes our prism spectrum (black), the best-fit model spectrum (red), and the synthetic spectrum with the same $T_{\rm eff}$ as the best-fit model but with $\log g = 3.5$ (roughly that expected for VL-G objects) in blue. In addition, we plot observed PS1/MKO/AllWISE photometry (green circles) and synthetic photometry for the best-fit model (orange squares). Upper limits for $W3$ (12 μm) and $W4$ (22 μm) are plotted with open triangles; the $W4$ detection for PSO J060.3+25 (open circle) is marginal at 2.6σ. The right-hand plots show the χ^2 surface for the model ($T_{\rm eff}$, $\log g$) fits (top) and the inferred radius in units of $R_{\rm Jup}$ (bottom). The best-fit models match the observed spectra fairly poorly, particular in the H- and K-band morphology. The observed excess flux relative to the best-fit models at $W2$ (4.6 μm) in all three objects may indicate the presence of a disk, but the excess is not seen relative to the low-gravity model spectra, and may therefore be the result of a systematic error in the model atmospheres.

Astrophysical Data System; the SIMBAD and Vizier databases operated at CDS, Strasbourg, France, and the Database of Ultracool Parallaxes, maintained by Trent Dupuy at https://www.cfa.harvard.edu/~tdupuy/plx. W.M.J.B. received support from NSF grant AST09-09222. W.M.B.J., M.C.L., and E.A.M. received support from NSF grant AST-

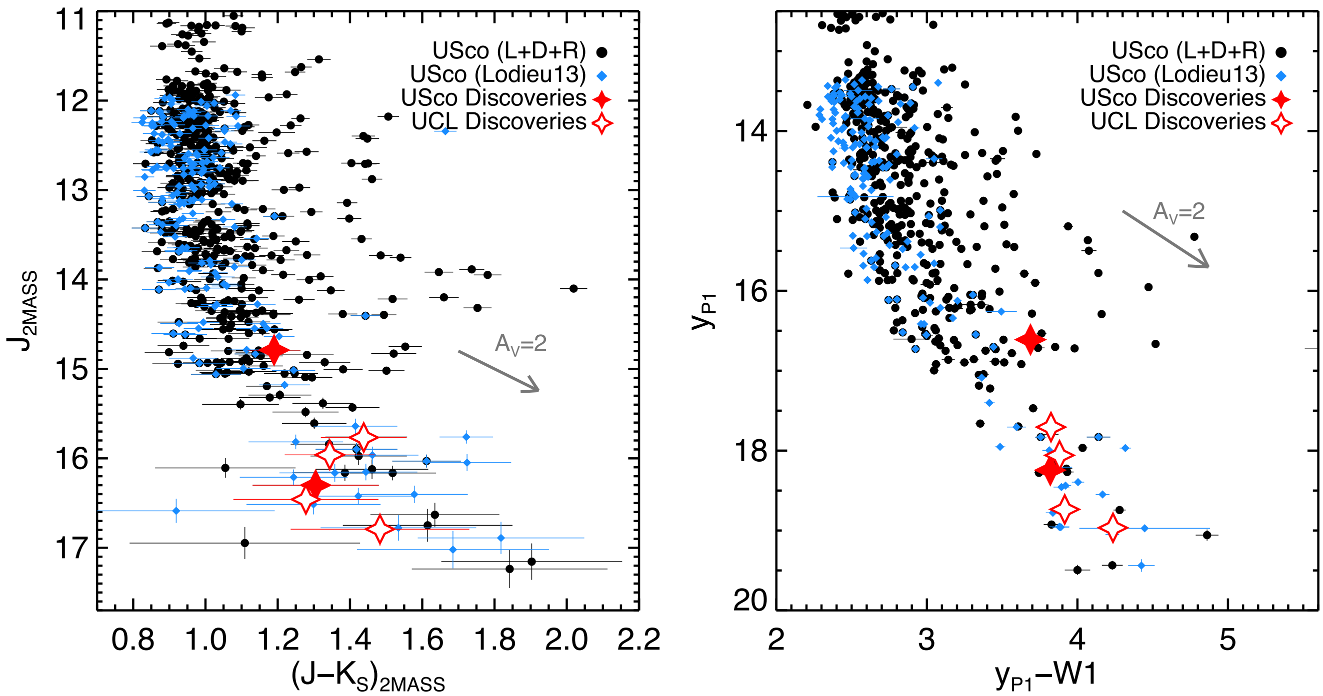

Figure 14. Comparison of the photometry of our discoveries in Upper Sco (USco, filled red stars) and Upper Centaurus–Lupus (UCL, open red stars) to known members of Upper Sco from Luhman & Mamajek (2012); Dawson et al. (2014), and Rizzuto et al. (2015; black circles, labeled "L+D+R" in the legend) and known and candidate Upper Sco members from UKIDSS GCS (Lodieu 2013, blue diamonds). Left: J vs. $J-K$ (MKO) diagram. Right: y_{P1} vs. $y_{P1}-W1$ diagram for non-saturated objects in PS1. We include reddening vectors (gray arrows) scaled to an extinction of $A_V = 2$ mag. All six of our discoveries have photometry lying along the cluster sequences. The brighter Upper Sco discovery, PSO J237.1−23, has a redder $y_{P1}-W1$ color suggesting the presence of a circumstellar disk (Section 6.3).

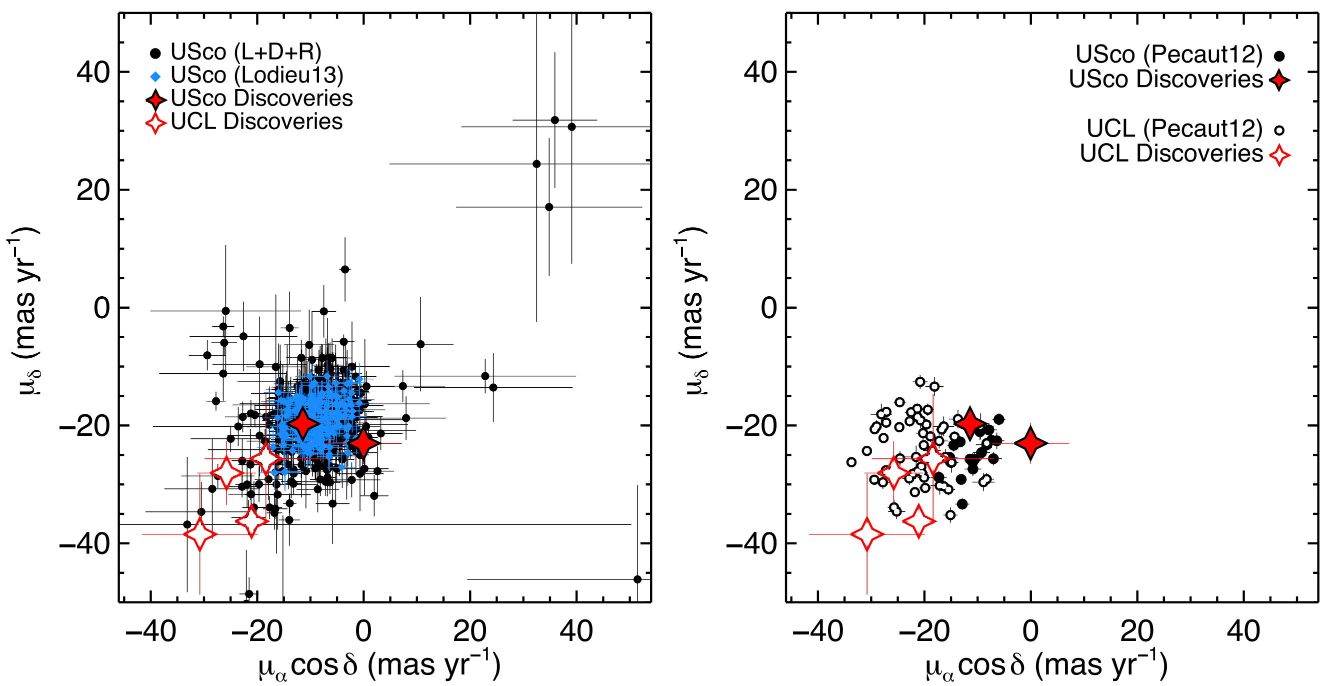

Figure 15. Vector-point diagrams comparing the proper motions of our discoveries in Upper Scorpius (USco, filled red stars) and Upper Centaurus–Lupus (UCL, open red stars) to those of Sco–Cen objects from the literature. Left: we show our proper motions for objects in the Upper Sco lists of LM12, Dawson et al. (2014), and Rizzuto et al. (2015; black circles, labeled "L+D+R" in the legend) that are not saturated in PS1 and have reliable proper motion fits, and the proper motions of known and candidate Upper Sco members from UKIDSS GCS (Lodieu 2013, blue diamonds). Right: proper motions of F-type stars in Upper Sco (black filled circles) and UCL (black open circles) from Pecaut et al. (2012). All six of our Sco–Cen discoveries have proper motions consistent with all literature sources.

1313455. Finally, the authors wish to recognize and acknowledge the very significant cultural role and reverence that the summit of Maunakea has always held within the indigenous Hawaiian community. We are most fortunate to have the opportunity to conduct observations from this mountain.

Facilities: IRTF (SpeX), PS1, UKIRT (WFCAM).

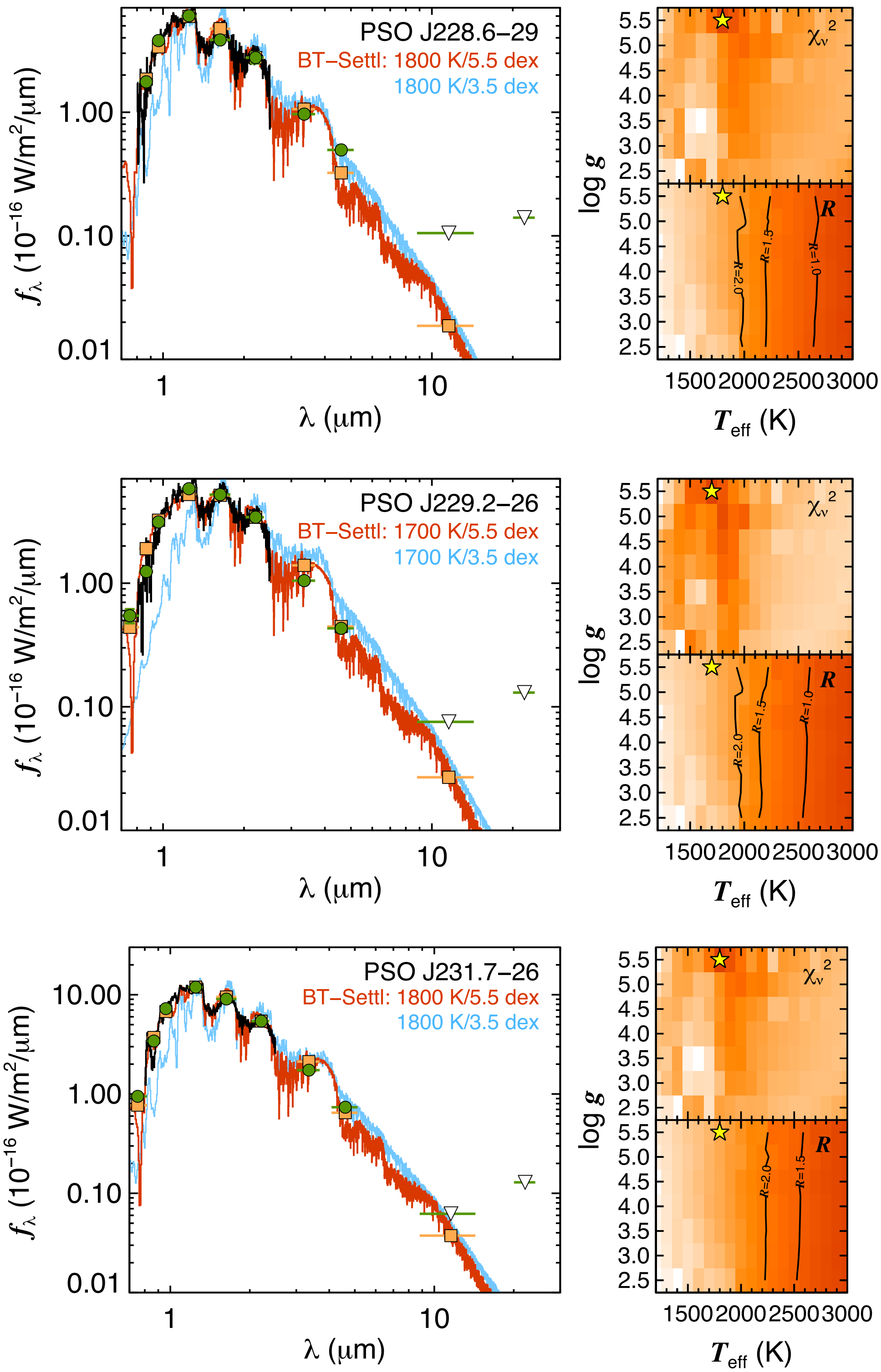

Figure 16. Same as Figure 13, but showing the best-fit BT-Settl model spectra (Baraffe et al. 2015) to our Sco–Cen discoveries. The best-fit models again match the observed spectra fairly poorly, particularly in the *H*- and *K*-band morphology. The observed excess flux at *W*2 (4.6 μm) seen in Figure 13 is seen here in three of the six objects, but the excess again disappears in two cases (PSO J228.6−29 and PSO J239.7−23) when compared to the low-gravity models expected for VL-G objects. However, PSO J237.1−23 does show a clear excess in flux relative to the models at all four *WISE* bands (⩾3.4 μm), implying the presence of a circumstellar disk.

Appendix A
Proper Motions of Known Low-mass Taurus Members

A.1. Pan-STARRS1 Proper Motions

We compiled a catalog of proper motions for low-mass members of Taurus using the Pan-STARRS1 3π (PS1) Survey, Processing Version 3.2 (PV3.2). Photometry and positions from PV3.2 were publically released as part of PS1 DR1 (K. Chambers et al. 2017, in preparation), with proper motions and parallaxes planned for a future PS1 release. PS1 astrometry includes Pan-STARRS1 observations from 2009 November to 2014 March, as well as detections

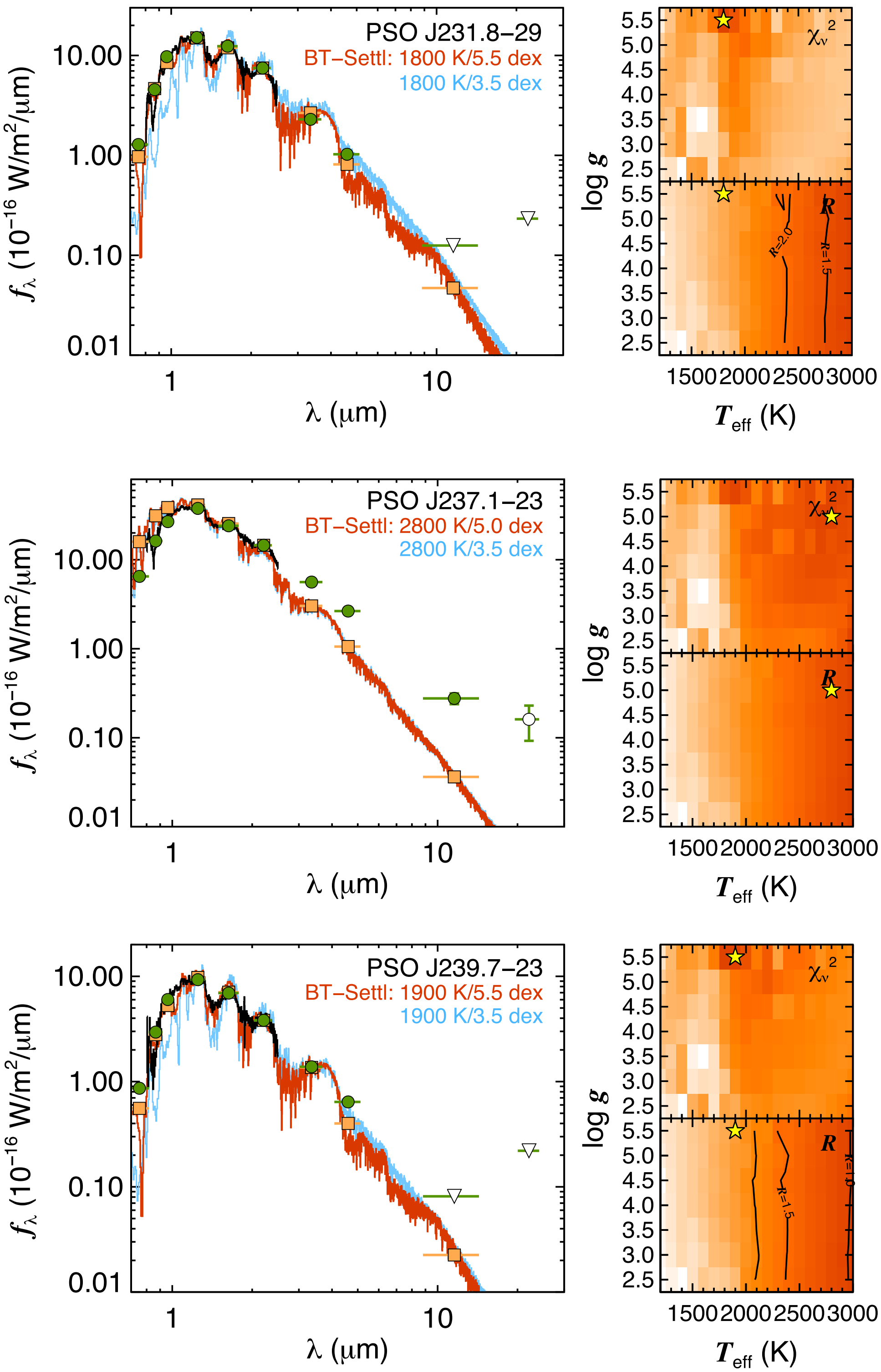

Figure 16. (Continued.)

from 2MASS (1997 October–2000 November) and *Gaia* DR1 (Epoch 2015.0; Gaia Collaboration et al. 2016; Lindegren et al. 2016) lying within 1″ of the mean PS1 position. PS1 astrometry, including proper motions, is calibrated to the *Gaia* DR1 reference frame.

A full description of the proper motion calculations can be found in E. Magnier et al. (2017, in preparation). Briefly, all PS1, 2MASS, and *Gaia* detections for an object were fit simultaneously for position, parallax, and proper motion using iteratively reweighted least squares regression with outlier clipping. Errors were estimated for each object using a bootstrapping approach, drawing random samples in a Monte Carlo fashion (allowing duplicates) from the set of detections not rejected in the astrometric fit.

Table 8
Proper Motions of Taurus Members

Name	Photometry			Proper Motion				
	i_{P1} (mag)	z_{P1} (mag)	y_{P1} (mag)	$\mu_\alpha \cos\delta$ (mas yr^{-1})	μ_δ (mas yr^{-1})	χ^2_ν	N_{ep}	Δt (years)
Reliable fits: $0.3 < \chi^2_\nu < 40$								
PSO J060.3200+25.9644	21.61 ± 0.04	20.06 ± 0.02	19.02 ± 0.02	19.0 ± 8.2	−38.1 ± 8.2	0.8	43	17.2
2MASS J04034997+2620382	16.27 ± 0.01	15.28 ± 0.01	14.73 ± 0.01	15.6 ± 6.3	−16.0 ± 5.3	14	62	15.1
2MASS J04064443+2540182	15.67 ± 0.01	14.68 ± 0.01	14.14 ± 0.01	12.4 ± 1.3	−15.5 ± 1.1	2.0	87	15.2
2MASS J04080782+2807280	15.19 ± 0.01	14.34 ± 0.01	13.91 ± 0.01	2.6 ± 1.5	−7.7 ± 1.5	3.5	91	17.2
2MASS J04102834+2051507	16.90 ± 0.01	15.87 ± 0.01	15.28 ± 0.01	−2.3 ± 2.6	−7.3 ± 1.0	1.7	69	17.2
2MASS J04105425+2501266	20.00 ± 0.03	19.74 ± 0.07	18.78 ± 0.04	9.2 ± 4.0	−15.7 ± 4.0	0.7	34	17.2
2MASS J04135328+2811233	20.37 ± 0.03	18.33 ± 0.01	16.93 ± 0.01	13.3 ± 9.9	−39.8 ± 12.3	22	45	17.2
2MASS J04135737+2918193	14.81 ± 0.08	14.79 ± 0.06	14.66 ± 0.01	5.9 ± 1.3	−26.4 ± 1.5	1.8	64	17.2
2MASS J04141760+2806096	15.14 ± 0.02	14.26 ± 0.02	13.64 ± 0.01	7.7 ± 3.8	−24.6 ± 2.8	14	67	17.2
2MASS J04142626+2806032	19.07 ± 0.05	17.21 ± 0.05	16.29 ± 0.03	8.1 ± 2.8	−18.4 ± 3.6	3.4	41	17.2
2MASS J04142639+2805597	16.51 ± 0.01	15.10 ± 0.01	14.17 ± 0.02	8.3 ± 2.9	−20.2 ± 2.6	4.3	63	17.2
2MASS J04143054+2805147	15.79 ± 0.03	14.63 ± 0.04	13.81 ± 0.04	11.8 ± 2.2	−19.5 ± 1.6	3.6	61	17.2
2MASS J04144158+2809583	⋯	20.76 ± 0.12	19.68 ± 0.05	−4.7 ± 5.9	−5.6 ± 5.7	0.4	15	15.9
2MASS J04151471+2800096	19.77 ± 0.01	18.07 ± 0.02	17.09 ± 0.01	15.5 ± 2.0	−24.3 ± 2.4	1.1	50	17.2
2MASS J04152409+2910434	17.90 ± 0.01	16.45 ± 0.01	15.59 ± 0.01	12.3 ± 1.8	−9.0 ± 1.8	4.3	60	17.2
2MASS J04153566+2847417	19.81 ± 0.02	18.62 ± 0.03	17.89 ± 0.01	8.1 ± 3.6	−29.6 ± 5.3	4.9	45	17.2
2MASS J04154131+2915078	16.09 ± 0.01	14.96 ± 0.01	14.34 ± 0.01	3.9 ± 3.1	−13.2 ± 2.6	6.1	59	17.2
2MASS J04154269+2909558	16.96 ± 0.01	15.50 ± 0.01	14.65 ± 0.01	13.9 ± 2.7	−1.5 ± 4.5	11	39	17.2
2MASS J04154807+2911331	20.61 ± 0.03	18.86 ± 0.01	17.84 ± 0.02	11.7 ± 3.5	−14.0 ± 3.5	0.7	35	17.2
2MASS J04155799+2746175	14.90 ± 0.01	13.83 ± 0.03	13.36 ± 0.03	9.9 ± 1.9	−23.2 ± 1.9	2.5	60	17.2
2MASS J04161210+2756385	15.50 ± 0.06	14.12 ± 0.01	13.55 ± 0.01	7.3 ± 2.1	−24.8 ± 1.4	1.4	71	17.2
2MASS J04161885+2752155	16.36 ± 0.01	15.09 ± 0.01	14.35 ± 0.01	5.0 ± 1.9	−24.2 ± 1.5	1.3	72	17.2
2MASS J04162725+2053091	14.96 ± 0.01	14.03 ± 0.01	13.50 ± 0.01	2.1 ± 1.2	−10.2 ± 1.3	1.8	98	17.2
2MASS J04163048+3037053	16.43 ± 0.01	15.53 ± 0.01	15.07 ± 0.01	6.6 ± 1.3	−6.2 ± 1.2	2.1	86	17.0
2MASS J04163911+2858491	16.42 ± 0.01	15.24 ± 0.01	14.45 ± 0.01	17.8 ± 3.7	−4.2 ± 5.4	17	56	17.2
2MASS J04181710+2828419	17.71 ± 0.01	16.14 ± 0.01	15.19 ± 0.01	16.2 ± 6.2	−19.1 ± 7.7	18	61	17.2
2MASS J04182909+2826191	⋯	⋯	19.55 ± 0.06	11.8 ± 11.1	−21.7 ± 4.8	1.4	13	15.9
2MASS J04183030+2743208	14.86 ± 0.01	⋯	13.33 ± 0.01	9.1 ± 1.7	−29.2 ± 2.4	2.2	48	17.2
2MASS J04183203+2831153	21.20 ± 0.07	19.38 ± 0.05	18.55 ± 0.12	11.0 ± 3.2	−19.3 ± 3.1	1.3	61	17.2
2MASS J04183444+2830302	⋯	19.80 ± 0.02	18.08 ± 0.03	9.9 ± 3.6	−22.7 ± 3.4	1.5	31	17.2
2MASS J04184023+2824245	21.16 ± 0.03	19.03 ± 0.03	17.44 ± 0.01	2.7 ± 5.9	−31.8 ± 4.9	8.6	54	17.2
2MASS J04184250+2818498	16.92 ± 0.01	15.52 ± 0.01	14.59 ± 0.01	8.2 ± 2.5	−13.1 ± 3.8	8.0	73	17.2
2MASS J04185115+2814332	17.75 ± 0.01	16.42 ± 0.01	15.65 ± 0.01	11.7 ± 4.5	−27.9 ± 2.9	4.3	87	17.2
2MASS J04185147+2820264	16.68 ± 0.03	15.54 ± 0.03	14.94 ± 0.02	2.3 ± 4.6	−6.0 ± 7.2	29	87	17.2
2MASS J04190126+2802487	20.96 ± 0.04	19.51 ± 0.01	18.46 ± 0.01	7.1 ± 5.6	−28.4 ± 5.3	1.2	53	17.2
2MASS J04190197+2822332	16.41 ± 0.01	15.02 ± 0.01	14.17 ± 0.01	−2.6 ± 3.8	−21.3 ± 4.9	23	83	17.2
2MASS J04194148+2716070	18.03 ± 0.04	17.33 ± 0.03	16.87 ± 0.03	29.0 ± 3.3	−19.3 ± 2.8	5.9	78	17.2
2MASS J04201611+2821325	17.25 ± 0.01	15.98 ± 0.01	15.26 ± 0.01	3.2 ± 4.3	−31.1 ± 6.1	12	73	17.2
2MASS J04202144+2813491	19.41 ± 0.02	18.54 ± 0.08	18.32 ± 0.02	−17.1 ± 14.9	5.2 ± 12.3	20	60	17.2
2MASS J04202555+2700355	16.39 ± 0.01	15.24 ± 0.01	14.58 ± 0.01	18.5 ± 3.5	−14.9 ± 1.1	7.3	82	17.2
2MASS J04202583+2819237	18.37 ± 0.01	17.09 ± 0.05	16.60 ± 0.03	25.2 ± 7.2	−36.6 ± 15.7	35	77	17.2
2MASS J04210795+2702204	18.21 ± 0.01	15.70 ± 0.01	14.89 ± 0.07	11.5 ± 8.0	−7.0 ± 3.3	11	69	17.2
2MASS J04213459+2701388	15.74 ± 0.01	14.47 ± 0.01	13.75 ± 0.01	8.1 ± 3.2	−13.5 ± 2.7	3.1	64	17.2
2MASS J04213965+2649143	16.27 ± 0.01	15.05 ± 0.01	14.35 ± 0.01	14.7 ± 2.7	−13.2 ± 5.1	5.5	68	17.2
2MASS J04214013+2814224	14.84 ± 0.01	13.86 ± 0.01	13.34 ± 0.01	13.5 ± 2.1	−25.3 ± 3.9	7.0	84	17.2
2MASS J04214631+2659296	18.11 ± 0.01	16.70 ± 0.01	15.84 ± 0.01	12.1 ± 1.6	−18.5 ± 1.8	1.2	73	17.2
2MASS J04215450+2652315	20.78 ± 0.02	18.87 ± 0.01	17.78 ± 0.02	12.0 ± 3.5	−9.5 ± 3.5	1.2	57	17.2
2MASS J04215482+2642372	15.34 ± 0.01	14.36 ± 0.01	13.84 ± 0.01	19.2 ± 7.8	−15.9 ± 3.3	6.4	63	17.2
2MASS J04215851+1520145	15.69 ± 0.01	15.05 ± 0.02	14.59 ± 0.01	−2.2 ± 3.6	2.2 ± 3.0	5.6	69	17.2
2MASS J04220069+2657324	18.50 ± 0.04	17.90 ± 0.02	17.12 ± 0.11	−11.3 ± 7.4	−12.8 ± 5.4	7.0	52	17.2
2MASS J04221332+1934392	16.93 ± 0.01	15.52 ± 0.01	14.70 ± 0.01	8.7 ± 2.1	−8.8 ± 1.7	1.6	90	17.2
2MASS J04221568+2657060	16.26 ± 0.01	15.85 ± 0.01	15.48 ± 0.01	10.6 ± 4.0	−4.0 ± 5.2	4.6	74	17.2
2MASS J04221644+2549118	17.07 ± 0.01	15.61 ± 0.01	14.85 ± 0.01	15.9 ± 2.6	−22.4 ± 1.3	2.1	79	17.2
2MASS J04221675+2654570	15.13 ± 0.07	⋯	14.14 ± 0.03	12.7 ± 2.1	−14.6 ± 3.3	13	79	17.2
2MASS J04223075+1526310	18.11 ± 0.01	16.85 ± 0.01	16.12 ± 0.01	1.3 ± 1.8	−3.5 ± 1.7	0.8	62	17.1
2MASS J04224786+2645530	15.36 ± 0.02	14.74 ± 0.13	14.27 ± 0.12	12.2 ± 1.9	−16.7 ± 1.4	1.6	54	17.2
2MASS J04230607+2801194	15.55 ± 0.01	14.45 ± 0.01	13.81 ± 0.01	11.5 ± 1.0	−25.2 ± 2.1	3.5	64	17.2
2MASS J04230776+2805573	16.34 ± 0.03	15.37 ± 0.01	15.04 ± 0.07	9.8 ± 1.2	−26.2 ± 2.0	1.8	78	17.2
2MASS J04231822+2641156	17.57 ± 0.01	16.10 ± 0.01	15.16 ± 0.01	14.9 ± 1.7	−13.1 ± 2.0	1.9	53	17.2
2MASS J04233539+2503026	14.76 ± 0.01	13.43 ± 0.01	12.64 ± 0.02	11.2 ± 4.2	−15.3 ± 4.8	23	69	17.2

Table 8
(Continued)

Name	Photometry			Proper Motion				
	i_{P1} (mag)	z_{P1} (mag)	y_{P1} (mag)	$\mu_\alpha \cos\delta$ (mas yr^{-1})	μ_δ (mas yr^{-1})	χ^2_ν	N_{ep}	Δt (years)
2MASS J04233573+2502596	20.19 ± 0.02	18.40 ± 0.02	17.21 ± 0.01	1.4 ± 5.9	−31.9 ± 5.5	4.0	34	17.2
2MASS J04242090+2630511	16.99 ± 0.01	15.75 ± 0.01	15.07 ± 0.01	12.0 ± 3.1	−25.9 ± 1.4	2.2	47	17.1
2MASS J04242646+2649503	16.28 ± 0.01	15.15 ± 0.01	14.50 ± 0.01	10.9 ± 1.4	−18.3 ± 1.3	1.2	64	17.1
2MASS J04245021+2641006	15.60 ± 0.01	14.51 ± 0.01	13.94 ± 0.01	9.3 ± 1.5	−13.4 ± 1.6	1.7	65	17.2
2MASS J04251550+2829275	14.64 ± 0.01	13.48 ± 0.01	12.84 ± 0.01	10.2 ± 1.5	−23.6 ± 1.3	1.5	72	17.2
2MASS J04262939+2624137	17.02 ± 0.01	15.83 ± 0.01	15.08 ± 0.01	6.2 ± 2.5	−14.8 ± 1.6	3.1	74	17.1
2MASS J04263055+2443558	19.51 ± 0.02	17.70 ± 0.01	16.67 ± 0.01	10.2 ± 3.1	−15.3 ± 4.1	2.5	56	17.1
2MASS J04264449+2756433	15.89 ± 0.01	14.77 ± 0.01	14.17 ± 0.01	4.5 ± 2.0	−30.4 ± 3.7	7.9	102	17.2
2MASS J04265732+2606284	14.95 ± 0.01	13.80 ± 0.01	13.09 ± 0.01	−1.6 ± 2.1	−16.3 ± 1.9	4.8	79	17.1
2MASS J04270266+2605304	20.03 ± 0.04	19.06 ± 0.03	18.41 ± 0.03	3.9 ± 10.5	−27.0 ± 11.5	8.1	47	16.0
2MASS J04270739+2215037	15.49 ± 0.01	14.39 ± 0.01	13.79 ± 0.01	7.9 ± 1.3	−15.3 ± 1.4	1.0	73	17.2
2MASS J04272799+2612052	20.34 ± 0.02	18.58 ± 0.03	17.57 ± 0.01	−0.9 ± 2.5	−25.6 ± 2.5	1.8	59	17.2
2MASS J04274538+2357243	19.27 ± 0.01	17.75 ± 0.01	16.84 ± 0.01	9.3 ± 2.9	−12.6 ± 2.7	3.5	62	17.2
2MASS J04275730+2619183	17.60 ± 0.08	16.66 ± 0.04	15.94 ± 0.04	−6.4 ± 5.4	8.1 ± 5.9	21	73	17.2
2MASS J04284199+1533535	15.46 ± 0.01	14.63 ± 0.01	14.20 ± 0.01	1.1 ± 1.3	−15.1 ± 1.6	1.9	68	17.2
2MASS J04284263+2714039	15.33 ± 0.01	14.45 ± 0.01	13.85 ± 0.01	2.5 ± 1.3	−15.7 ± 3.1	5.8	71	17.2
2MASS J04285053+1844361	14.65 ± 0.01	13.46 ± 0.01	12.70 ± 0.01	9.3 ± 2.9	−9.0 ± 3.8	11	89	17.2
2MASS J04290068+2755033	17.99 ± 0.01	16.55 ± 0.01	15.72 ± 0.01	8.7 ± 1.9	−25.2 ± 1.7	1.8	57	17.2
2MASS J04290498+2649073	18.01 ± 0.01	17.14 ± 0.02	16.64 ± 0.02	12.2 ± 5.5	−9.4 ± 6.2	2.8	69	17.2
2MASS J04292165+2701259	15.67 ± 0.01	14.18 ± 0.01	13.17 ± 0.02	3.9 ± 1.5	−18.9 ± 1.5	1.8	83	17.2
2MASS J04293008+2439550	18.71 ± 0.04	17.92 ± 0.10	16.92 ± 0.12	18.9 ± 3.3	−29.4 ± 3.6	13	71	17.1
2MASS J04294568+2630468	16.31 ± 0.01	15.05 ± 0.01	14.29 ± 0.01	7.4 ± 1.2	−23.0 ± 1.4	1.6	65	17.2
2MASS J04295422+1754041	15.98 ± 0.03	15.18 ± 0.05	14.46 ± 0.11	8.8 ± 4.0	−19.5 ± 2.8	3.1	70	17.2
2MASS J04295950+2433078	16.00 ± 0.07	14.51 ± 0.01	14.01 ± 0.03	10.0 ± 1.6	−15.5 ± 2.3	1.8	66	17.1
2MASS J04300724+2608207	19.24 ± 0.01	17.70 ± 0.01	16.78 ± 0.01	4.4 ± 1.6	−19.4 ± 1.8	1.3	63	17.2
2MASS J04302365+2359129	19.25 ± 0.01	17.70 ± 0.01	16.79 ± 0.01	1.2 ± 2.4	−16.3 ± 2.2	1.6	55	17.2
2MASS J04305171+2441475	16.63 ± 0.01	15.71 ± 0.01	15.11 ± 0.04	1.8 ± 5.2	−16.5 ± 2.5	11	74	17.1
2MASS J04305718+2556394	18.55 ± 0.01	17.10 ± 0.01	16.28 ± 0.01	12.6 ± 1.6	−21.4 ± 1.9	1.4	71	17.2
2MASS J04311907+2335047	17.86 ± 0.01	16.35 ± 0.01	15.47 ± 0.01	6.4 ± 2.2	−9.8 ± 2.0	1.4	58	15.2
2MASS J04312405+1800215	15.46 ± 0.01	14.18 ± 0.01	13.39 ± 0.01	13.9 ± 4.3	−8.8 ± 3.6	4.7	62	15.2
2MASS J04312669+2703188	19.25 ± 0.01	17.69 ± 0.02	16.77 ± 0.01	16.7 ± 2.8	−17.3 ± 1.6	0.6	42	17.2
2MASS J04313407+1808049	19.56 ± 0.03	18.37 ± 0.14	17.27 ± 0.03	−79.0 ± 25.7	−28.5 ± 12.6	39	36	15.2
2MASS J04313613+1813432	16.81 ± 0.02	16.19 ± 0.03	15.57 ± 0.03	21.5 ± 6.9	−18.2 ± 6.8	22	57	15.2
2MASS J04313747+1812244	17.71 ± 0.10	17.36 ± 0.03	17.07 ± 0.10	14.8 ± 5.7	−22.6 ± 7.5	27	64	15.2
2MASS J04314644+2506236	15.13 ± 0.01	14.13 ± 0.01	13.57 ± 0.01	11.3 ± 1.5	−27.8 ± 1.4	1.9	50	17.2
2MASS J04315968+1821305	16.10 ± 0.02	15.08 ± 0.15	14.05 ± 0.07	5.2 ± 6.7	−23.1 ± 3.4	13	80	14.2
2MASS J04320329+2528078	15.07 ± 0.01	13.91 ± 0.01	13.28 ± 0.01	2.8 ± 2.0	−17.9 ± 2.5	3.4	44	17.1
2MASS J04321540+2428597	14.69 ± 0.02	13.32 ± 0.09	12.59 ± 0.04	14.2 ± 4.6	−8.3 ± 6.1	13	69	17.1
2MASS J04321786+2422149	15.13 ± 0.01	13.93 ± 0.01	13.23 ± 0.01	−1.0 ± 3.2	−16.9 ± 2.6	12	76	17.2
2MASS J04322210+1827426	14.61 ± 0.01	13.69 ± 0.01	13.20 ± 0.01	16.3 ± 1.8	−20.3 ± 1.8	3.4	81	14.3
2MASS J04322329+2403013	16.29 ± 0.02	14.85 ± 0.01	14.08 ± 0.01	6.6 ± 2.4	−18.8 ± 2.2	1.9	69	17.2
2MASS J04322415+2251083	14.55 ± 0.01	13.64 ± 0.01	13.11 ± 0.01	10.8 ± 1.6	−19.9 ± 1.6	1.0	58	14.3
2MASS J04323205+2257266	⋯	20.05 ± 0.11	19.08 ± 0.07	13.5 ± 5.1	−7.1 ± 5.2	3.7	18	13.3
2MASS J04324938+2253082	15.37 ± 0.16	13.89 ± 0.01	13.16 ± 0.01	18.8 ± 6.3	−18.8 ± 4.1	29	78	14.3
2MASS J04325026+2422115	20.85 ± 0.03	18.56 ± 0.02	17.12 ± 0.02	1.8 ± 2.9	−18.1 ± 2.7	1.2	41	17.2
2MASS J04325119+1730092	19.08 ± 0.02	17.43 ± 0.01	16.53 ± 0.01	12.6 ± 1.7	−20.8 ± 1.6	0.7	61	17.3
2MASS J04330197+2421000	14.56 ± 0.01	13.32 ± 0.01	12.60 ± 0.01	4.9 ± 1.8	−19.1 ± 2.1	2.4	51	17.2
2MASS J04330781+2616066	16.40 ± 0.01	14.89 ± 0.01	14.00 ± 0.01	9.0 ± 1.8	−16.0 ± 1.5	2.3	74	17.2
2MASS J04330945+2246487	17.51 ± 0.02	15.98 ± 0.01	15.20 ± 0.01	−0.6 ± 3.3	−16.8 ± 1.5	2.3	67	16.2
2MASS J04331435+2614235	18.61 ± 0.01	17.52 ± 0.02	16.88 ± 0.01	9.7 ± 4.3	−10.4 ± 4.1	3.5	61	17.2
2MASS J04331907+2246342	15.71 ± 0.04	14.64 ± 0.01	13.89 ± 0.05	7.0 ± 2.4	−18.7 ± 1.9	3.2	74	16.2
2MASS J04332621+2245293	15.93 ± 0.01	14.70 ± 0.01	13.93 ± 0.01	8.0 ± 2.9	−12.4 ± 2.2	3.9	69	16.2
2MASS J04332789+1758436	17.90 ± 0.03	17.19 ± 0.03	16.40 ± 0.07	11.5 ± 1.6	−14.9 ± 1.6	0.7	76	17.3
2MASS J04333905+2227207	16.04 ± 0.01	15.53 ± 0.02	15.10 ± 0.01	6.3 ± 1.9	−10.3 ± 4.8	4.3	77	16.2
2MASS J04334291+2526470	19.29 ± 0.01	17.61 ± 0.01	16.61 ± 0.01	6.0 ± 2.2	−24.5 ± 3.0	1.3	43	17.2
2MASS J04334465+2615005	15.98 ± 0.02	14.92 ± 0.05	13.82 ± 0.03	1.8 ± 2.9	−17.1 ± 2.7	6.4	104	17.2
2MASS J04335245+2612548	20.78 ± 0.02	19.03 ± 0.02	17.93 ± 0.02	9.0 ± 3.6	−15.9 ± 3.5	1.0	73	17.2
2MASS J04340619+2418508	17.99 ± 0.01	16.57 ± 0.01	15.75 ± 0.01	8.1 ± 2.9	−19.9 ± 2.0	3.2	53	17.2
2MASS J04341527+2250309	18.78 ± 0.01	17.09 ± 0.01	16.09 ± 0.01	17.5 ± 9.3	−12.4 ± 2.8	13	45	16.2
2MASS J04344544+2308027	16.14 ± 0.01	15.03 ± 0.01	14.40 ± 0.01	9.7 ± 1.2	−16.1 ± 1.2	1.4	82	16.3
2MASS J04345973+2807017	19.39 ± 0.02	18.22 ± 0.01	17.48 ± 0.01	7.0 ± 3.5	−15.6 ± 3.2	0.8	37	17.1
2MASS J04350850+2311398	15.73 ± 0.01	14.63 ± 0.01	14.01 ± 0.01	9.4 ± 1.3	−19.8 ± 1.1	1.2	89	16.3

Table 8
(Continued)

Name	Photometry			Proper Motion				
	i_{P1} (mag)	z_{P1} (mag)	y_{P1} (mag)	$\mu_\alpha \cos\delta$ (mas yr^{-1})	μ_δ (mas yr^{-1})	χ^2_ν	N_{ep}	Δt (years)
2MASS J04354093+2411087	14.85 ± 0.02	14.12 ± 0.04	13.29 ± 0.03	10.9 ± 4.4	−7.7 ± 6.2	16	74	17.2
2MASS J04354183+2234115	16.26 ± 0.01	15.15 ± 0.01	14.50 ± 0.01	9.6 ± 1.3	−16.1 ± 1.5	1.6	88	16.3
2MASS J04354203+2252226	14.68 ± 0.01	13.59 ± 0.01	13.00 ± 0.01	8.4 ± 1.9	−13.0 ± 1.6	1.6	71	16.3
2MASS J04354526+2737130	19.65 ± 0.01	17.94 ± 0.01	16.99 ± 0.01	8.7 ± 4.3	−24.7 ± 1.7	2.0	57	15.2
2MASS J04355143+2249119	20.23 ± 0.01	18.55 ± 0.01	17.53 ± 0.02	20.7 ± 6.4	−14.3 ± 2.5	2.7	59	16.3
2MASS J04355209+2255039	14.78 ± 0.01	13.74 ± 0.01	13.14 ± 0.01	5.9 ± 1.9	−4.4 ± 2.2	3.2	71	16.3
2MASS J04355760+2253574	18.57 ± 0.01	17.55 ± 0.01	17.00 ± 0.02	20.0 ± 5.4	−12.6 ± 2.3	4.6	69	16.3
2MASS J04355949+2238291	17.21 ± 0.03	16.73 ± 0.02	16.25 ± 0.01	13.8 ± 3.2	−14.0 ± 3.8	4.8	89	16.3
2MASS J04361030+2159364	19.19 ± 0.01	17.65 ± 0.02	16.71 ± 0.01	7.7 ± 2.8	−21.9 ± 2.9	3.8	70	16.3
2MASS J04361038+2259560	18.33 ± 0.01	16.79 ± 0.01	15.84 ± 0.01	12.6 ± 3.1	−15.1 ± 2.4	3.1	64	16.3
2MASS J04362151+2351165	16.02 ± 0.01	15.05 ± 0.01	14.55 ± 0.01	−0.4 ± 1.2	−16.7 ± 1.5	2.7	54	16.3
2MASS J04363248+2421395	15.57 ± 0.01	14.24 ± 0.01	13.41 ± 0.01	12.3 ± 1.9	−10.0 ± 1.4	1.6	58	14.3
2MASS J04363893+2258119	18.02 ± 0.01	16.48 ± 0.01	15.55 ± 0.01	13.3 ± 5.7	−24.9 ± 6.7	32	62	16.3
2MASS J04373705+2331080	⋯	20.75 ± 0.03	19.67 ± 0.10	15.9 ± 13.5	−54.8 ± 13.4	0.6	16	15.0
2MASS J04374333+3056563	15.99 ± 0.01	15.09 ± 0.01	14.56 ± 0.01	6.4 ± 3.6	−10.6 ± 2.0	6.5	81	15.1
2MASS J04375670+2546229	17.21 ± 0.06	16.46 ± 0.07	16.00 ± 0.06	−4.6 ± 1.6	7.6 ± 3.4	4.9	62	16.2
2MASS J04380083+2558572	15.79 ± 0.01	14.34 ± 0.01	13.49 ± 0.01	−9.0 ± 5.3	−35.6 ± 7.5	15	77	16.2
2MASS J04380191+2519266	16.87 ± 0.01	16.07 ± 0.02	15.57 ± 0.01	29.6 ± 10.0	−45.3 ± 23.5	35	78	16.2
2MASS J04381486+2611399	18.98 ± 0.01	17.66 ± 0.01	16.92 ± 0.01	9.5 ± 2.8	−17.0 ± 4.6	4.6	77	16.2
2MASS J04381630+2326402	14.50 ± 0.01	13.65 ± 0.01	13.18 ± 0.01	8.6 ± 2.9	−16.2 ± 1.7	3.9	69	16.2
2MASS J04382134+2609137	⋯	14.88 ± 0.07	13.82 ± 0.01	21.8 ± 2.9	−17.1 ± 3.1	5.7	54	16.2
2MASS J04384725+1737260	15.57 ± 0.01	14.67 ± 0.01	14.19 ± 0.01	6.0 ± 1.5	−19.7 ± 1.8	1.9	76	17.2
2MASS J04385859+2336351	14.99 ± 0.01	14.00 ± 0.01	13.44 ± 0.01	11.1 ± 1.5	−20.3 ± 2.7	1.8	62	16.3
2MASS J04385871+2323595	15.60 ± 0.01	14.53 ± 0.01	13.94 ± 0.01	5.3 ± 1.7	−20.0 ± 2.0	1.6	70	16.3
2MASS J04390396+2544264	16.74 ± 0.02	15.29 ± 0.01	14.47 ± 0.01	5.2 ± 2.2	−25.9 ± 2.7	4.5	66	16.3
2MASS J04390525+2337450	14.92 ± 0.02	14.57 ± 0.01	14.66 ± 0.02	31.8 ± 16.2	−31.5 ± 5.6	11	77	16.3
2MASS J04390637+2334179	15.20 ± 0.01	14.11 ± 0.01	13.51 ± 0.01	4.5 ± 1.2	−20.4 ± 1.2	1.3	67	16.3
2MASS J04394748+2601407	17.54 ± 0.02	15.79 ± 0.01	14.68 ± 0.01	3.5 ± 2.1	−11.1 ± 4.0	4.7	56	16.3
2MASS J04400067+2358211	15.70 ± 0.01	14.57 ± 0.01	13.95 ± 0.01	−7.8 ± 4.0	−37.2 ± 4.6	8.7	64	16.3
2MASS J04400174+2556292	18.99 ± 0.01	17.25 ± 0.01	16.08 ± 0.02	2.3 ± 3.9	3.9 ± 10.1	15	46	16.3
2MASS J04400800+2605253	18.34 ± 0.01	16.66 ± 0.01	15.68 ± 0.01	−2.2 ± 2.6	−11.4 ± 2.8	2.1	47	16.3
2MASS J04403979+2519061	15.89 ± 0.01	14.59 ± 0.01	13.81 ± 0.01	−0.1 ± 5.8	−8.2 ± 9.8	17	89	16.3
2MASS J04410826+2556074	16.98 ± 0.02	16.25 ± 0.03	15.86 ± 0.04	4.9 ± 4.5	−16.2 ± 6.6	19	69	16.3
2MASS J04411078+2555116	17.90 ± 0.07	16.31 ± 0.07	15.57 ± 0.04	−11.8 ± 7.4	−25.9 ± 4.1	20	68	16.3
2MASS J04413882+2556267	15.09 ± 0.02	14.21 ± 0.02	13.46 ± 0.05	0.0 ± 5.5	−27.4 ± 4.2	23	79	16.3
2MASS J04414489+2301513	18.37 ± 0.01	16.96 ± 0.01	16.10 ± 0.01	6.9 ± 2.2	−19.9 ± 1.5	1.4	59	16.2
2MASS J04414825+2534304	17.81 ± 0.02	16.82 ± 0.01	15.77 ± 0.02	10.9 ± 2.4	−16.6 ± 2.7	3.6	69	16.3
2MASS J04422101+2520343	14.61 ± 0.01	13.60 ± 0.01	13.03 ± 0.01	4.6 ± 2.2	−18.3 ± 2.0	16	64	16.3
2MASS J04440164+1621324	16.64 ± 0.01	15.52 ± 0.01	14.89 ± 0.01	11.3 ± 2.0	−21.0 ± 2.3	5.3	85	17.2
2MASS J04442713+2512164	14.95 ± 0.03	13.91 ± 0.08	13.53 ± 0.04	4.2 ± 1.7	−15.3 ± 1.5	2.6	84	16.2
2MASS J04480632+1551251	17.47 ± 0.01	16.31 ± 0.01	15.59 ± 0.01	13.8 ± 2.0	−19.0 ± 1.2	3.4	71	17.2
2MASS J04484189+1703374	17.09 ± 0.01	15.84 ± 0.01	15.13 ± 0.01	3.8 ± 1.8	−14.8 ± 2.0	3.5	76	17.2
2MASS J04485745+2913521	14.97 ± 0.01	13.94 ± 0.01	13.38 ± 0.01	12.9 ± 6.1	−17.5 ± 6.3	21	71	17.1
2MASS J04485789+2913548	16.59 ± 0.01	15.73 ± 0.04	15.31 ± 0.01	8.7 ± 6.5	−24.0 ± 6.3	19	70	17.1
2MASS J04520668+3047175	19.42 ± 0.02	18.21 ± 0.03	17.31 ± 0.01	9.2 ± 2.6	−31.6 ± 1.9	3.9	65	17.0
2MASS J04520970+3037454	16.02 ± 0.03	15.40 ± 0.05	15.02 ± 0.10	1.9 ± 1.3	−29.8 ± 2.0	3.0	82	17.0
2MASS J04552333+3027366	16.55 ± 0.01	15.38 ± 0.01	14.70 ± 0.01	−6.1 ± 4.5	−23.6 ± 1.8	6.5	71	17.0
2MASS J04554046+3039057	15.63 ± 0.01	14.70 ± 0.01	14.19 ± 0.01	5.0 ± 1.6	−22.9 ± 1.5	2.7	73	17.0
2MASS J04554801+3028050	16.45 ± 0.01	15.37 ± 0.01	14.74 ± 0.01	4.2 ± 4.0	−22.9 ± 2.4	3.1	69	17.0
2MASS J04554969+3019400	15.93 ± 0.01	14.88 ± 0.01	14.29 ± 0.01	5.8 ± 1.7	−22.5 ± 1.4	1.8	49	17.0
2MASS J04555288+3006523	14.51 ± 0.01	13.61 ± 0.01	13.07 ± 0.01	10.8 ± 2.1	−8.7 ± 1.1	1.8	53	16.9
2MASS J04555636+3049374	14.79 ± 0.01	13.88 ± 0.01	13.40 ± 0.01	5.9 ± 0.9	−23.6 ± 2.1	4.6	77	17.0
2MASS J04574903+3015195	20.54 ± 0.03	18.82 ± 0.02	17.80 ± 0.01	−5.2 ± 4.1	−24.1 ± 4.0	0.9	48	17.0
2MASS J04591661+2840468	18.14 ± 0.01	17.54 ± 0.08	17.56 ± 0.02	3.1 ± 3.3	3.1 ± 2.3	1.1	48	17.0
2MASS J05052286+2531312	14.86 ± 0.12	13.71 ± 0.07	13.40 ± 0.08	−0.2 ± 2.8	−17.9 ± 4.7	21	79	14.9
2MASS J05064662+2104296	14.90 ± 0.01	13.95 ± 0.01	13.44 ± 0.01	8.6 ± 2.3	−18.2 ± 2.2	4.3	53	17.1
2MASS J05073903+2311068	14.75 ± 0.01	14.08 ± 0.01	13.55 ± 0.01	6.5 ± 1.7	−17.4 ± 3.2	3.6	36	17.2
PSO J077.1033+24.3809	21.62 ± 0.10	20.18 ± 0.05	19.21 ± 0.06	14.1 ± 12.5	−27.1 ± 12.1	0.6	27	16.0
Unreliable fits: $\chi^2_\nu \leqslant 0.3$ or $\chi^2_\nu \geqslant 40$								
2MASS J04141188+2811535	16.76 ± 0.05	15.78 ± 0.03	14.99 ± 0.01	11.8 ± 5.5	−25.0 ± 19.5	81	53	17.2

Table 8
(Continued)

Name	Photometry			Proper Motion				
	i_{P1} (mag)	z_{P1} (mag)	y_{P1} (mag)	$\mu_\alpha \cos\delta$ (mas yr^{-1})	μ_δ (mas yr^{-1})	χ^2_ν	N_{ep}	Δt (years)
2MASS J04174955+2813318	15.70 ± 0.02	15.00 ± 0.01	14.47 ± 0.01	−6.0 ± 4.4	−3.3 ± 12.2	59	90	17.2
2MASS J04180796+2826036	15.14 ± 0.01	13.91 ± 0.01	13.21 ± 0.01	15.0 ± 3.9	1.1 ± 12.1	51	87	17.2
2MASS J04185813+2812234	17.16 ± 0.02	16.04 ± 0.08	15.40 ± 0.06	25.4 ± 6.3	−81.7 ± 36.5	61	97	17.2
2MASS J04292373+2433002	15.51 ± 0.04	14.93 ± 0.10	14.41 ± 0.14	−23.6 ± 14.6	68.5 ± 27.1	66	71	17.1
WISE J043835.50+261041.9	16.20 ± 0.04	15.69 ± 0.07	15.12 ± 0.02	2.2 ± 6.1	−21.7 ± 7.0	44	65	5.1[a]
2MASS J04391389+2553208	…	…	19.75 ± 0.14	−2.0 ± 462.7	−5.4 ± 65.0	0.2	7	15.0

Notes. The objects in this table are taken from the catalog of Esplin et al. (2014), except for PSO J060.3200+25.9644 and PSO J077.1033+24.3809, which are new discoveries presented in this paper. We adopt a photometric precision floor of 0.01 mag for the PS1 photometry, following the analysis of Schlafly et al. (2012). The errors reported in the PS1 database are formal errors that do not include systematics and are often smaller.
[a] This object does not have a 2MASS detection.

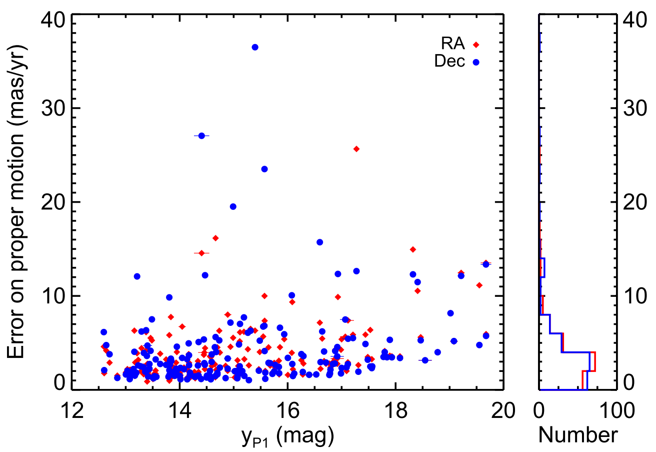

Figure 17. Errors on our $\mu_\alpha \cos\delta$ (red diamonds) and μ_δ (blue dots) as a function of y_{P1} for known Taurus members that are not saturated in PS1. The histogram on the right shows the distributions of the errors. Most errors are $\lesssim$5 mas yr^{-1}.

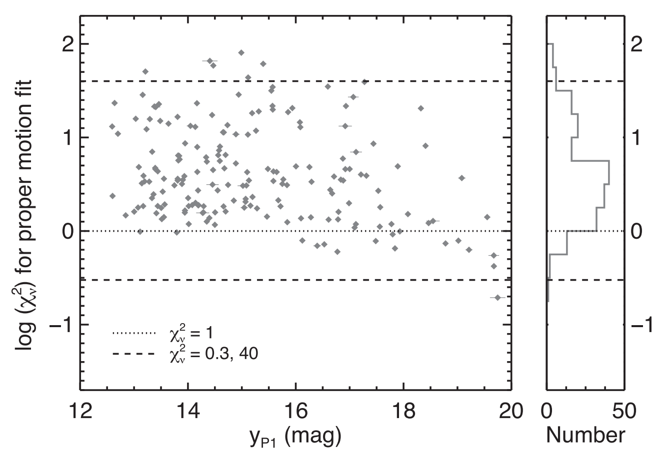

Figure 18. Reduced χ^2 for our proper motions as a function of y_{P1} for known Taurus members that are not saturated in PS1. The histogram on the right shows the distribution of χ^2_ν. The two dashed lines mark $\chi^2_\nu = 0.3$ and $\chi^2_\nu = 40$, values between which we regard our proper motion fits and errors as reliable (Figure 19). The dotted line marks $\chi^2_\nu = 1$. The fact that most of the fits have $\chi^2_\nu > 1$ suggests that our estimates for the PS1 astrometric errors are small compared to the scatter in positions between epochs.

A.2. Catalog

To create our catalog, we began with the list of 414 Taurus members from Esplin et al. (2014). Using the 2MASS positions (or *WISE* positions for the seven objects with no 2MASS detection), we cross-matched this list with the PS1 database using a 3″ matching radius and found 363 matches with a proper motion measured by PS1. We supplemented these matches with our two Taurus discoveries presented in the paper. We verified that none of the PS1 sources were identified as quasars, transients, periodic variables, or solar system objects in the PS1 database and we excluded any objects with poor PSF fits (`psf_qf` < 0.85). To avoid saturation in PS1 we also excluded objects having $i_{P1} < 14.5$ mag or $y_{P1} < 12.5$ mag (corresponding roughly to a spectral type of M3–M4). This left us with 187 members of Taurus having proper motions measured by PS1. Almost every object in the catalog of Esplin et al. (2014) was detected by 2MASS, so the PS1 proper motions have time baselines of ≈14–17 years. Our catalog includes 27 objects with no previously published proper motion and 93 measurements that improve on the best available literature values drawn from NOMAD (Zacharias et al. 2005), PPMXL (Roeser et al. 2010), SDSS DR9 (Ahn et al. 2012), UCAC4 (Zacharias et al. 2013), UKIDSS GCS DR9 (Lawrence et al. 2013), URAT1 (Finch & Zacharias 2016), USNO-B (Monet et al. 2003), and Riaz et al. (2013). It is the largest catalog to date for proper motions of low-mass (spectral types $\gtrsim$M3) members of Taurus.

We list our proper motions in Table 8, along with the i_{P1} and y_{P1} photometry, the number of epochs used, the reduced χ^2, and the time baseline for each proper motion fit. We adopt a photometric precision floor of 0.01 mag for the PS1 photometry, following the analysis of Schlafly et al. (2012). The errors reported in the PS1 database are formal errors that do not include systematics and are often smaller than 0.01 mag. We do not report photometry with errors larger than 0.2 mag. Figure 17 shows the proper motion errors as a function of the y_{P1} magnitude of each source and indicates that most of the errors are $\lesssim$5 mas yr^{-1}.

In Figure 18, we plot the reduced χ^2 for the proper motion fits as a function of y_{P1}. Most of our proper motion fits have $\chi^2_\nu > 1$, suggesting that the astrometric uncertainties of the individual PS1 epochs are small compared to the scatter in R.A. and decl. of the epochs. The proper motion errors may therefore be underestimated (by a factor of ≈2).

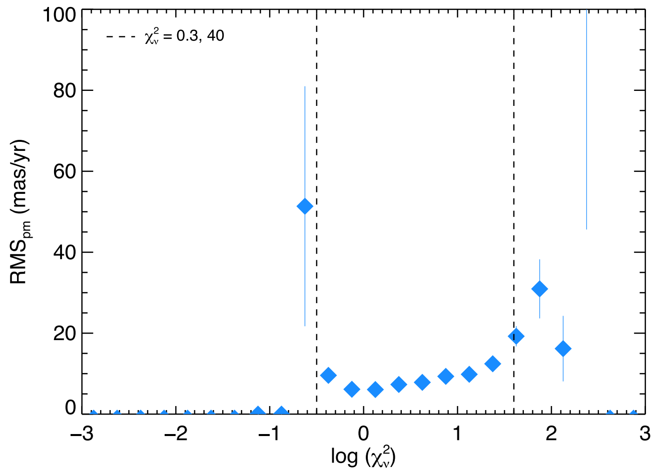

Figure 19. rms of PS1 proper motions of well-detected objects in a 0.5 deg^2 patch of sky near Taurus, for bins of 0.25 in $\log(\chi^2_\nu)$. More than 97% of the proper motions in this patch of sky are less than 50 mas yr^{-1}. The low rms for proper motions with $-0.5 < \log(\chi^2_\nu) < 1.6$ (between the vertical dashed black lines), i.e., $0.3 < \chi^2_\nu < 40$, implies that those proper motion measurements are reliable, while measurements with larger or smaller χ^2_ν are less reliable.

To assess the reliability of our proper motions, we calculated proper motions and χ^2_ν for objects in a 0.5 deg^2 patch of sky near Taurus ($80° < \alpha < 81°$, $5\overset{\circ}{.}5 < \delta < 6\overset{\circ}{.}0$), in which more than 97% of objects have proper motions less than 50 mas yr^{-1}. We used all 8962 objects in this patch meeting the same criteria as our Taurus catalog and also having $y_{\rm P1} < 19.75$ mag to match the faintness limit of our Taurus catalog. Because the proper motions of this sample are small, the rms of the proper motions gives us an estimate of the quality of the measurements. Figure 19 shows that proper motions measurements with $0.3 < \chi^2_\nu < 40$ had rms ≈5–15 mas yr^{-1}, while proper motions with larger or smaller χ^2_ν had significantly greater spread. We therefore adopted these χ^2_ν values as the limits between which we regard our proper motions as reliable measurements. Table 8 separates our Taurus proper motions into those we regard as reliable (all but five of the objects) and unreliable. We report all of our proper motions for completeness, but when $\chi^2_\nu \leqslant 0.3$ or $\chi^2_\nu \geqslant 40$ the proper motions should be treated with caution.

Using the reliable proper motions and inverse variance weighting, we calculate a weighted mean proper motion for Taurus of ($\mu_\alpha \cos\delta = 7.6 \pm 0.2$, $\mu_\delta = -17.4 \pm 0.2$ mas yr^{-1}), with a weighted rms of 4.9 mas yr^{-1} in R.A. and 6.4 mas yr^{-1} in decl. We compare this to the catalog of brighter Taurus members compiled by Ducourant et al. (2005, hereinafter D05), whose proper motions were similarly calculated using optical and 2MASS data and whose time baselines range from 10 to more than 100 years. Using the proper motions from the full D05 Taurus catalog, we calculate a weighted mean proper motion of (7.9 ± 1.1, -20.5 ± 1.0 mas yr^{-1}). We note a ≈3 mas yr^{-1} discrepancy with the mean proper motion for our Taurus list, which is likely due to differences in the astrometric reference frames used for the two samples. The Pan-STARRS1 PV3.2 astrometry is tied to the *Gaia* DR1 reference frame, while the D05 proper motions use data from many sources with different astrometric reference frames. Only 10 Taurus objects in the D05 catalog are not saturated in PS1 and have reliable proper motions, preventing a robust object-by-object comparison of the PS1 proper motions with those from D05. The 10 shared objects mostly have proper motions from the two catalogs that are consistent within errors.

Appendix B
Proper Motions of Known Upper Scorpius Members

We calculated proper motions for 482 members of Upper Sco from the lists of Luhman & Mamajek (2012), Dawson et al. (2014), Rizzuto et al. (2015), and this paper, that met the same selection criteria we used for Taurus members in Appendix A.2. Our catalog comprises the largest set of proper motions for low-mass (spectral types ≳M3) members of Upper Sco published to date. It includes 40 objects for which no proper motion has previously been published and 266 that improve on existing literature values, which were drawn from NOMAD (Zacharias et al. 2005), PPMXL (Roeser et al. 2010), SDSS DR9 (Ahn et al. 2012), UCAC4 (Zacharias et al. 2013), UKIDSS GCS DR9 (Lawrence et al. 2013), USNO-B (Monet et al. 2003), Dawson et al. (2011); Lodieu et al. (2007, 2013), and Lodieu (2013). We list our proper motions, number of epochs used, reduced χ^2, and time baseline for each proper motion fit in Table 9.

Figure 20 shows the distribution of errors for our Upper Sco proper motions as a function of the $y_{\rm P1}$ magnitude of each source. As with our Taurus sample (Appendix A), most of the errors are ≲5 mas yr^{-1}. Figure 21 shows the reduced χ^2 for the proper motion fits as a function of $y_{\rm P1}$. Again like Taurus, most of our proper motion fits have $\chi^2_\nu > 1$, implying that the proper motion errors may be underestimated (by a factor of ≈2).

Using the reliable fits from our Upper Sco list, we calculate a weighted mean proper motion for Upper Sco of ($\mu_\alpha \cos\delta = -8.5 \pm 0.1$, $\mu_\delta = -19.6 \pm 0.1$ mas yr^{-1}), with a weighted rms of 4.3 mas yr^{-1} in R.A. and 5.6 mas yr^{-1} in decl. We compare our proper motions to those listed in Pecaut et al. (2012, hereinafter P12) for F stars in Upper Sco, which were determined by *Hipparcos* (van Leeuwen 2007) or Tycho-2 (Høg et al. 2000). These stars are all saturated in PS1, so we are not able to measure accurate proper motions using PS1 data and compare them directly to the P12 proper motions. For the P12 Upper Sco catalog, we calculate a weighted mean proper motion of (-11.5 ± 0.3, -25.0 ± 0.2 mas yr^{-1}). We also cross-matched the P12 objects with the UCAC4 catalog (Zacharias et al. 2013), and using those proper motions obtained a weighted mean of (-9.9 ± 0.2, -21.6 ± 0.2 mas yr^{-1}). The source of the discrepancy between these two mean proper motion vectors for Upper Sco and our determination from PS1 PV3.2 is unclear and may indicate a difference in the bulk motions of higher mass stars (from P12) and low-mass stars and brown dwarfs (our catalog) in Upper Sco.

Appendix C
A New SpeX Prism Spectrum for the L0 Field Standard

We identified a wavelength offset in the spectrum of 2MASS J03454316+2540233 (hereinafter 2MASS J0345+2540) publically available from the SpeX Prism Library.[12] 2MASS J0345+2540 is the field L0 spectral standard for both optical (Kirkpatrick et al. 1999) and near-infrared (Kirkpatrick et al. 2010) wavelengths. The spectrum, first published in Burgasser & McElwain (2006, hereinafter BM06), is shifted ≈0.01 μm toward longer wavelengths (Figure 22). The offset is insignificant when visually compared to

[12] http://pono.ucsd.edu/ãdam/browndwarfs/spexprism

Table 9
Proper Motions of Upper Scorpius Members

Name	Photometry			Proper Motion				
	i_{P1} (mag)	z_{P1} (mag)	y_{P1} (mag)	$\mu_\alpha \cos\delta$ (mas yr^{-1})	μ_δ (mas yr^{-1})	χ^2_ν	N_{ep}	Δt (years)
Reliable fits: $0.3 < \chi^2_\nu < 40$								
2MASS J15350863−2532397	17.98 ± 0.01	16.86 ± 0.01	16.28 ± 0.01	−10.2 ± 6.8	−13.5 ± 4.8	4.7	47	16.5
2MASS J15355111−2021008	18.73 ± 0.01	17.32 ± 0.01	16.50 ± 0.01	−11.2 ± 1.6	−17.6 ± 2.2	1.2	38	16.6
2MASS J15411302−2308161	18.14 ± 0.01	17.02 ± 0.01	16.40 ± 0.01	−12.1 ± 2.2	−22.8 ± 1.9	1.1	48	15.3
2MASS J15420830−2621138	16.83 ± 0.01	15.85 ± 0.01	15.32 ± 0.01	−10.9 ± 3.3	−16.8 ± 6.6	3.7	53	15.7
2MASS J15423609−2108428	18.39 ± 0.01	17.02 ± 0.01	16.22 ± 0.01	−11.1 ± 6.3	−13.5 ± 5.0	6.3	37	16.6
2MASS J15433947−2535549	20.47 ± 0.03	18.85 ± 0.02	17.83 ± 0.02	−15.9 ± 4.5	−16.6 ± 4.4	0.7	41	15.3
2MASS J15442275−2136092	18.29 ± 0.01	17.23 ± 0.01	16.60 ± 0.01	−13.2 ± 2.2	−28.2 ± 2.1	0.9	52	16.6
2MASS J15453662−2510493	17.85 ± 0.01	16.70 ± 0.01	16.05 ± 0.01	−10.9 ± 1.8	−20.2 ± 2.1	2.0	55	15.7
2MASS J15465432−2556520	15.93 ± 0.01	14.93 ± 0.01	14.40 ± 0.01	−11.3 ± 1.9	−15.3 ± 4.1	4.2	64	15.7
2MASS J15470494−2137403	15.55 ± 0.01	14.68 ± 0.01	14.21 ± 0.01	−5.9 ± 3.7	−8.5 ± 3.3	4.0	51	16.6
2MASS J15472282−2139141	20.13 ± 0.02	18.72 ± 0.02	17.83 ± 0.03	−9.2 ± 2.3	−21.1 ± 2.3	1.0	45	16.6
2MASS J15472572−2609185	17.22 ± 0.02	16.10 ± 0.01	15.45 ± 0.01	−13.2 ± 2.0	−27.5 ± 2.6	2.0	54	15.3
2MASS J15480057−1815003	18.72 ± 0.01	17.38 ± 0.01	16.62 ± 0.01	−10.8 ± 2.3	−21.7 ± 2.3	1.2	37	15.9
PSO J237.1470−23.1489	18.69 ± 0.01	17.41 ± 0.01	16.61 ± 0.01	−11.4 ± 2.8	−19.7 ± 2.8	2.1	34	16.6
2MASS J15490414−2120150	17.14 ± 0.01	16.03 ± 0.01	15.43 ± 0.01	−6.6 ± 2.2	−8.5 ± 2.5	2.0	59	16.6
2MASS J15490803−2839550	16.39 ± 0.01	15.49 ± 0.01	15.02 ± 0.01	−20.4 ± 3.2	−18.2 ± 1.9	4.9	67	15.7
2MASS J15491602−2547146	15.92 ± 0.01	14.97 ± 0.01	14.49 ± 0.01	−21.2 ± 1.8	−18.0 ± 2.3	2.3	47	15.3
2MASS J15492260−2146574	14.61 ± 0.01	13.87 ± 0.01	13.49 ± 0.01	−17.1 ± 1.6	−18.2 ± 1.4	2.2	66	16.6
2MASS J15492909−2815384	16.01 ± 0.01	15.03 ± 0.01	14.47 ± 0.01	−15.9 ± 1.5	−22.4 ± 3.4	2.2	54	15.3
2MASS J15493660−2815141	16.31 ± 0.01	15.35 ± 0.01	14.86 ± 0.01	−14.5 ± 1.2	−14.9 ± 4.1	2.1	66	15.7
2MASS J15493784−2514102	18.73 ± 0.01	17.38 ± 0.01	16.60 ± 0.01	−22.8 ± 2.0	−26.0 ± 3.7	1.5	45	15.7
2MASS J15495069−2233511	17.51 ± 0.01	16.20 ± 0.01	15.47 ± 0.01	24.4 ± 14.9	−13.6 ± 5.8	10	54	16.1
2MASS J15495733−2201256	16.69 ± 0.01	15.59 ± 0.01	14.98 ± 0.01	−9.1 ± 12.7	−18.5 ± 2.6	8.8	59	16.6
2MASS J15501958−2805237	17.78 ± 0.01	16.70 ± 0.01	16.11 ± 0.01	−14.6 ± 1.4	−16.3 ± 4.8	4.3	71	15.7
2MASS J15511870−2145235	14.76 ± 0.01	13.98 ± 0.01	13.57 ± 0.01	−10.6 ± 2.3	−19.6 ± 4.7	9.4	60	16.6
2MASS J15514032−2146103	14.70 ± 0.01	13.88 ± 0.01	13.45 ± 0.01	−13.1 ± 2.9	−17.1 ± 2.0	4.1	58	16.6
2MASS J15514709−2113234	16.44 ± 0.08	15.61 ± 0.07	15.32 ± 0.01	−9.6 ± 1.0	−15.3 ± 1.6	1.3	70	16.6
2MASS J15514758−2329332	18.31 ± 0.01	16.96 ± 0.01	16.17 ± 0.01	−11.5 ± 1.5	−16.8 ± 3.8	1.4	45	16.6
2MASS J15521088−2125372	17.22 ± 0.01	16.90 ± 0.12	16.73 ± 0.19	−9.9 ± 3.9	−16.1 ± 2.6	2.3	64	16.6
2MASS J15522255−2313361	17.33 ± 0.01	16.11 ± 0.01	15.45 ± 0.01	−16.5 ± 1.5	−17.8 ± 5.0	1.7	55	16.6
2MASS J15524857−2621453	16.25 ± 0.01	15.30 ± 0.01	14.78 ± 0.01	−16.0 ± 1.3	−13.9 ± 7.8	6.3	46	15.7
2MASS J15530132−2114135	14.78 ± 0.01	13.93 ± 0.01	13.47 ± 0.01	−9.5 ± 1.5	−20.8 ± 1.9	1.5	59	16.3
2MASS J15541998−2135428	19.00 ± 0.01	17.56 ± 0.01	16.70 ± 0.01	−7.3 ± 3.0	−24.1 ± 2.7	1.0	42	16.3
2MASS J15543065−2536054	18.67 ± 0.01	17.41 ± 0.01	16.73 ± 0.01	−10.6 ± 2.3	−19.0 ± 4.6	1.6	47	15.7
2MASS J15543190−2221564	17.95 ± 0.01	16.65 ± 0.01	15.92 ± 0.01	−18.3 ± 3.5	−18.5 ± 3.0	2.8	38	16.6
2MASS J15544486−2843078	17.16 ± 0.01	16.15 ± 0.01	15.62 ± 0.01	−21.1 ± 4.3	−31.7 ± 3.6	5.4	64	15.1
2MASS J15550531−2117402	15.52 ± 0.01	14.59 ± 0.01	14.08 ± 0.01	−10.8 ± 1.7	−18.1 ± 2.6	3.7	50	16.3
2MASS J15551960−2751207	17.45 ± 0.01	16.30 ± 0.01	15.64 ± 0.01	−17.7 ± 2.3	−33.9 ± 2.0	1.5	56	15.1
2MASS J15552561−1817484	15.69 ± 0.01	14.56 ± 0.01	13.95 ± 0.01	−8.2 ± 1.4	−20.2 ± 1.7	2.8	73	16.6
2MASS J15553243−2308171	15.57 ± 0.01	15.12 ± 0.02	14.87 ± 0.01	35.9 ± 7.9	31.8 ± 11.5	19	57	16.6
2MASS J15555600−2045187	16.99 ± 0.01	16.13 ± 0.05	15.37 ± 0.01	−11.2 ± 1.6	−24.4 ± 1.6	1.3	60	16.1
2MASS J15560104−2338081	17.18 ± 0.01	16.04 ± 0.01	15.43 ± 0.01	−13.6 ± 1.5	−20.0 ± 3.2	2.4	75	16.6
2MASS J15560497−2106461	17.82 ± 0.01	16.52 ± 0.01	15.77 ± 0.01	−13.8 ± 1.1	−16.9 ± 4.6	1.5	50	16.6
2MASS J15561216−2354076	⋯	⋯	12.51 ± 0.02	−19.7 ± 3.9	−30.0 ± 3.0	3.3	28	15.7
2MASS J15561978−2423288	16.26 ± 0.01	15.32 ± 0.01	14.83 ± 0.01	−3.1 ± 10.5	−19.0 ± 3.8	21	76	15.7
2MASS J15562060−2336099	⋯	⋯	12.62 ± 0.01	−12.1 ± 3.1	−14.2 ± 3.8	3.6	64	16.6
2MASS J15563425−2003332	14.63 ± 0.01	13.73 ± 0.01	13.26 ± 0.01	−11.3 ± 1.9	−17.9 ± 2.8	3.5	51	16.6
2MASS J15570641−2206060	14.93 ± 0.01	14.06 ± 0.01	13.65 ± 0.01	−11.3 ± 2.9	−17.1 ± 2.8	3.0	50	15.7
2MASS J15571279−2343465	16.64 ± 0.01	15.59 ± 0.01	14.99 ± 0.01	−11.9 ± 1.4	−15.7 ± 2.2	2.5	52	15.7
2MASS J15572343−2924290	18.30 ± 0.01	17.08 ± 0.01	16.37 ± 0.01	−17.9 ± 2.6	−29.1 ± 3.6	2.0	39	15.1
2MASS J15572692−2715094	16.45 ± 0.01	15.57 ± 0.01	15.11 ± 0.01	−21.5 ± 1.8	−48.6 ± 2.8	2.6	62	14.9
2MASS J15572849−2219051	15.37 ± 0.01	14.48 ± 0.01	14.01 ± 0.01	−16.0 ± 5.2	−14.6 ± 3.1	12	51	14.6
2MASS J15572919−2215237	16.00 ± 0.01	15.22 ± 0.01	14.82 ± 0.01	−29.4 ± 3.5	−8.1 ± 2.6	14	53	14.6
2MASS J15572986−2258438	14.77 ± 0.01	13.94 ± 0.01	13.51 ± 0.01	−26.4 ± 12.0	−11.2 ± 4.6	17	73	14.6
2MASS J15573718−2245251	15.65 ± 0.01	15.06 ± 0.01	14.77 ± 0.01	−9.8 ± 1.6	−12.0 ± 1.5	1.8	65	14.1
2MASS J15574250−2226055	14.73 ± 0.01	14.03 ± 0.01	13.67 ± 0.01	−13.2 ± 1.5	−21.0 ± 2.7	3.2	53	14.6
2MASS J15574757−2444121	15.66 ± 0.01	14.81 ± 0.01	14.40 ± 0.01	−12.7 ± 1.3	−19.1 ± 5.0	2.6	62	15.7
2MASS J15581571−2021368	14.66 ± 0.01	13.81 ± 0.01	13.39 ± 0.01	−11.1 ± 2.0	−21.5 ± 2.9	4.4	63	15.7
2MASS J15581884−1915448	⋯	⋯	12.57 ± 0.01	−8.2 ± 2.3	−16.7 ± 3.9	3.0	76	15.7
2MASS J15582337−2151588	15.19 ± 0.01	14.25 ± 0.01	13.73 ± 0.01	−7.5 ± 2.2	−19.1 ± 3.2	2.1	57	15.1
2MASS J15582376−2721435	15.96 ± 0.01	15.04 ± 0.01	14.56 ± 0.01	−6.4 ± 2.1	−22.9 ± 2.3	1.9	66	15.1
2MASS J15582981−2310077	14.96 ± 0.01	14.08 ± 0.01	13.67 ± 0.01	−9.4 ± 1.5	−18.0 ± 4.9	3.6	66	15.7
2MASS J15583162−2402538	16.07 ± 0.03	15.16 ± 0.01	14.65 ± 0.01	−13.5 ± 4.2	−21.1 ± 4.2	9.1	45	15.1
2MASS J15583598−2348136	15.88 ± 0.01	14.96 ± 0.01	14.46 ± 0.01	−10.3 ± 3.0	−24.2 ± 2.4	23	68	15.1
2MASS J15584813−2141338	16.49 ± 0.01	15.51 ± 0.01	15.00 ± 0.01	−21.9 ± 1.7	−30.0 ± 4.0	2.1	45	15.7
PSO J239.7015−23.2665	20.88 ± 0.05	19.26 ± 0.01	18.24 ± 0.02	−0.1 ± 7.2	−23.0 ± 3.5	0.7	38	15.7
2MASS J15590193−2616329	14.84 ± 0.01	13.97 ± 0.01	13.52 ± 0.01	−13.7 ± 1.2	−17.1 ± 5.4	2.8	50	16.5
2MASS J15591135−2338002	17.89 ± 0.01	16.66 ± 0.01	15.97 ± 0.01	−11.0 ± 1.1	−20.9 ± 2.3	3.1	56	14.6
2MASS J15591244−2236502	15.64 ± 0.01	14.73 ± 0.01	14.21 ± 0.01	−10.7 ± 2.1	−16.7 ± 2.9	4.8	60	14.6
2MASS J15591513−2840411	15.58 ± 0.01	14.79 ± 0.01	14.39 ± 0.01	−13.9 ± 2.2	−16.5 ± 2.2	4.0	61	16.5
2MASS J15592591−2305081	15.64 ± 0.01	14.58 ± 0.01	14.01 ± 0.01	−9.1 ± 1.6	−27.3 ± 1.9	2.4	60	15.1
2MASS J15594366−2014396	17.93 ± 0.01	16.63 ± 0.01	15.87 ± 0.01	−11.9 ± 2.3	−24.0 ± 2.0	2.0	54	15.1
2MASS J15594439−1928191	18.37 ± 0.01	17.02 ± 0.01	16.25 ± 0.01	−23.6 ± 16.0	−20.2 ± 3.3	23	41	15.1

Table 9
(Continued)

Name	Photometry i_{P1} (mag)	z_{P1} (mag)	y_{P1} (mag)	Proper Motion $\mu_\alpha \cos\delta$ (mas yr^{-1})	μ_δ (mas yr^{-1})	χ^2_ν	N_{ep}	Δt (years)
2MASS J15594802−2227162	17.80 ± 0.01	16.56 ± 0.01	15.85 ± 0.01	−9.8 ± 2.0	−16.3 ± 3.2	1.4	57	15.7
2MASS J15594970−2301576	15.74 ± 0.01	14.78 ± 0.01	14.25 ± 0.01	−5.7 ± 1.9	−21.4 ± 1.9	2.2	68	15.1
2MASS J15595868−1836520	16.83 ± 0.01	15.67 ± 0.01	15.05 ± 0.01	−7.6 ± 3.0	−16.9 ± 1.8	1.5	61	15.7
2MASS J16000713−2224066	15.86 ± 0.01	15.17 ± 0.01	14.83 ± 0.01	−26.4 ± 2.1	−3.2 ± 1.7	3.3	55	15.7
2MASS J16001610−1726071	18.04 ± 0.01	16.78 ± 0.01	16.07 ± 0.01	−8.5 ± 1.2	−10.6 ± 1.9	1.4	84	16.7
2MASS J16001730−2236504	⋯	⋯	12.61 ± 0.04	−16.4 ± 7.7	−30.0 ± 11.8	13	40	15.7
2MASS J16001944−2256287	18.33 ± 0.01	17.00 ± 0.01	16.24 ± 0.01	−11.0 ± 2.1	−19.2 ± 4.8	1.5	56	15.7
2MASS J16002323−2329595	18.40 ± 0.02	17.04 ± 0.01	16.23 ± 0.02	51.4 ± 32.0	−46.1 ± 16.0	23	36	15.7
2MASS J16002631−2259412	15.31 ± 0.01	14.32 ± 0.01	13.78 ± 0.01	−10.0 ± 1.8	−23.5 ± 2.0	2.7	69	15.1
2MASS J16002669−2056316	16.45 ± 0.01	15.50 ± 0.01	14.97 ± 0.01	−3.4 ± 3.1	−11.1 ± 5.5	7.0	75	15.7
2MASS J16003023−2334457	15.85 ± 0.01	14.83 ± 0.01	14.30 ± 0.01	−10.8 ± 1.1	−15.6 ± 2.7	2.7	57	15.7
2MASS J16004318−2229143	19.17 ± 0.01	17.77 ± 0.01	17.00 ± 0.01	−10.8 ± 1.6	−17.2 ± 3.4	1.5	54	15.7
2MASS J16005065−1927502	15.71 ± 0.01	14.61 ± 0.02	13.95 ± 0.01	−4.2 ± 2.1	−18.1 ± 2.2	4.5	69	15.1
2MASS J16005265−2812087	16.65 ± 0.01	15.66 ± 0.01	15.10 ± 0.01	−6.8 ± 1.6	−28.8 ± 1.6	1.5	73	15.9
2MASS J16010605−2215246	14.90 ± 0.01	14.12 ± 0.01	13.70 ± 0.01	−8.1 ± 1.9	−29.2 ± 2.8	2.7	57	15.1
2MASS J16011915−2306394	16.86 ± 0.01	15.78 ± 0.01	15.19 ± 0.01	−16.6 ± 2.3	−27.9 ± 3.7	3.4	50	15.1
2MASS J16012238−2708194	18.80 ± 0.01	17.38 ± 0.01	16.55 ± 0.01	−6.7 ± 2.4	−20.1 ± 3.8	2.1	58	16.5
2MASS J16012902−2509069	⋯	⋯	12.67 ± 0.01	−10.9 ± 1.6	−100.6 ± 32.4	27	69	16.5
2MASS J16014157−2111380	15.88 ± 0.02	14.89 ± 0.04	14.38 ± 0.01	−10.2 ± 1.4	−17.5 ± 2.2	1.7	76	16.5
2MASS J16014528−2138551	18.91 ± 0.01	17.64 ± 0.01	16.92 ± 0.01	−6.3 ± 2.3	−10.4 ± 1.7	1.8	64	16.5
2MASS J16014769−2441011	16.85 ± 0.01	15.89 ± 0.01	15.38 ± 0.01	−7.9 ± 1.7	−15.7 ± 5.7	2.1	46	16.5
2MASS J16014955−2351082	15.64 ± 0.01	14.76 ± 0.01	14.30 ± 0.01	−10.4 ± 1.9	−19.3 ± 1.7	4.1	54	16.5
2MASS J16015498−2131230	16.22 ± 0.01	15.23 ± 0.01	14.69 ± 0.01	−14.6 ± 3.4	−23.2 ± 1.6	12	66	16.0
2MASS J16015976−1952202	15.29 ± 0.01	14.36 ± 0.01	13.89 ± 0.01	−15.3 ± 2.0	−27.8 ± 2.2	3.1	66	16.0
2MASS J16020287−2236139	14.77 ± 0.01	14.32 ± 0.01	14.10 ± 0.01	−22.0 ± 8.6	−50.3 ± 9.1	15	50	16.5
2MASS J16020429−2050425	16.05 ± 0.01	14.98 ± 0.01	14.38 ± 0.01	−5.1 ± 1.6	−18.0 ± 3.9	2.8	79	16.5
2MASS J16021096−2007495	15.16 ± 0.01	14.28 ± 0.01	13.83 ± 0.01	−6.0 ± 1.6	−13.9 ± 3.6	3.1	78	16.5
2MASS J16021489−2438325	14.93 ± 0.01	14.01 ± 0.01	13.52 ± 0.01	−16.8 ± 1.5	−34.8 ± 2.9	2.4	41	15.9
2MASS J16022357−2259332	14.89 ± 0.01	13.91 ± 0.01	13.38 ± 0.01	−10.8 ± 2.0	−17.2 ± 5.1	2.9	56	16.5
2MASS J16022616−2002403	14.65 ± 0.01	13.79 ± 0.01	13.34 ± 0.01	−6.9 ± 1.1	−14.2 ± 7.5	4.4	83	16.5
2MASS J16023185−2132340	15.65 ± 0.01	14.73 ± 0.01	14.20 ± 0.01	−7.2 ± 3.6	−16.6 ± 3.4	4.5	39	16.5
2MASS J16023227−2200486	16.57 ± 0.01	15.48 ± 0.01	14.88 ± 0.01	−10.4 ± 1.5	−20.2 ± 1.8	1.4	64	16.0
2MASS J16023418−2200354	16.25 ± 0.01	15.02 ± 0.01	14.37 ± 0.01	−11.9 ± 1.7	−22.9 ± 1.3	1.7	70	16.0
2MASS J16023587−2320170	⋯	⋯	12.53 ± 0.01	−10.8 ± 3.4	−27.7 ± 6.3	8.8	39	16.5
2MASS J16024142−2248419	16.20 ± 0.01	15.17 ± 0.01	14.56 ± 0.01	−10.9 ± 2.0	−20.1 ± 6.2	3.6	42	16.5
2MASS J16024152−2138245	15.05 ± 0.01	14.22 ± 0.01	13.72 ± 0.01	−11.7 ± 1.6	−13.9 ± 2.8	3.5	71	16.5
2MASS J16024448−2543323	14.68 ± 0.01	13.93 ± 0.01	13.57 ± 0.01	−12.5 ± 3.3	−16.2 ± 4.2	5.9	75	16.5
2MASS J16024544−1930377	15.08 ± 0.01	14.12 ± 0.01	13.60 ± 0.01	−6.7 ± 1.1	−14.9 ± 2.6	3.0	87	16.0
2MASS J16024546−1946034	15.25 ± 0.01	14.65 ± 0.01	14.33 ± 0.01	−3.5 ± 1.1	6.5 ± 5.5	3.1	95	16.5
2MASS J16024575−2304509	15.35 ± 0.01	14.38 ± 0.01	13.87 ± 0.01	−21.3 ± 1.8	−26.6 ± 6.1	3.3	56	16.5
2MASS J16025116−2401502	15.67 ± 0.01	14.65 ± 0.01	14.04 ± 0.01	−16.5 ± 5.6	−10.1 ± 12.3	24	46	16.5
2MASS J16025214−2121296	18.52 ± 0.01	17.10 ± 0.02	16.34 ± 0.01	−5.4 ± 1.9	−17.6 ± 1.9	2.1	54	16.5
2MASS J16025529−1922431	16.06 ± 0.01	14.95 ± 0.01	14.33 ± 0.01	−11.0 ± 1.8	−19.5 ± 1.5	2.2	97	16.0
2MASS J16030161−2207523	15.70 ± 0.01	14.78 ± 0.01	14.27 ± 0.01	−9.1 ± 2.1	−18.7 ± 4.4	4.1	51	16.5
2MASS J16031329−2112569	14.98 ± 0.01	14.12 ± 0.01	13.62 ± 0.01	−9.5 ± 1.9	−19.3 ± 3.1	3.3	83	16.5
2MASS J16031491−2234454	14.59 ± 0.01	13.62 ± 0.01	13.13 ± 0.01	−9.7 ± 1.4	−19.0 ± 7.0	3.9	51	16.5
2MASS J16032625−2155378	15.46 ± 0.01	14.56 ± 0.01	14.05 ± 0.01	−11.3 ± 1.5	−19.1 ± 2.9	2.2	67	16.5
2MASS J16032940−1955038	14.62 ± 0.01	13.81 ± 0.01	13.39 ± 0.01	−3.9 ± 1.1	−12.8 ± 2.8	5.2	93	16.5
2MASS J16033471−1829303	15.54 ± 0.01	14.56 ± 0.01	14.02 ± 0.01	−7.0 ± 1.0	−16.5 ± 1.5	2.3	84	16.5
2MASS J16034030−2335237	14.79 ± 0.01	14.01 ± 0.01	13.61 ± 0.01	−10.2 ± 2.9	−16.9 ± 6.9	5.6	51	16.5
2MASS J16035175−2140154	14.57 ± 0.01	13.55 ± 0.01	13.00 ± 0.01	−9.3 ± 1.5	−24.4 ± 2.1	2.1	70	16.0
2MASS J16035404−2509393	14.91 ± 0.01	14.08 ± 0.01	13.64 ± 0.01	−10.5 ± 2.0	−21.9 ± 5.4	6.3	61	16.5
2MASS J16035652−2357250	16.51 ± 0.01	15.59 ± 0.01	15.08 ± 0.01	−8.6 ± 1.1	−16.1 ± 4.2	1.9	47	16.5
2MASS J16041792−1941505	16.65 ± 0.01	15.47 ± 0.01	14.91 ± 0.01	−5.7 ± 1.4	−16.2 ± 2.2	1.5	78	16.5
2MASS J16042796−1904337	14.77 ± 0.01	13.93 ± 0.01	13.46 ± 0.01	−1.8 ± 1.7	−16.9 ± 4.4	8.5	78	16.5
2MASS J16043565−1948302	15.02 ± 0.01	14.10 ± 0.01	13.58 ± 0.01	−9.1 ± 1.7	−21.8 ± 2.3	3.2	70	15.9
2MASS J16044026−2254323	18.00 ± 0.01	16.72 ± 0.01	16.18 ± 0.04	−10.6 ± 3.3	−17.4 ± 2.7	5.0	49	16.5
2MASS J16044068−1946538	16.56 ± 0.01	15.53 ± 0.01	14.96 ± 0.01	−5.8 ± 1.9	−14.8 ± 3.5	5.7	91	16.5
2MASS J16044075−1936525	17.04 ± 0.01	15.84 ± 0.01	15.15 ± 0.01	−8.7 ± 2.9	−16.5 ± 4.8	2.0	74	16.5
2MASS J16044303−2318258	17.14 ± 0.01	15.98 ± 0.01	15.31 ± 0.01	−8.7 ± 1.5	−17.9 ± 2.4	1.5	88	16.5
2MASS J16044930−2045581	19.21 ± 0.01	17.76 ± 0.01	16.90 ± 0.01	−6.0 ± 1.6	−16.9 ± 2.4	1.4	47	16.5
2MASS J16044997−2038353	14.86 ± 0.01	13.90 ± 0.01	13.40 ± 0.01	−6.9 ± 2.0	−16.1 ± 5.2	4.8	74	16.5
2MASS J16045199−2224108	17.85 ± 0.01	16.44 ± 0.01	15.65 ± 0.01	−9.1 ± 2.1	−20.4 ± 2.1	1.0	52	15.9
2MASS J16045379−2002271	16.38 ± 0.01	15.40 ± 0.01	14.87 ± 0.01	−7.8 ± 0.8	−16.1 ± 2.0	1.6	81	16.5
2MASS J16045581−2307438	17.38 ± 0.01	16.14 ± 0.01	15.42 ± 0.01	−6.4 ± 3.6	−18.2 ± 5.7	2.4	72	16.5
2MASS J16045716−2104160	15.07 ± 0.01	14.27 ± 0.01	13.84 ± 0.01	−7.5 ± 2.2	−19.5 ± 5.8	2.5	67	16.5
2MASS J16050231−1941554	15.14 ± 0.01	14.32 ± 0.01	13.89 ± 0.01	−7.2 ± 2.3	−14.8 ± 6.0	7.1	79	16.5
2MASS J16050474−1956274	⋯	⋯	12.54 ± 0.01	−0.7 ± 4.7	−17.4 ± 5.6	24	81	16.5
2MASS J16051403−2406524	16.16 ± 0.01	15.01 ± 0.01	14.39 ± 0.01	−12.0 ± 1.4	−24.1 ± 1.7	1.6	80	16.0
2MASS J16051615−1938310	15.03 ± 0.01	14.21 ± 0.01	13.80 ± 0.01	−6.0 ± 2.3	−18.3 ± 5.3	3.4	59	16.5
2MASS J16052556−2035397	15.05 ± 0.01	14.09 ± 0.01	13.57 ± 0.01	−5.8 ± 3.2	−33.3 ± 6.8	4.7	71	16.5
2MASS J16052787−2115510	15.87 ± 0.01	15.00 ± 0.01	14.51 ± 0.01	−7.2 ± 1.8	−14.1 ± 2.6	2.5	85	16.5
2MASS J16053077−2246200	17.18 ± 0.01	16.03 ± 0.01	15.38 ± 0.01	−12.1 ± 3.0	−21.9 ± 2.2	2.1	71	15.1
2MASS J16053128−1926240	15.35 ± 0.01	14.43 ± 0.01	13.93 ± 0.01	−8.4 ± 2.1	−21.1 ± 1.7	1.6	64	15.1

Table 9
(Continued)

Name	Photometry			Proper Motion				
	i_{P1} (mag)	z_{P1} (mag)	y_{P1} (mag)	$\mu_\alpha \cos\delta$ (mas yr^{-1})	μ_δ (mas yr^{-1})	χ^2_ν	N_{ep}	Δt (years)
2MASS J16053215−1933159	15.49 ± 0.01	14.67 ± 0.01	14.28 ± 0.01	−7.4 ± 1.2	−15.6 ± 3.4	2.0	57	15.7
2MASS J16054416−2155054	14.91 ± 0.01	13.94 ± 0.01	13.40 ± 0.01	−14.0 ± 2.0	−36.0 ± 4.4	4.3	67	15.1
2MASS J16054565−1948353	15.49 ± 0.01	14.61 ± 0.01	14.14 ± 0.01	−7.5 ± 1.4	−15.4 ± 4.4	2.6	64	15.7
2MASS J16054778−1945263	14.88 ± 0.01	14.05 ± 0.01	13.63 ± 0.01	−5.2 ± 1.1	−13.6 ± 4.8	2.9	76	15.7
2MASS J16055407−1818443	16.78 ± 0.01	15.64 ± 0.01	15.00 ± 0.01	−4.8 ± 2.0	−14.7 ± 1.4	1.6	68	15.7
2MASS J16055409−1818488	21.26 ± 0.10	19.66 ± 0.03	18.71 ± 0.09	−16.2 ± 6.2	−31.7 ± 5.9	1.2	15	14.1
2MASS J16060374−2219298	20.55 ± 0.04	18.94 ± 0.02	17.97 ± 0.01	7.4 ± 7.9	−13.3 ± 2.7	0.9	36	15.7
2MASS J16060391−2056443	17.34 ± 0.01	16.02 ± 0.01	15.27 ± 0.01	−8.6 ± 2.1	−20.0 ± 4.4	2.9	62	15.1
2MASS J16060629−2335133	20.70 ± 0.04	19.23 ± 0.01	18.28 ± 0.01	−7.5 ± 6.5	−18.1 ± 6.4	1.0	31	15.1
2MASS J16061144−1935405	15.82 ± 0.03	14.96 ± 0.01	14.32 ± 0.01	−4.7 ± 3.4	−13.1 ± 1.7	2.4	65	15.7
2MASS J16061199−1935331	15.05 ± 0.01	14.05 ± 0.01	13.50 ± 0.01	−6.0 ± 1.7	−15.0 ± 1.7	2.2	62	15.7
2MASS J16061935−1923326	15.20 ± 0.01	14.31 ± 0.01	13.84 ± 0.01	−4.1 ± 2.8	−25.2 ± 2.7	5.1	71	15.1
2MASS J16062277−2011243	14.61 ± 0.01	13.84 ± 0.01	13.42 ± 0.01	−8.1 ± 3.3	−15.3 ± 2.9	4.2	80	15.7
2MASS J16062389−1941165	14.77 ± 0.01	13.82 ± 0.01	13.30 ± 0.01	−6.0 ± 1.2	−21.9 ± 1.9	1.7	78	15.1
2MASS J16062637−2306113	16.08 ± 0.01	15.17 ± 0.01	14.69 ± 0.01	−5.8 ± 2.3	−14.2 ± 4.2	2.7	74	15.7
2MASS J16062860−2043317	14.65 ± 0.01	13.71 ± 0.01	13.16 ± 0.01	−12.4 ± 1.2	−13.3 ± 4.9	3.4	87	15.7
2MASS J16062870−2856580	16.54 ± 0.01	15.57 ± 0.01	15.04 ± 0.01	−3.9 ± 1.7	−19.4 ± 1.7	1.7	72	15.9
2MASS J16063210−2020538	15.87 ± 0.01	14.95 ± 0.01	14.46 ± 0.01	−19.5 ± 8.9	−9.6 ± 8.1	18	75	15.8
2MASS J16063461−2255043	14.72 ± 0.01	13.86 ± 0.01	13.39 ± 0.01	−10.0 ± 1.6	−21.0 ± 2.4	2.5	51	15.9
2MASS J16063539−2516510	15.26 ± 0.01	14.41 ± 0.01	13.97 ± 0.01	−9.6 ± 1.4	−20.6 ± 5.1	3.5	53	16.5
2MASS J16063922−2248340	15.09 ± 0.01	14.24 ± 0.01	13.78 ± 0.01	−4.0 ± 2.3	−25.8 ± 4.9	12	77	16.4
2MASS J16064102−2455489	15.70 ± 0.01	14.89 ± 0.01	14.41 ± 0.01	−10.3 ± 1.8	−20.0 ± 4.1	4.7	64	16.5
2MASS J16064266−1851140	18.26 ± 0.01	16.86 ± 0.01	16.04 ± 0.01	−7.4 ± 2.1	−20.8 ± 2.1	1.4	47	15.9
2MASS J16064818−2230400	19.06 ± 0.01	17.61 ± 0.01	16.75 ± 0.01	−8.0 ± 1.4	−16.3 ± 4.0	1.2	42	16.4
2MASS J16065018−2309539	14.57 ± 0.01	13.74 ± 0.01	13.29 ± 0.01	−7.0 ± 1.9	−22.4 ± 2.4	5.2	74	16.4
2MASS J16070009−2043102	14.50 ± 0.01	13.70 ± 0.01	13.25 ± 0.01	−7.9 ± 1.4	−20.7 ± 3.8	6.1	76	15.7
2MASS J16070051−2206362	⋯	13.05 ± 0.01	12.71 ± 0.01	−12.2 ± 1.1	−19.9 ± 2.3	1.9	92	15.7
2MASS J16070169−2028579	16.67 ± 0.01	15.74 ± 0.01	15.04 ± 0.01	−8.5 ± 2.2	−24.7 ± 3.1	3.2	70	15.1
2MASS J16070474−2015557	15.14 ± 0.01	14.32 ± 0.01	13.88 ± 0.01	−5.0 ± 1.2	−14.7 ± 5.0	3.0	84	15.7
2MASS J16070700−2515127	14.51 ± 0.01	13.76 ± 0.01	13.37 ± 0.01	−11.6 ± 2.2	−16.7 ± 9.6	6.4	48	16.5
2MASS J16070873−1927341	14.71 ± 0.01	13.95 ± 0.01	13.51 ± 0.01	−9.0 ± 2.4	−14.3 ± 2.0	4.3	75	15.7
2MASS J16071007−1917046	15.64 ± 0.01	14.66 ± 0.01	14.14 ± 0.01	−13.6 ± 2.0	−23.7 ± 3.1	3.7	81	15.1
2MASS J16071348−2106016	15.35 ± 0.01	14.41 ± 0.01	13.89 ± 0.01	−10.0 ± 1.3	−24.6 ± 2.2	2.3	85	15.1
2MASS J16071478−2321011	⋯	19.81 ± 0.01	18.74 ± 0.02	0.2 ± 12.2	−16.3 ± 11.0	0.7	17	14.3
2MASS J16071750−1820348	18.95 ± 0.01	17.48 ± 0.01	16.72 ± 0.04	−4.5 ± 2.6	−21.1 ± 3.3	2.9	50	15.7
2MASS J16072240−2011581	15.75 ± 0.01	14.76 ± 0.01	14.19 ± 0.01	−7.2 ± 1.9	−25.8 ± 2.0	4.8	85	15.1
2MASS J16072382−2211018	19.51 ± 0.02	17.93 ± 0.01	17.05 ± 0.01	−19.5 ± 6.0	−21.7 ± 6.9	4.1	53	15.7
2MASS J16072641−2144169	17.98 ± 0.01	16.85 ± 0.01	16.21 ± 0.01	−9.2 ± 2.4	−20.7 ± 4.3	2.7	62	15.1
2MASS J16072754−2018344	15.76 ± 0.01	14.66 ± 0.01	14.04 ± 0.01	−6.2 ± 3.6	−23.6 ± 2.3	13	70	15.1
2MASS J16072853−2407543	⋯	⋯	12.55 ± 0.01	−3.2 ± 13.0	−20.8 ± 11.8	16	62	16.5
2MASS J16073556−2027134	15.80 ± 0.01	14.92 ± 0.01	14.43 ± 0.01	−8.2 ± 1.5	−22.8 ± 2.7	2.6	64	15.1
2MASS J16073799−2242468	⋯	19.99 ± 0.02	18.93 ± 0.03	−14.4 ± 10.3	−16.5 ± 10.3	0.9	36	14.8
2MASS J16074036−2357019	16.88 ± 0.01	15.80 ± 0.01	15.21 ± 0.01	−7.0 ± 1.8	−20.3 ± 2.5	3.0	73	15.7
2MASS J16074200−2107302	15.12 ± 0.01	14.23 ± 0.01	13.77 ± 0.01	−4.7 ± 2.2	−14.4 ± 4.5	4.5	82	15.7
2MASS J16074522−2222574	15.30 ± 0.01	14.41 ± 0.01	13.91 ± 0.01	−9.7 ± 1.4	−11.9 ± 3.6	3.1	73	15.7
2MASS J16075039−2221021	15.18 ± 0.01	14.27 ± 0.01	13.79 ± 0.01	−8.3 ± 2.8	−19.9 ± 3.1	4.2	70	15.1
2MASS J16075567−2443267	16.75 ± 0.01	15.78 ± 0.01	15.28 ± 0.01	−8.2 ± 7.5	−17.1 ± 2.9	16	60	16.5
2MASS J16075850−2039485	16.88 ± 0.01	15.78 ± 0.01	15.18 ± 0.01	−4.6 ± 3.1	−22.6 ± 6.0	7.2	85	15.7
2MASS J16080051−2040289	15.27 ± 0.01	14.33 ± 0.01	13.81 ± 0.01	−0.7 ± 4.5	−28.2 ± 6.3	13	84	15.1
2MASS J16080217−2259057	15.15 ± 0.01	14.18 ± 0.01	13.68 ± 0.01	−8.4 ± 1.2	−14.8 ± 3.7	2.2	62	15.7
2MASS J16080245−2531392	14.61 ± 0.01	13.75 ± 0.01	13.28 ± 0.01	−14.8 ± 2.7	−17.8 ± 3.5	4.1	57	16.5
2MASS J16080370−1812385	16.78 ± 0.01	16.10 ± 0.01	15.79 ± 0.01	34.8 ± 17.5	17.1 ± 11.7	10	65	15.7
2MASS J16080745−2345055	17.93 ± 0.01	16.74 ± 0.01	16.05 ± 0.01	−5.0 ± 7.0	−17.7 ± 4.8	3.1	63	15.7
2MASS J16081081−2229428	15.62 ± 0.01	14.61 ± 0.01	14.08 ± 0.01	−4.4 ± 2.1	−20.7 ± 3.2	2.0	68	15.7
2MASS J16081758−2348508	16.66 ± 0.01	15.64 ± 0.01	15.08 ± 0.02	−6.5 ± 5.7	−18.9 ± 5.2	3.3	57	15.7
2MASS J16081843−2232248	20.92 ± 0.04	19.26 ± 0.02	18.18 ± 0.01	−11.7 ± 5.6	−26.7 ± 5.5	0.7	46	15.1
2MASS J16082096−1832197	17.66 ± 0.01	16.52 ± 0.01	15.87 ± 0.01	−15.6 ± 1.6	−18.3 ± 3.3	2.7	57	15.7
2MASS J16082229−2217029	15.96 ± 0.01	15.00 ± 0.01	14.47 ± 0.01	−19.1 ± 4.1	−25.9 ± 1.9	11	53	15.7
2MASS J16082751−1949047	14.52 ± 0.01	13.61 ± 0.01	13.10 ± 0.01	10.7 ± 6.2	−6.2 ± 8.0	5.0	74	15.7
2MASS J16082847−2315103	20.03 ± 0.02	18.43 ± 0.01	17.47 ± 0.01	−8.6 ± 4.0	−30.8 ± 3.9	1.2	41	15.1
2MASS J16083048−2335109	19.08 ± 0.01	17.58 ± 0.01	16.75 ± 0.01	−12.3 ± 4.1	−18.7 ± 4.4	1.4	45	15.7
2MASS J16083455−2211559	15.36 ± 0.01	14.47 ± 0.01	13.97 ± 0.01	−9.8 ± 1.7	−18.7 ± 3.8	3.4	81	15.7
2MASS J16083659−1802497	16.26 ± 0.01	15.10 ± 0.01	14.42 ± 0.01	−5.4 ± 1.5	−17.7 ± 4.7	4.1	88	15.7
2MASS J16084171−1856107	15.46 ± 0.01	14.38 ± 0.01	13.79 ± 0.01	−6.5 ± 1.5	−18.6 ± 1.6	1.9	73	15.1
2MASS J16084565−2430000	14.73 ± 0.01	13.93 ± 0.01	13.54 ± 0.01	−10.6 ± 1.4	−14.3 ± 5.2	3.3	75	16.5
2MASS J16084744−2235477	20.14 ± 0.02	18.56 ± 0.01	17.66 ± 0.01	0.1 ± 4.5	−27.3 ± 4.5	0.8	46	15.1
2MASS J16084836−2341209	15.43 ± 0.01	14.46 ± 0.01	13.98 ± 0.01	−9.4 ± 2.3	−17.6 ± 4.9	3.9	72	15.7
2MASS J16085871−2449363	14.86 ± 0.01	14.08 ± 0.01	13.68 ± 0.01	−10.0 ± 1.8	−15.4 ± 4.9	7.2	82	16.5
2MASS J16090002−1908368	14.75 ± 0.01	13.87 ± 0.01	13.43 ± 0.01	−4.9 ± 1.2	−19.2 ± 3.8	2.3	74	15.7
2MASS J16090051−2745194	14.95 ± 0.01	14.04 ± 0.01	13.53 ± 0.01	−14.0 ± 3.0	−17.8 ± 3.2	3.9	58	16.5
2MASS J16090071−2029086	17.83 ± 0.01	16.63 ± 0.01	15.95 ± 0.01	−4.5 ± 3.4	−22.4 ± 1.8	2.2	46	15.7
2MASS J16090168−2740521	16.21 ± 0.01	15.08 ± 0.01	14.46 ± 0.01	−11.3 ± 2.2	−24.4 ± 2.1	2.3	68	15.9
2MASS J16090197−2151225	17.15 ± 0.01	15.96 ± 0.01	15.29 ± 0.01	−8.1 ± 2.7	−15.9 ± 2.7	2.8	59	15.7
2MASS J16090407−2417588	15.01 ± 0.01	13.86 ± 0.01	13.35 ± 0.02	−8.4 ± 2.1	−25.6 ± 3.6	14	74	16.0

Table 9
(Continued)

Name	Photometry			Proper Motion				
	i_{P1} (mag)	z_{P1} (mag)	y_{P1} (mag)	$\mu_\alpha \cos\delta$ (mas yr^{-1})	μ_δ (mas yr^{-1})	χ^2_ν	N_{ep}	Δt (years)
2MASS J16090451−2224523	16.60 ± 0.01	15.37 ± 0.01	14.65 ± 0.01	−6.1 ± 2.1	−16.5 ± 2.0	1.4	68	15.1
2MASS J16090776−2339545	15.04 ± 0.01	14.09 ± 0.01	13.56 ± 0.01	−8.4 ± 2.1	−26.7 ± 1.9	2.4	77	15.1
2MASS J16090884−2217466	15.74 ± 0.01	14.82 ± 0.01	14.36 ± 0.01	−15.9 ± 1.7	−26.0 ± 3.0	3.0	73	15.7
2MASS J16091580−1937063	15.03 ± 0.01	14.22 ± 0.01	13.78 ± 0.01	−3.2 ± 1.6	−13.5 ± 2.0	2.3	77	15.7
2MASS J16091689−2341324	14.74 ± 0.01	13.83 ± 0.01	13.38 ± 0.01	−15.2 ± 2.7	−15.2 ± 5.7	5.6	72	15.7
2MASS J16091837−2007349	16.40 ± 0.01	15.23 ± 0.01	14.61 ± 0.01	−11.7 ± 3.4	−25.6 ± 3.3	3.6	47	15.1
2MASS J16092054−1926318	16.32 ± 0.03	15.21 ± 0.01	14.61 ± 0.01	−9.5 ± 3.3	−18.6 ± 3.6	4.8	58	15.7
2MASS J16092136−2139342	15.11 ± 0.01	14.12 ± 0.02	13.58 ± 0.01	−10.2 ± 4.7	−6.3 ± 6.0	28	64	15.1
2MASS J16092619−2403030	14.94 ± 0.01	14.09 ± 0.01	13.66 ± 0.01	−8.0 ± 1.1	−18.6 ± 4.1	2.6	77	16.5
2MASS J16092938−2343121	17.83 ± 0.01	16.57 ± 0.01	15.87 ± 0.01	−8.3 ± 1.4	−16.1 ± 2.0	1.3	59	15.7
2MASS J16093019−2059536	17.30 ± 0.01	16.17 ± 0.01	15.56 ± 0.01	−5.8 ± 3.4	−13.7 ± 6.1	1.9	63	15.7
2MASS J16093245−2405593	16.11 ± 0.01	15.05 ± 0.01	14.43 ± 0.01	−4.8 ± 1.9	−17.5 ± 7.9	8.3	74	16.5
2MASS J16093558−1828232	14.62 ± 0.01	13.81 ± 0.01	13.38 ± 0.01	−2.6 ± 1.4	−14.7 ± 5.3	4.6	90	15.7
2MASS J16093706−2052529	15.82 ± 0.01	14.90 ± 0.01	14.39 ± 0.01	−5.9 ± 1.6	−15.4 ± 2.3	2.0	83	15.1
2MASS J16094634−2255335	14.71 ± 0.01	13.87 ± 0.01	13.44 ± 0.01	−7.1 ± 4.6	−15.1 ± 7.7	5.3	70	15.7
2MASS J16095060−1848521	18.73 ± 0.01	17.25 ± 0.01	16.37 ± 0.01	−6.0 ± 3.6	−20.6 ± 3.7	1.9	41	15.1
2MASS J16095107−2722418	16.72 ± 0.01	15.58 ± 0.01	14.92 ± 0.01	−11.1 ± 3.9	−20.1 ± 2.7	2.9	64	16.5
2MASS J16095217−2136277	16.11 ± 0.01	14.91 ± 0.01	14.23 ± 0.01	−5.1 ± 1.7	−27.4 ± 2.2	2.2	61	15.1
2MASS J16095287−2441535	14.77 ± 0.01	13.86 ± 0.01	13.35 ± 0.01	−7.2 ± 1.7	−26.6 ± 2.6	3.6	63	16.0
2MASS J16095307−1948169	16.04 ± 0.01	14.94 ± 0.01	14.33 ± 0.01	−3.7 ± 2.2	−10.6 ± 4.7	7.0	61	15.1
2MASS J16095361−1754474	15.50 ± 0.01	14.56 ± 0.01	14.11 ± 0.01	−8.3 ± 2.8	−17.3 ± 2.6	3.7	81	15.7
2MASS J16095695−2212027	16.69 ± 0.01	15.69 ± 0.01	15.13 ± 0.01	−6.8 ± 1.1	−17.4 ± 4.2	1.5	73	15.7
2MASS J16095852−2345186	16.09 ± 0.01	14.92 ± 0.01	14.26 ± 0.01	−7.2 ± 2.2	−25.2 ± 2.4	11	87	15.1
2MASS J16095990−2155424	17.54 ± 0.01	16.45 ± 0.01	15.86 ± 0.01	−7.4 ± 1.3	−16.4 ± 6.1	2.0	77	15.7
2MASS J16100129−2152243	15.82 ± 0.01	14.78 ± 0.01	14.18 ± 0.01	−0.7 ± 1.7	−25.0 ± 2.3	3.1	79	15.1
2MASS J16100394−2728479	14.65 ± 0.01	13.85 ± 0.01	13.44 ± 0.01	−7.7 ± 1.2	−14.9 ± 3.5	2.9	68	16.5
2MASS J16100541−1919362	17.93 ± 0.01	16.66 ± 0.03	15.90 ± 0.02	0.5 ± 5.3	−13.4 ± 2.6	7.1	49	15.7
2MASS J16100608−2127440	19.16 ± 0.02	17.61 ± 0.01	16.73 ± 0.01	−6.1 ± 3.6	−19.1 ± 2.8	2.4	46	15.7
2MASS J16100753−1810568	16.16 ± 0.01	14.99 ± 0.01	14.35 ± 0.01	−4.2 ± 1.6	−22.2 ± 1.8	1.7	76	15.1
2MASS J16101100−1946040	15.09 ± 0.01	14.22 ± 0.01	13.77 ± 0.01	−9.3 ± 1.2	−15.5 ± 2.6	4.6	89	15.7
2MASS J16101191−2101550	16.81 ± 0.01	15.72 ± 0.01	15.06 ± 0.01	−5.6 ± 1.7	−19.4 ± 1.9	2.5	79	15.1
2MASS J16101316−2856308	17.53 ± 0.01	16.34 ± 0.01	15.68 ± 0.01	−15.0 ± 2.8	−15.2 ± 3.1	1.3	51	16.5
2MASS J16101445−1951377	…	…	12.61 ± 0.01	−2.3 ± 2.9	−15.3 ± 2.6	1.9	46	15.7
2MASS J16101888−2502325	14.90 ± 0.01	14.02 ± 0.01	13.59 ± 0.02	−28.4 ± 9.0	−30.8 ± 8.5	28	46	16.5
2MASS J16101942−2331089	16.66 ± 0.01	15.67 ± 0.01	15.13 ± 0.01	−5.1 ± 1.2	−13.6 ± 2.3	1.6	62	15.7
2MASS J16102087−2331556	14.76 ± 0.01	13.86 ± 0.01	13.35 ± 0.01	−13.5 ± 2.1	−24.2 ± 3.6	5.0	76	15.1
2MASS J16102564−2411250	18.81 ± 0.01	17.46 ± 0.01	16.68 ± 0.01	−16.2 ± 5.9	−20.2 ± 2.4	1.9	51	16.0
2MASS J16102819−1910444	15.90 ± 0.01	14.93 ± 0.01	14.40 ± 0.01	−6.8 ± 2.4	−11.1 ± 1.9	6.2	80	15.7
2MASS J16102988−2403497	15.65 ± 0.01	14.82 ± 0.01	14.36 ± 0.01	−7.2 ± 3.1	−21.4 ± 2.3	5.9	66	16.0
2MASS J16103008−1839065	14.86 ± 0.01	13.86 ± 0.01	13.28 ± 0.01	−5.8 ± 1.2	−19.2 ± 2.8	3.4	86	15.7
2MASS J16103014−2315167	18.10 ± 0.01	16.83 ± 0.01	16.09 ± 0.01	−6.3 ± 2.0	−29.7 ± 2.0	1.4	64	15.1
2MASS J16103525−2029168	15.73 ± 0.01	14.74 ± 0.01	14.21 ± 0.01	−8.1 ± 1.2	−16.7 ± 3.1	2.4	74	15.7
2MASS J16103876−1829235	17.66 ± 0.01	16.46 ± 0.01	15.72 ± 0.01	−4.0 ± 1.3	−12.9 ± 2.0	1.4	67	15.7
2MASS J16104636−1840598	15.50 ± 0.01	14.58 ± 0.01	14.01 ± 0.01	−0.2 ± 2.7	−24.6 ± 2.2	3.0	82	15.1
2MASS J16104714−2239492	19.75 ± 0.02	18.13 ± 0.01	17.22 ± 0.01	−4.3 ± 3.9	−17.0 ± 4.6	2.4	50	15.7
2MASS J16104996−2212515	15.95 ± 0.01	14.89 ± 0.01	14.28 ± 0.01	−5.0 ± 1.5	−18.7 ± 2.8	2.4	54	15.7
2MASS J16105429−2309108	15.84 ± 0.01	14.92 ± 0.01	14.45 ± 0.01	−21.7 ± 3.2	−35.6 ± 3.0	5.4	78	15.1
2MASS J16105499−2126139	16.05 ± 0.01	14.98 ± 0.01	14.36 ± 0.01	22.8 ± 17.1	−11.6 ± 2.9	37	71	15.1
2MASS J16105728−2359540	15.58 ± 0.01	14.72 ± 0.01	14.27 ± 0.01	−11.4 ± 5.5	−12.9 ± 4.0	6.7	70	16.5
2MASS J16110142−1924489	16.44 ± 0.01	15.44 ± 0.01	14.87 ± 0.01	−4.9 ± 1.7	−14.6 ± 1.8	2.0	83	15.1
2MASS J16110212−2335504	14.63 ± 0.01	13.80 ± 0.01	13.34 ± 0.01	−5.7 ± 1.5	−20.5 ± 4.2	2.9	64	15.7
2MASS J16110360−2426429	18.98 ± 0.01	17.46 ± 0.01	16.61 ± 0.01	−9.1 ± 1.6	−24.4 ± 3.8	5.7	55	14.6
2MASS J16110737−2228501	15.51 ± 0.01	14.43 ± 0.01	13.83 ± 0.01	−3.4 ± 2.0	−18.9 ± 2.0	2.0	73	15.1
2MASS J16111095−1933320	15.08 ± 0.01	14.19 ± 0.01	13.72 ± 0.01	−1.6 ± 1.4	−18.0 ± 1.8	2.9	83	15.7
2MASS J16111237−1927374	16.01 ± 0.01	14.93 ± 0.01	14.31 ± 0.01	−0.8 ± 1.5	−17.0 ± 1.6	2.6	81	15.7
2MASS J16111687−2639331	14.79 ± 0.01	14.00 ± 0.01	13.62 ± 0.01	−7.0 ± 1.5	−20.1 ± 2.3	3.5	57	14.6
2MASS J16111711−2217173	17.96 ± 0.01	16.73 ± 0.01	16.04 ± 0.01	−2.9 ± 1.4	−14.7 ± 3.6	1.4	62	15.7
2MASS J16111744−2441203	…	…	12.73 ± 0.01	−7.9 ± 2.2	−18.6 ± 2.8	3.6	59	14.6
2MASS J16111820−1803585	16.04 ± 0.01	14.93 ± 0.01	14.32 ± 0.01	−9.7 ± 1.6	−17.7 ± 2.6	2.8	76	15.1
2MASS J16111907−2319202	15.67 ± 0.01	15.15 ± 0.10	13.71 ± 0.03	−8.1 ± 1.4	−23.9 ± 2.1	2.0	74	15.1
2MASS J16111935−1905080	17.49 ± 0.01	16.21 ± 0.01	15.47 ± 0.01	−2.9 ± 1.5	−17.3 ± 7.0	2.9	37	15.7
2MASS J16112023−1847554	15.96 ± 0.01	14.89 ± 0.01	14.32 ± 0.01	−1.4 ± 1.7	−18.6 ± 2.6	2.9	81	15.1
2MASS J16112479−2655461	18.50 ± 0.01	17.24 ± 0.01	16.52 ± 0.01	−12.9 ± 2.4	−17.6 ± 2.4	1.1	50	14.6
2MASS J16112630−2340059	16.48 ± 0.01	15.51 ± 0.01	14.96 ± 0.01	−7.1 ± 2.4	−13.6 ± 8.3	7.6	74	15.7
2MASS J16112939−1942246	15.14 ± 0.01	14.22 ± 0.01	13.67 ± 0.01	−4.3 ± 1.2	−19.4 ± 4.8	3.0	76	15.7
2MASS J16112959−1900292	17.37 ± 0.01	16.11 ± 0.01	15.39 ± 0.01	−5.4 ± 1.8	−18.5 ± 2.8	1.3	48	15.7
2MASS J16113180−2237082	15.79 ± 0.01	14.83 ± 0.01	14.29 ± 0.01	−4.8 ± 1.9	−17.2 ± 5.2	3.0	82	15.7
2MASS J16113363−1914003	…	…	12.57 ± 0.01	−12.9 ± 6.2	−16.3 ± 2.8	16	83	15.7
2MASS J16113470−2219442	16.35 ± 0.01	15.37 ± 0.01	14.83 ± 0.01	−7.6 ± 1.5	−16.3 ± 5.0	2.4	81	15.7
2MASS J16113761−2346147	14.81 ± 0.01	14.00 ± 0.01	13.56 ± 0.01	−7.9 ± 0.9	−18.3 ± 3.4	2.5	83	15.7
2MASS J16113837−2307072	17.00 ± 0.01	15.95 ± 0.01	15.34 ± 0.01	−6.5 ± 3.0	−21.4 ± 2.3	4.0	82	15.7
2MASS J16114040−2311347	15.62 ± 0.01	14.63 ± 0.01	14.09 ± 0.01	−15.2 ± 4.4	−51.4 ± 16.1	10	77	15.7
2MASS J16114353−2527073	14.69 ± 0.01	13.74 ± 0.01	13.23 ± 0.01	−13.6 ± 1.9	−29.5 ± 2.8	3.9	48	15.9
2MASS J16114530−2254329	15.99 ± 0.01	14.95 ± 0.01	14.36 ± 0.01	−6.7 ± 1.7	−27.4 ± 2.2	2.4	83	15.1

Table 9
(Continued)

Name	Photometry			Proper Motion				
	i_{P1} (mag)	z_{P1} (mag)	y_{P1} (mag)	$\mu_\alpha \cos\delta$ (mas yr^{-1})	μ_δ (mas yr^{-1})	χ^2_ν	N_{ep}	Δt (years)
2MASS J16114534−1928132	16.08 ± 0.01	15.02 ± 0.01	14.44 ± 0.01	−7.6 ± 3.0	−14.7 ± 2.7	4.1	56	15.7
2MASS J16114612−1907429	15.28 ± 0.01	14.31 ± 0.01	13.79 ± 0.01	−7.0 ± 2.0	−27.5 ± 2.7	3.9	75	15.1
2MASS J16114735−2242062	16.45 ± 0.01	15.47 ± 0.01	14.97 ± 0.01	−6.8 ± 3.0	−9.7 ± 7.9	4.3	64	15.7
2MASS J16114920−1947431	14.66 ± 0.01	13.76 ± 0.01	13.28 ± 0.01	−9.1 ± 1.5	−18.0 ± 6.5	4.2	67	15.7
2MASS J16115436−2157025	18.50 ± 0.01	17.04 ± 0.01	16.18 ± 0.01	−2.2 ± 7.1	−10.0 ± 7.6	11	40	15.7
2MASS J16115439−2236491	17.59 ± 0.01	16.49 ± 0.01	15.89 ± 0.01	−8.4 ± 1.1	−12.2 ± 5.0	1.5	68	15.7
2MASS J16115737−2215066	16.78 ± 0.01	15.80 ± 0.01	15.23 ± 0.01	−8.8 ± 1.6	−16.4 ± 1.8	1.3	73	15.1
2MASS J16121016−2758305	18.94 ± 0.02	17.63 ± 0.01	16.86 ± 0.02	32.5 ± 27.6	24.4 ± 26.9	17	42	16.5
2MASS J16121043−1932275	15.29 ± 0.01	14.30 ± 0.01	13.76 ± 0.01	−5.8 ± 1.1	−13.6 ± 1.6	2.9	78	15.7
2MASS J16121185−2047267	17.14 ± 0.01	15.95 ± 0.01	15.29 ± 0.01	−6.6 ± 1.7	−22.2 ± 1.4	1.8	74	15.7
2MASS J16121492−2218038	15.05 ± 0.01	14.22 ± 0.01	13.78 ± 0.01	−5.2 ± 2.4	−18.7 ± 4.7	8.3	67	15.7
2MASS J16121609−2344248	16.11 ± 0.01	15.18 ± 0.01	14.68 ± 0.01	−15.4 ± 2.8	−15.4 ± 3.1	4.9	67	15.7
2MASS J16121723−2839082	14.75 ± 0.01	13.94 ± 0.01	13.54 ± 0.01	−2.6 ± 4.6	−15.7 ± 2.5	11	62	16.5
2MASS J16122737−2009596	15.70 ± 0.01	14.68 ± 0.01	14.10 ± 0.01	−8.3 ± 1.5	−23.8 ± 2.7	2.3	73	15.1
2MASS J16122764−2156407	⋯	20.33 ± 0.02	19.44 ± 0.06	−5.2 ± 13.6	−19.8 ± 13.5	0.8	17	14.8
2MASS J16122768−2406485	15.94 ± 0.01	14.95 ± 0.01	14.39 ± 0.01	−6.7 ± 1.9	−23.9 ± 1.6	2.4	68	16.0
2MASS J16122895−2159358	⋯	20.32 ± 0.04	19.06 ± 0.07	−33.1 ± 83.4	−36.8 ± 11.5	1.2	14	13.9
2MASS J16123458−2458341	14.96 ± 0.01	13.98 ± 0.01	13.46 ± 0.01	−8.3 ± 3.1	−25.0 ± 4.3	4.0	67	15.9
2MASS J16123759−2349234	16.93 ± 0.01	15.93 ± 0.01	15.37 ± 0.01	−6.8 ± 1.7	−26.5 ± 2.2	1.7	69	15.1
2MASS J16124374−2308231	14.59 ± 0.01	13.79 ± 0.01	13.33 ± 0.01	−8.3 ± 1.0	−23.6 ± 4.8	4.1	77	15.7
2MASS J16124506−2305303	16.56 ± 0.01	15.57 ± 0.01	14.99 ± 0.01	−8.8 ± 1.0	−24.2 ± 3.3	2.1	70	15.7
2MASS J16124692−2338408	17.00 ± 0.01	15.87 ± 0.01	15.24 ± 0.01	−8.8 ± 2.7	−19.3 ± 1.6	1.9	69	15.1
2MASS J16124726−1903531	16.06 ± 0.01	15.01 ± 0.01	14.45 ± 0.01	−2.2 ± 5.4	−29.2 ± 3.0	6.2	62	15.1
2MASS J16125528−2226542	15.15 ± 0.01	14.28 ± 0.01	13.81 ± 0.01	−14.6 ± 4.9	−23.0 ± 3.5	16	71	15.1
2MASS J16130232−2124283	⋯	20.63 ± 0.04	19.50 ± 0.06	−9.0 ± 6.2	−23.3 ± 6.1	0.8	24	14.8
2MASS J16130235−1904450	17.72 ± 0.02	16.60 ± 0.02	15.79 ± 0.02	−10.8 ± 2.1	−18.0 ± 2.2	1.0	52	15.1
2MASS J16130306−1929319	16.72 ± 0.01	15.64 ± 0.01	15.03 ± 0.01	−9.7 ± 1.5	−25.3 ± 1.7	1.7	71	15.1
2MASS J16130762−1703524	16.74 ± 0.01	15.73 ± 0.01	15.17 ± 0.01	−22.6 ± 10.1	−4.9 ± 5.9	32	68	15.2
2MASS J16130996−1904269	14.52 ± 0.03	13.68 ± 0.01	13.23 ± 0.01	−5.5 ± 1.6	−17.3 ± 2.9	2.9	67	15.7
2MASS J16131082−2313514	15.23 ± 0.01	14.36 ± 0.01	13.90 ± 0.01	−13.9 ± 1.3	−33.2 ± 1.7	1.6	71	15.1
2MASS J16131211−2305031	17.55 ± 0.01	16.35 ± 0.01	15.68 ± 0.01	−6.0 ± 2.1	−24.5 ± 2.1	2.3	69	15.1
2MASS J16132665−2230348	16.97 ± 0.01	15.80 ± 0.01	15.18 ± 0.01	−3.9 ± 2.2	−17.6 ± 5.3	2.0	48	15.7
2MASS J16132809−1924524	16.22 ± 0.01	15.14 ± 0.01	14.53 ± 0.01	−3.9 ± 1.3	−19.8 ± 3.3	1.9	77	15.7
2MASS J16133476−2328156	16.40 ± 0.01	15.49 ± 0.01	14.98 ± 0.01	−5.9 ± 1.1	−14.9 ± 2.7	1.9	75	15.7
2MASS J16133647−2327353	15.05 ± 0.01	14.12 ± 0.01	13.63 ± 0.01	−10.0 ± 1.2	−24.5 ± 2.2	2.1	74	15.1
2MASS J16133834−2158518	14.58 ± 0.01	13.79 ± 0.01	13.36 ± 0.01	−1.5 ± 3.9	−11.7 ± 2.5	7.5	58	15.7
2MASS J16133840−2443309	⋯	13.09 ± 0.01	12.72 ± 0.01	−12.2 ± 3.0	−15.9 ± 3.1	5.4	64	16.5
2MASS J16134045−2233156	16.02 ± 0.01	14.99 ± 0.01	14.42 ± 0.01	−2.5 ± 1.8	−23.6 ± 2.1	4.0	64	15.1
2MASS J16134079−2219459	18.60 ± 0.01	17.25 ± 0.01	16.47 ± 0.01	−2.7 ± 2.7	−20.7 ± 3.1	2.4	43	15.1
2MASS J16134264−2301279	16.98 ± 0.01	15.91 ± 0.01	15.31 ± 0.01	−5.3 ± 1.6	−14.8 ± 3.6	1.4	84	15.7
2MASS J16134490−2434143	⋯	⋯	12.58 ± 0.01	−6.5 ± 2.4	−19.2 ± 5.9	4.1	55	16.5
2MASS J16134880−2509006	16.84 ± 0.01	15.75 ± 0.01	15.19 ± 0.01	−5.3 ± 1.9	−18.3 ± 3.8	1.6	70	16.5
2MASS J16135765−2053447	17.18 ± 0.01	16.12 ± 0.01	15.54 ± 0.01	−22.8 ± 2.8	−30.4 ± 1.8	1.4	56	15.1
2MASS J16140514−2042017	18.04 ± 0.02	16.79 ± 0.01	16.09 ± 0.01	−9.4 ± 2.4	−18.8 ± 2.4	1.4	56	15.1
2MASS J16141352−2244578	15.03 ± 0.01	14.22 ± 0.01	13.81 ± 0.01	−10.8 ± 7.5	−13.8 ± 7.5	31	70	15.7
2MASS J16141484−2427081	15.66 ± 0.01	14.58 ± 0.01	14.00 ± 0.01	0.5 ± 2.6	−20.1 ± 2.3	7.6	71	16.5
2MASS J16141974−2428404	17.13 ± 0.01	16.01 ± 0.01	15.37 ± 0.01	−9.9 ± 2.8	−15.0 ± 3.4	5.1	49	16.5
2MASS J16142144−2339146	18.53 ± 0.01	17.31 ± 0.01	16.64 ± 0.01	−16.0 ± 3.2	−15.9 ± 2.9	2.5	51	15.1
2MASS J16142312−2219338	14.82 ± 0.01	13.86 ± 0.01	13.30 ± 0.01	−2.8 ± 3.3	−19.6 ± 3.4	10	56	15.7
2MASS J16142478−1733329	18.86 ± 0.01	17.47 ± 0.01	16.68 ± 0.01	−11.1 ± 2.5	−22.0 ± 2.7	2.1	45	15.2
2MASS J16143287−2242133	17.81 ± 0.01	16.57 ± 0.01	15.90 ± 0.01	−4.4 ± 7.0	−18.7 ± 6.7	3.7	53	15.7
2MASS J16143751−1858240	14.92 ± 0.01	14.27 ± 0.01	13.95 ± 0.01	−20.6 ± 2.2	−33.9 ± 4.5	14	75	15.7
2MASS J16144169−2351058	20.96 ± 0.05	19.29 ± 0.01	18.23 ± 0.03	−15.6 ± 7.7	−16.2 ± 7.2	1.3	30	15.1
2MASS J16145258−2017133	19.59 ± 0.02	18.07 ± 0.01	17.19 ± 0.01	−1.2 ± 4.9	−16.6 ± 3.0	2.5	51	15.7
2MASS J16145392−2504305	14.94 ± 0.01	14.09 ± 0.01	13.64 ± 0.01	−5.2 ± 1.5	−22.0 ± 4.0	2.5	51	16.5
2MASS J16145928−2459308	14.80 ± 0.01	13.99 ± 0.01	13.55 ± 0.01	−7.3 ± 1.9	−17.8 ± 1.7	2.8	45	16.5
2MASS J16150524−2459351	15.63 ± 0.01	14.64 ± 0.01	14.09 ± 0.01	−5.4 ± 1.9	−21.2 ± 2.3	3.7	57	15.9
2MASS J16150702−2535528	17.63 ± 0.01	16.44 ± 0.01	15.78 ± 0.01	−9.0 ± 1.7	−17.3 ± 1.9	1.4	73	15.9
2MASS J16150891−2345048	14.89 ± 0.01	14.08 ± 0.01	13.68 ± 0.01	−9.3 ± 2.0	−17.4 ± 2.4	3.5	58	15.7
2MASS J16151116−2420153	17.43 ± 0.01	16.39 ± 0.01	15.78 ± 0.01	−7.9 ± 1.9	−12.1 ± 4.6	1.7	52	16.5
2MASS J16151239−2420091	15.97 ± 0.01	15.06 ± 0.01	14.57 ± 0.01	−14.0 ± 2.1	−19.3 ± 2.4	2.1	53	15.9
2MASS J16151361−2304261	18.30 ± 0.01	17.11 ± 0.01	16.45 ± 0.01	−14.4 ± 1.5	−17.2 ± 3.4	1.7	56	15.7
2MASS J16151602−2345103	15.31 ± 0.01	14.36 ± 0.01	13.83 ± 0.01	−6.8 ± 3.1	−17.4 ± 8.1	7.1	56	15.7
2MASS J16151667−2340462	20.44 ± 0.03	18.71 ± 0.01	17.70 ± 0.01	−8.0 ± 5.0	−19.5 ± 4.6	1.1	35	15.1
2MASS J16152009−2333545	16.24 ± 0.01	15.15 ± 0.01	14.53 ± 0.01	−2.3 ± 2.1	−20.9 ± 2.0	1.7	61	15.1
2MASS J16152750−2627281	14.76 ± 0.01	14.01 ± 0.01	13.60 ± 0.01	−3.6 ± 2.5	−15.6 ± 2.8	4.3	51	16.5
2MASS J16152819−2315439	15.88 ± 0.01	15.04 ± 0.01	14.60 ± 0.01	−13.5 ± 1.2	−24.5 ± 4.2	2.2	79	15.7
2MASS J16153648−2315175	16.92 ± 0.01	15.98 ± 0.01	15.49 ± 0.01	−7.9 ± 1.6	−23.3 ± 1.6	1.8	54	15.1
2MASS J16153844−2341558	14.93 ± 0.01	14.11 ± 0.01	13.69 ± 0.01	−7.9 ± 5.3	−12.2 ± 6.0	8.3	86	15.7
2MASS J16153866−2240371	15.51 ± 0.01	14.57 ± 0.01	14.10 ± 0.01	−10.1 ± 5.6	−17.1 ± 4.6	7.5	60	15.7
2MASS J16153913−1917005	15.13 ± 0.01	14.04 ± 0.01	13.42 ± 0.01	−2.8 ± 1.1	−22.4 ± 2.2	3.3	89	15.1
2MASS J16155507−2444365	16.92 ± 0.01	15.73 ± 0.01	15.05 ± 0.01	−9.6 ± 2.4	−25.2 ± 3.5	2.5	49	15.9
2MASS J16155926−2329363	14.94 ± 0.01	14.11 ± 0.01	13.69 ± 0.01	−10.4 ± 1.4	−16.3 ± 2.6	3.2	78	15.7
2MASS J16160080−2214192	14.72 ± 0.01	13.80 ± 0.01	13.34 ± 0.01	−6.3 ± 1.5	−16.0 ± 2.2	2.8	57	15.7

Table 9
(Continued)

Name	Photometry			Proper Motion				
	i_{P1} (mag)	z_{P1} (mag)	y_{P1} (mag)	$\mu_\alpha \cos\delta$ (mas yr^{-1})	μ_δ (mas yr^{-1})	χ^2_ν	N_{ep}	Δt (years)
2MASS J16161183−2316268	15.60 ± 0.01	14.70 ± 0.01	14.25 ± 0.01	−11.0 ± 1.6	−24.1 ± 2.3	2.4	61	15.1
2MASS J16161948−2405301	15.63 ± 0.01	14.75 ± 0.01	14.29 ± 0.01	−9.2 ± 1.7	−20.4 ± 2.1	3.6	70	15.9
2MASS J16162399−2408301	16.16 ± 0.01	15.20 ± 0.01	14.67 ± 0.01	−10.4 ± 3.5	−18.1 ± 3.4	7.4	64	15.9
2MASS J16162531−2412057	16.60 ± 0.01	15.65 ± 0.02	15.03 ± 0.01	−8.1 ± 1.3	−13.2 ± 3.3	1.6	62	16.5
2MASS J16162598−2112227	17.36 ± 0.01	16.33 ± 0.01	15.78 ± 0.01	−11.7 ± 2.8	−8.5 ± 3.1	3.1	51	15.7
2MASS J16163068−2512201	15.95 ± 0.01	14.96 ± 0.01	14.46 ± 0.01	−8.2 ± 1.7	−16.2 ± 1.9	3.3	65	15.9
2MASS J16163226−2205201	16.81 ± 0.01	15.76 ± 0.01	15.20 ± 0.01	−3.7 ± 2.3	−17.8 ± 2.4	1.8	43	15.1
2MASS J16163343−2327210	15.23 ± 0.01	14.27 ± 0.01	13.76 ± 0.01	−15.9 ± 3.2	−19.2 ± 2.2	15	84	15.1
2MASS J16163345−2521505	⋯	⋯	12.60 ± 0.01	−6.8 ± 2.8	−20.5 ± 3.1	3.1	56	16.5
2MASS J16163503−2057551	15.28 ± 0.01	14.27 ± 0.01	13.73 ± 0.01	−6.6 ± 1.3	−24.4 ± 1.7	1.9	74	15.1
2MASS J16164539−2333413	16.82 ± 0.01	15.82 ± 0.01	15.30 ± 0.01	−13.2 ± 1.5	−29.9 ± 1.8	1.9	102	15.1
2MASS J16165158−2048537	14.77 ± 0.01	13.95 ± 0.01	13.53 ± 0.01	−5.4 ± 2.6	−15.3 ± 2.7	6.6	59	15.7
2MASS J16165430−2459590	14.56 ± 0.01	13.75 ± 0.01	13.30 ± 0.01	−8.2 ± 2.9	−14.8 ± 8.3	23	67	16.5
2MASS J16170606−2225414	14.79 ± 0.01	13.98 ± 0.01	13.58 ± 0.01	−7.5 ± 2.3	−0.6 ± 4.5	7.9	58	15.1
2MASS J16171901−2137129	16.69 ± 0.01	15.63 ± 0.01	15.03 ± 0.01	−3.6 ± 1.5	−21.2 ± 1.9	2.1	76	15.1
2MASS J16172505−2350380	17.09 ± 0.01	16.01 ± 0.01	15.40 ± 0.01	−4.5 ± 1.5	−16.9 ± 4.6	1.7	58	15.7
2MASS J16173103−2050469	16.49 ± 0.01	15.31 ± 0.01	14.65 ± 0.01	−5.9 ± 2.1	−23.6 ± 2.3	2.7	68	15.1
2MASS J16173236−2040362	18.06 ± 0.01	16.85 ± 0.01	16.11 ± 0.01	−1.2 ± 2.2	−14.3 ± 2.4	1.4	55	15.1
2MASS J16173786−2119159	14.96 ± 0.01	14.11 ± 0.01	13.68 ± 0.01	−12.3 ± 1.2	−20.4 ± 2.7	2.2	65	15.7
2MASS J16174366−2111552	17.11 ± 0.01	16.30 ± 0.01	15.87 ± 0.01	−7.7 ± 2.3	−8.5 ± 2.3	1.2	55	15.1
2MASS J16174539−2353360	17.53 ± 0.01	16.33 ± 0.01	15.66 ± 0.01	−7.1 ± 5.6	−29.6 ± 2.4	3.8	55	15.9
2MASS J16174583−2414436	16.72 ± 0.01	15.72 ± 0.01	15.16 ± 0.01	−2.5 ± 1.3	−20.0 ± 1.8	3.4	57	16.5
2MASS J16181201−2413326	15.82 ± 0.01	14.81 ± 0.01	14.26 ± 0.01	−6.2 ± 2.1	−11.3 ± 2.7	3.6	67	15.9
2MASS J16181568−2347084	16.24 ± 0.01	15.00 ± 0.01	14.29 ± 0.01	−27.4 ± 6.9	−28.6 ± 2.1	3.8	73	15.7
2MASS J16181600−2437266	14.79 ± 0.01	13.78 ± 0.01	13.24 ± 0.01	−4.2 ± 1.6	−17.8 ± 2.1	2.1	57	15.9
2MASS J16181618−2619080	15.41 ± 0.01	14.41 ± 0.01	13.84 ± 0.01	−18.5 ± 3.5	−22.7 ± 2.0	10	70	15.9
2MASS J16181904−2028479	15.35 ± 0.01	14.36 ± 0.01	13.82 ± 0.01	−1.4 ± 1.7	−20.6 ± 1.8	2.1	78	15.1
2MASS J16182082−2401502	18.46 ± 0.01	17.24 ± 0.01	16.56 ± 0.01	−9.3 ± 2.2	−23.6 ± 2.6	1.4	54	15.9
2MASS J16182501−2338106	17.23 ± 0.01	16.08 ± 0.01	15.45 ± 0.01	−7.0 ± 2.0	−25.1 ± 1.8	1.5	78	15.1
2MASS J16183317−2517504	16.21 ± 0.01	15.07 ± 0.02	14.37 ± 0.01	39.1 ± 20.8	30.7 ± 23.2	24	62	16.5
2MASS J16183618−2425333	14.82 ± 0.01	13.97 ± 0.01	13.52 ± 0.01	−1.3 ± 2.8	−15.8 ± 3.3	2.2	69	16.5
2MASS J16184074−2209482	17.22 ± 0.01	16.05 ± 0.01	15.38 ± 0.01	−11.3 ± 3.5	−21.9 ± 2.4	4.4	50	15.7
2MASS J16184955−2541499	19.11 ± 0.01	17.82 ± 0.01	17.04 ± 0.01	−4.0 ± 4.9	−14.1 ± 4.0	1.9	55	16.5
2MASS J16185037−2424319	16.84 ± 0.01	15.77 ± 0.01	15.16 ± 0.01	−6.6 ± 1.9	−27.0 ± 1.6	1.5	57	15.9
2MASS J16185430−2346075	18.88 ± 0.01	17.65 ± 0.01	16.92 ± 0.01	−6.0 ± 1.6	−15.5 ± 4.5	1.0	46	15.7
2MASS J16190341−2344085	17.98 ± 0.01	16.72 ± 0.01	16.01 ± 0.01	−6.7 ± 1.4	−24.3 ± 4.5	1.6	61	15.7
2MASS J16190474−2307526	16.21 ± 0.01	15.14 ± 0.01	14.56 ± 0.01	2.6 ± 3.1	−27.7 ± 4.2	3.6	52	15.1
2MASS J16191521−2417241	15.22 ± 0.01	14.24 ± 0.01	13.70 ± 0.01	−14.1 ± 1.2	−15.3 ± 2.8	1.8	59	16.5
2MASS J16191646−2347235	18.95 ± 0.01	17.58 ± 0.01	16.78 ± 0.01	−7.6 ± 1.5	−14.3 ± 1.8	1.2	75	15.7
2MASS J16192634−2412444	16.93 ± 0.01	15.80 ± 0.01	15.18 ± 0.01	−9.7 ± 2.0	−8.9 ± 8.1	4.7	62	16.5
2MASS J16192988−2440469	18.39 ± 0.01	16.90 ± 0.01	16.07 ± 0.01	−7.4 ± 1.2	−24.4 ± 3.7	1.5	59	16.5
2MASS J16192992−2425540	14.63 ± 0.01	13.70 ± 0.01	13.21 ± 0.01	−7.3 ± 1.5	−23.6 ± 2.3	2.7	77	15.9
2MASS J16193976−2145349	16.58 ± 0.01	15.43 ± 0.01	14.77 ± 0.01	−5.1 ± 1.6	−22.7 ± 2.4	3.4	59	15.1
2MASS J16194210−2504323	18.87 ± 0.01	17.58 ± 0.01	16.86 ± 0.01	−15.7 ± 8.0	−12.5 ± 6.2	15	62	16.5
2MASS J16194309−2216175	14.73 ± 0.01	13.99 ± 0.01	13.62 ± 0.01	−15.0 ± 3.4	−18.8 ± 4.1	2.5	70	15.7
2MASS J16194836−2212519	⋯	⋯	12.53 ± 0.01	−6.5 ± 1.8	−14.6 ± 5.4	5.2	77	15.7
2MASS J16195143−2241332	18.28 ± 0.01	16.99 ± 0.01	16.21 ± 0.01	−5.3 ± 1.5	−13.2 ± 5.6	1.8	51	15.7
2MASS J16195827−2832276	20.98 ± 0.04	19.37 ± 0.02	18.27 ± 0.03	−17.7 ± 6.5	−19.9 ± 6.5	0.9	49	15.7
2MASS J16200757−2359150	16.76 ± 0.01	15.55 ± 0.01	14.87 ± 0.01	−14.4 ± 3.7	−22.7 ± 2.0	2.8	63	14.4
2MASS J16201318−2425014	16.25 ± 0.01	15.49 ± 0.01	15.10 ± 0.01	−3.7 ± 2.0	−5.8 ± 1.2	4.2	61	14.8
2MASS J16202128−2120289	16.65 ± 0.01	15.55 ± 0.01	14.90 ± 0.01	−5.6 ± 1.0	−16.6 ± 3.6	1.3	67	15.7
2MASS J16202163−2005348	14.94 ± 0.01	14.03 ± 0.01	13.56 ± 0.01	−16.5 ± 2.8	−23.9 ± 3.6	10	76	15.1
2MASS J16202523−2316033	17.89 ± 0.01	16.72 ± 0.01	16.08 ± 0.01	−9.5 ± 1.3	−20.3 ± 2.0	1.7	60	15.7
2MASS J16203456−2430205	18.93 ± 0.01	17.26 ± 0.01	16.29 ± 0.01	8.0 ± 7.5	−18.7 ± 3.7	5.7	38	14.2
2MASS J16204144−2425491	18.44 ± 0.01	17.08 ± 0.01	16.29 ± 0.01	−11.8 ± 3.3	−15.2 ± 2.0	1.5	60	14.8
2MASS J16210222−2358395	18.87 ± 0.01	17.51 ± 0.01	16.70 ± 0.01	−7.4 ± 2.6	−16.7 ± 3.0	2.9	54	15.7
2MASS J16211563−2436117	14.54 ± 0.01	13.95 ± 0.01	13.67 ± 0.01	−27.7 ± 1.8	−15.9 ± 1.6	3.9	64	15.5
2MASS J16211920−2425525	15.75 ± 0.01	14.66 ± 0.01	14.00 ± 0.01	−0.5 ± 1.6	−14.5 ± 1.6	1.8	70	15.1
2MASS J16212488−2426145	16.17 ± 0.01	15.15 ± 0.01	14.57 ± 0.01	−6.5 ± 2.4	−17.3 ± 1.0	2.3	74	15.5
2MASS J16212953−2529431	⋯	⋯	12.54 ± 0.01	−5.1 ± 2.1	−18.8 ± 2.3	2.3	77	15.5
2MASS J16212961−2129038	15.02 ± 0.01	14.07 ± 0.01	13.61 ± 0.01	−3.1 ± 3.0	−18.7 ± 11.6	21	71	15.7
2MASS J16213591−2355035	17.65 ± 0.01	16.40 ± 0.01	15.67 ± 0.01	−9.6 ± 1.3	−17.8 ± 2.2	1.6	72	15.7
2MASS J16214853−2517266	⋯	⋯	12.53 ± 0.01	−8.1 ± 1.9	−20.0 ± 1.4	1.2	58	16.8
2MASS J16215975−2706366	14.68 ± 0.01	13.91 ± 0.01	13.51 ± 0.01	−9.0 ± 1.6	−22.1 ± 2.2	2.5	66	16.2
2MASS J16221693−1825131	⋯	⋯	17.80 ± 0.04	−25.9 ± 14.2	−0.6 ± 11.2	24	14	14.3
2MASS J16222160−2217307	16.56 ± 0.01	15.51 ± 0.01	14.96 ± 0.01	−22.7 ± 3.3	−18.6 ± 2.6	4.0	66	15.1
2MASS J16222521−2405139	18.27 ± 0.01	17.00 ± 0.01	16.23 ± 0.01	−13.9 ± 1.7	−3.4 ± 6.2	3.7	62	16.8
2MASS J16223834−2541017	18.50 ± 0.01	17.28 ± 0.03	16.53 ± 0.02	−8.8 ± 4.0	−13.0 ± 3.4	1.6	59	16.8
2MASS J16224385−1951057	16.63 ± 0.01	15.14 ± 0.01	14.25 ± 0.01	3.2 ± 4.1	−21.4 ± 2.9	7.2	51	15.7
2MASS J16230646−2528419	19.09 ± 0.01	17.71 ± 0.01	16.90 ± 0.01	−14.9 ± 2.6	−24.4 ± 2.6	1.0	50	16.0
2MASS J16232202−2609553	18.88 ± 0.02	17.66 ± 0.01	16.89 ± 0.03	−6.8 ± 2.6	−18.5 ± 4.5	1.2	49	16.8
2MASS J16235155−2317270	17.43 ± 0.01	16.07 ± 0.01	15.24 ± 0.01	−14.1 ± 9.4	−26.7 ± 4.1	3.9	59	15.7
2MASS J16235470−2438319	17.23 ± 0.01	15.94 ± 0.01	15.17 ± 0.01	−2.2 ± 2.7	−17.0 ± 4.3	1.4	61	16.8
2MASS J16250277−3006556	18.31 ± 0.01	17.14 ± 0.01	16.50 ± 0.01	−7.0 ± 4.2	−22.3 ± 6.7	4.2	50	16.5

Table 9
(Continued)

Name	Photometry			Proper Motion				
	i_{P1} (mag)	z_{P1} (mag)	y_{P1} (mag)	$\mu_\alpha \cos\delta$ (mas yr^{-1})	μ_δ (mas yr^{-1})	χ^2_ν	N_{ep}	Δt (years)
2MASS J16252860−1658509	17.44 ± 0.01	16.14 ± 0.01	15.40 ± 0.01	−6.3 ± 3.2	−8.5 ± 2.5	1.6	63	16.7
2MASS J16252969−2214543	16.52 ± 0.01	15.42 ± 0.01	14.82 ± 0.01	−5.9 ± 2.0	−15.7 ± 1.8	1.7	51	15.7
2MASS J16253274−2611386	14.63 ± 0.01	13.76 ± 0.01	13.30 ± 0.01	−7.1 ± 4.8	−14.6 ± 4.6	11	90	16.5
2MASS J16253672−2224285	17.03 ± 0.01	15.88 ± 0.01	15.16 ± 0.01	−5.2 ± 2.7	−15.8 ± 7.4	2.1	47	15.7
2MASS J16254322−2230026	15.98 ± 0.01	15.02 ± 0.01	14.49 ± 0.01	−5.9 ± 3.1	−18.2 ± 2.3	3.1	58	15.7
2MASS J16254808−2154195	14.63 ± 0.01	13.87 ± 0.01	13.46 ± 0.01	−9.4 ± 2.4	−18.6 ± 3.6	2.6	72	15.7
2MASS J16255066−2155454	17.24 ± 0.01	16.26 ± 0.01	15.74 ± 0.01	−16.1 ± 13.2	−24.1 ± 2.2	11	66	15.7
2MASS J16260625−2334030	16.90 ± 0.01	15.69 ± 0.01	14.96 ± 0.01	2.0 ± 2.7	−31.9 ± 3.5	3.3	80	15.3
2MASS J16263026−2336551	17.68 ± 0.03	16.27 ± 0.01	15.50 ± 0.04	−3.5 ± 1.1	−16.9 ± 4.5	1.4	55	15.7
2MASS J16263276−2622589	14.50 ± 0.01	13.49 ± 0.01	12.92 ± 0.01	−6.8 ± 1.8	−27.2 ± 4.9	4.5	53	15.1
2MASS J16265619−2213519	16.84 ± 0.01	15.72 ± 0.01	15.05 ± 0.01	−7.9 ± 1.8	−20.6 ± 2.3	1.6	62	15.3
2MASS J16270217−2542346	18.98 ± 0.01	17.59 ± 0.01	16.72 ± 0.01	−10.2 ± 1.7	−13.0 ± 2.7	1.1	32	15.7
2MASS J16270942−2148457	16.30 ± 0.01	15.22 ± 0.03	14.79 ± 0.02	−8.7 ± 1.7	−18.4 ± 1.7	2.4	70	15.7
2MASS J16272034−2844302	18.47 ± 0.01	17.31 ± 0.04	16.54 ± 0.01	−30.5 ± 10.5	−34.7 ± 5.1	18	57	15.3
2MASS J16272553−2138036	15.10 ± 0.01	14.24 ± 0.01	13.80 ± 0.01	−7.6 ± 1.3	−17.7 ± 3.7	2.8	69	15.7
2MASS J16274799−2457134	17.47 ± 0.01	16.19 ± 0.01	15.42 ± 0.01	−6.7 ± 1.8	−21.6 ± 1.9	1.1	64	15.3
2MASS J16281808−2428358	16.61 ± 0.01	15.30 ± 0.01	14.54 ± 0.01	−3.5 ± 1.3	−25.2 ± 1.9	1.1	62	15.7
2MASS J16284703−2428138	16.65 ± 0.04	15.81 ± 0.01	15.19 ± 0.02	−6.6 ± 1.6	−18.5 ± 1.9	1.9	58	15.7
2MASS J16292211−1742091	15.41 ± 0.01	14.49 ± 0.01	14.02 ± 0.01	−25.0 ± 7.5	−22.3 ± 2.2	6.3	61	16.7
2MASS J16293624−2456527	16.51 ± 0.01	15.52 ± 0.01	14.90 ± 0.01	−12.8 ± 4.2	−19.5 ± 2.6	4.6	80	15.7
2MASS J16293662−1708413	14.83 ± 0.01	13.94 ± 0.01	13.47 ± 0.01	−2.3 ± 1.2	−19.5 ± 3.7	2.5	75	16.7
2MASS J16293934−1614570	14.54 ± 0.01	13.89 ± 0.01	13.57 ± 0.01	−26.2 ± 2.4	−6.0 ± 2.2	5.2	72	16.7
2MASS J16294879−2137086	15.50 ± 0.01	14.55 ± 0.01	14.02 ± 0.01	−4.0 ± 5.5	−17.6 ± 4.7	15	64	15.7
2MASS J16302673−2359087	16.07 ± 0.01	14.95 ± 0.02	14.30 ± 0.01	−1.5 ± 1.8	−24.4 ± 4.0	3.0	61	15.1
2MASS J16303390−2428062	14.72 ± 0.01	13.76 ± 0.01	13.22 ± 0.01	−4.3 ± 1.7	−19.3 ± 1.9	1.8	63	15.1
2MASS J16305349−2424538	15.69 ± 0.01	14.61 ± 0.01	13.99 ± 0.01	−1.6 ± 2.1	−21.9 ± 1.6	1.9	79	16.1
2MASS J16310240−2408431	14.73 ± 0.01	13.78 ± 0.01	13.24 ± 0.01	0.9 ± 1.8	−22.0 ± 2.1	2.3	69	16.1
2MASS J16313519−2542261	18.41 ± 0.01	17.05 ± 0.01	16.26 ± 0.01	−11.8 ± 5.9	−18.7 ± 8.1	4.1	43	14.6
2MASS J16320136−2237081	17.70 ± 0.01	16.50 ± 0.01	15.78 ± 0.01	−5.1 ± 2.3	−17.2 ± 3.7	2.2	55	16.0
2MASS J16324221−2316562	14.66 ± 0.01	13.66 ± 0.01	13.14 ± 0.01	−16.6 ± 2.3	−34.1 ± 1.7	2.7	62	16.2
2MASS J16324727−2059375	16.55 ± 0.01	15.53 ± 0.02	14.97 ± 0.01	−12.4 ± 8.0	−17.3 ± 3.0	19	65	16.6
2MASS J16332000−2741076	17.80 ± 0.01	16.71 ± 0.01	16.12 ± 0.01	−13.2 ± 2.2	−17.8 ± 1.8	2.4	54	16.5
2MASS J16342850−2201119	16.81 ± 0.01	15.64 ± 0.01	14.99 ± 0.01	−8.9 ± 1.8	−25.8 ± 2.2	1.9	62	16.1
2MASS J16370753−2432395	19.35 ± 0.01	17.69 ± 0.01	16.67 ± 0.01	−2.9 ± 2.4	−13.6 ± 4.1	1.3	50	16.5
Unreliable fits: $\chi^2_\nu \leqslant 0.3$ or $\chi^2_\nu \geqslant 40$								
2MASS J16002535−2644060	16.03 ± 0.01	15.09 ± 0.01	14.54 ± 0.01	−23.2 ± 6.0	19.9 ± 21.0	64	64	15.9
2MASS J16070211−2019387	15.74 ± 0.02	14.82 ± 0.04	14.35 ± 0.04	102.4 ± 41.2	48.9 ± 28.7	89	79	15.7
2MASS J16090405−1934000	14.85 ± 0.02	14.02 ± 0.03	13.49 ± 0.01	−70.2 ± 36.1	95.5 ± 54.7	130	65	15.7
2MASS J16125723−2428013	15.80 ± 0.01	14.89 ± 0.01	14.41 ± 0.01	−8.5 ± 5.8	1.0 ± 31.0	110	70	16.5
2MASS J16273320−2821097	⋯	⋯	12.67 ± 0.01	−17.2 ± 11.7	−9.8 ± 7.3	58	65	15.7

Note. The objects in this table are taken from the catalogs of Luhman & Mamajek (2012), Dawson et al. (2014), and Rizzuto et al. (2015), except for PSO J237.1470 −23.1489 and PSO J239.7015−23.2665, which are new discoveries presented in this paper. We adopt a photometric precision floor of 0.01 mag for the PS1 photometry, following the analysis of Schlafly et al. (2012). The errors reported in the PS1 database are formal errors that do not include systematics and are often smaller.

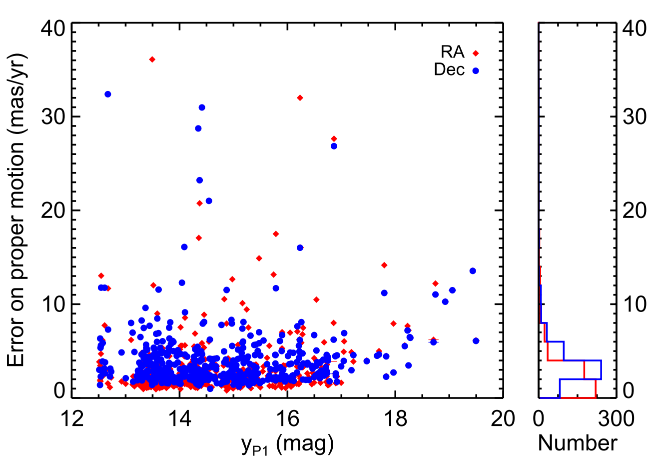

Figure 20. Errors on our $\mu_\alpha \cos\delta$ and μ_δ as a function of y_{P1} for known Upper Sco members that are not saturated in PS1, using the same format as Figure 17. Most errors are $\lesssim$5 mas yr^{-1}.

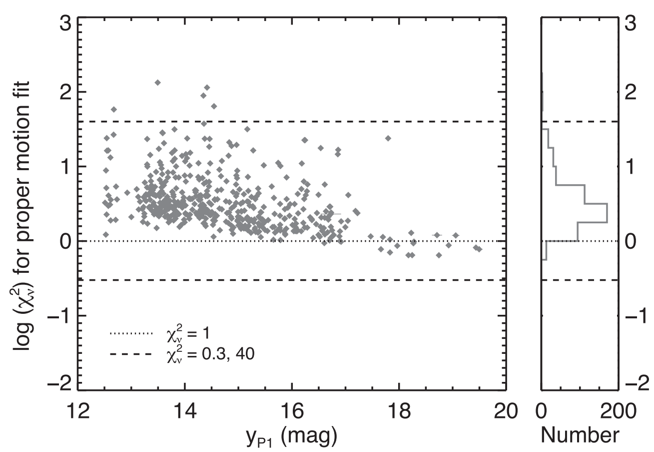

Figure 21. Reduced χ^2 for our proper motion fits as a function of y_{P1} for known Upper Sco members that are not saturated in PS1, using the same format as Figure 18. The two dashed lines mark $\chi^2_\nu = 0.3$ and $\chi^2_\nu = 40$, values between which we regard our proper motion fits and errors as reliable (Appendix A.2). The dotted line marks $\chi^2_\nu = 1$. As in Taurus, most of the proper motion fits have $\chi^2_\nu > 1$.

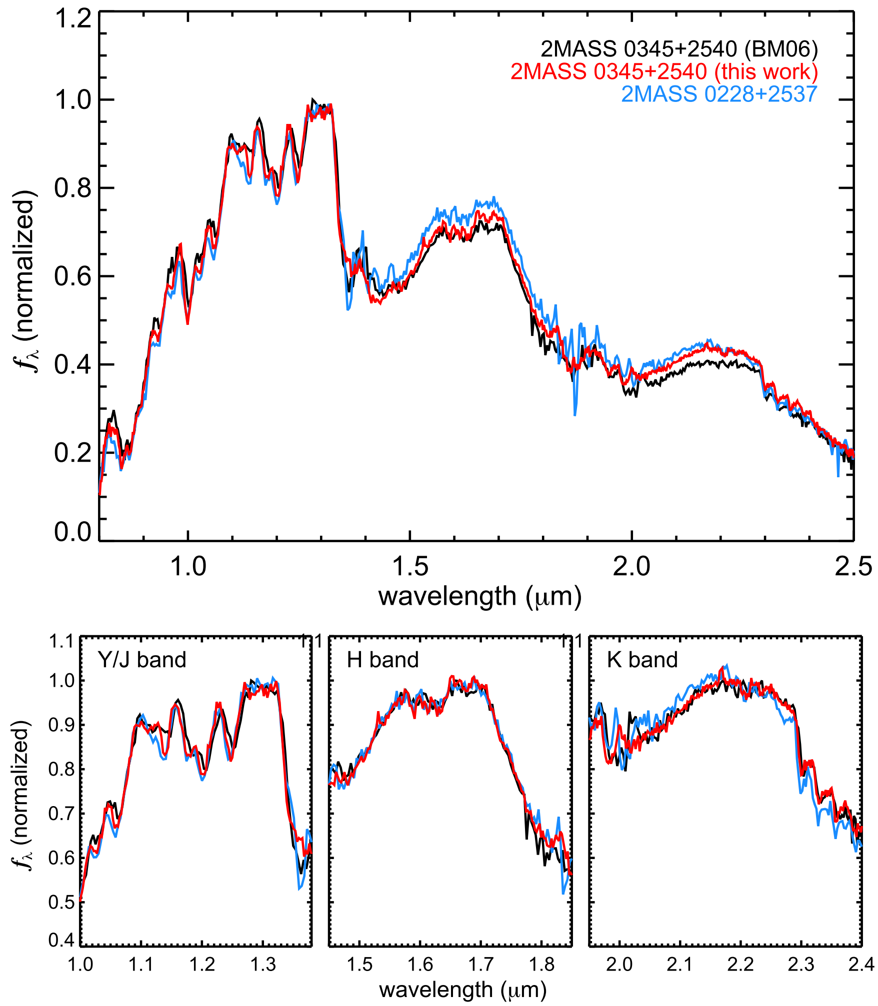

Figure 22. Top: SpeX Prism Library spectra for the L0 field standard 2MASS J0345+2540 (Burgasser & McElwain 2006, BM06, black) and the L0 dwarf 2MASS J0228+2537 (Burgasser et al. 2008, blue), compared with our new SpeX prism spectrum for 2MASS J0345+2540 (red). Bottom: same three spectra normalized and plotted separately for Y/J, H, and K bands to compare the spectral shapes in each band. The offset of the BM06 2MASS J0345+2540 spectrum toward longer wavelengths is evident in the J-band absorption features. We use our new spectrum for 2MASS J0345+2540 for analysis in this paper.

other spectra over the full 0.8–2.5 μm range of SpeX prism spectra, but is large enough to impact calculations of the Allers & Liu (2013a) gravity-sensitive spectral indices that use $\approx$0.02 μm-wide J-band absorption features (Section 4.3). The offset is equivalent to a velocity of $\approx$2400 km s^{-1}, two orders of magnitude larger than the radial velocities typical of nearby late-M and early-L dwarfs (Burgasser et al. 2015), so the offset is almost certainly due to a wavelength calibration error.

To obtain a spectrum for 2MASS J0345+2540 with an accurate wavelength calibration, we observed the object on 2016 February 03 UT with IRTF/SpeX in prism mode, using the 0$''$.5 slit. Conditions were clear. Observations were made at an airmass of 1.01 and comprised six exposures of 120 s using an ABBA nodding pattern. Immediately after we observed the A0V star HD 19600 for telluric calibration. We reduced the 2MASS J0345+2540 spectrum using Spextool v. 4.0 in standard fashion. The final spectrum has a mean S/N of 115 in J band (1.20–1.31 μm). Figure 22 shows our spectrum compared with the BM06 spectrum for 2MASS J0345+2540 and the SpeX Prism Library spectrum for the L0 dwarf 2MASS J02281101+2537380 (Burgasser et al. 2008). The redward offset on the BM06 spectrum is evident in the J-band absorption features. We therefore used our new spectrum for 2MASS J0345+2540 in our analysis (Sections 4.2 and 4.3).

References

Ahn, C. P., Alexandroff, R., Allende Prieto, C., et al. 2012, ApJS, 203, 21
Aller, K. M., Kraus, A. L., Liu, M. C., et al. 2013, ApJ, 773, 63
Aller, K. M., Liu, M. C., Magnier, E. A., et al. 2016, ApJ, 821, 120
Allers, K. N., Gallimore, J. F., Liu, M. C., & Dupuy, T. J. 2016, ApJ, 819, 133
Allers, K. N., & Liu, M. C. 2013a, ApJ, 772, 79
Allers, K. N., & Liu, M. C. 2013b, MmSAI, 84, 1089
Alves de Oliveira, C., Moraux, E., Bouvier, J., et al. 2013, A&A, 549, 123
Andrews, S. M., Rosenfeld, K. A., Kraus, A. L., & Wilner, D. J. 2013, ApJ, 771, 129
Baraffe, I., Homeier, D., Allard, F., & Chabrier, G. 2015, A&A, 577, A42
Bardalez Gagliuffi, D. C., Burgasser, A. J., Gelino, C. R., et al. 2014, ApJ, 794, 143
Best, W. M. J., Liu, M. C., Magnier, E. A., et al. 2013, ApJ, 777, 84
Best, W. M. J., Liu, M. C., Magnier, E. A., et al. 2015, ApJ, 814, 118
Bihain, G., Rebolo, R., Béjar, V. J. S., et al. 2006, A&A, 458, 805
Bihain, G., Rebolo, R., Zapatero Osorio, M. R., Béjar, V. J. S., & Caballero, J. A. 2010, A&A, 519, 93
Bouy, H., Bertin, E., Sarro, L. M., et al. 2015, A&A, 577, A148
Bowler, B. P., & Hillenbrand, L. A. 2015, ApJL, 811, L30
Bowler, B. P., Liu, M. C., Kraus, A. L., & Mann, A. W. 2014, ApJ, 784, 65
Bowler, B. P., Liu, M. C., Kraus, A. L., Mann, A. W., & Ireland, M. J. 2011, ApJ, 743, 148

Burgasser, A. J. 2007, ApJ, 659, 655
Burgasser, A. J., Geballe, T. R., Leggett, S. K., Kirkpatrick, J. D., & Golimowski, D. A. 2006, ApJ, 637, 1067
Burgasser, A. J., Liu, M. C., Ireland, M. J., Cruz, K. L., & Dupuy, T. J. 2008, ApJ, 681, 579
Burgasser, A. J., Logsdon, S. E., Gagné, J., et al. 2015, ApJS, 220, 18
Burgasser, A. J., & McElwain, M. W. 2006, AJ, 131, 1007
Burrows, A. S., Marley, M., Hubbard, W. B., et al. 1997, ApJ, 491, 856
Chabrier, G., Baraffe, I., Allard, F., & Hauschildt, P. 2000, ApJ, 542, 464
Cruz, K. L., Reid, I. N., Liebert, J., Kirkpatrick, J. D., & Lowrance, P. J. 2003, AJ, 126, 2421
Cushing, M. C., Marley, M. S., Saumon, D., et al. 2008, ApJ, 678, 1372
Cushing, M. C., Vacca, W. D., & Rayner, J. T. 2004, PASP, 116, 362
Cutri, R. M., Skrutskie, M. F., Van Dyk, S., et al. 2003, yCat, II/246, 0
Cutri, R. M., Wright, E. L., Conrow, T., et al. 2012, yCat, II/311, 0
Cutri, R. M., Wright, E. L., Conrow, T., et al. 2014, yCat, II/328, 0
Daemgen, S., Bonavita, M., Jayawardhana, R., Lafreniere, D., & Janson, M. 2015, ApJ, 799, 155
Danilov, V. M., & Loktin, A. V. 2015, AstBu, 70, 414
Davenport, J. R. A., Ivezić, Ž., Becker, A. C., et al. 2014, MNRAS, 440, 3430
Dawson, P., Scholz, A., & Ray, T. P. 2011, MNRAS, 418, 1231
Dawson, P., Scholz, A., Ray, T. P., et al. 2013, MNRAS, 429, 903
Dawson, P., Scholz, A., Ray, T. P., et al. 2014, MNRAS, 442, 1586
de Bruijne, J. H. J. 1999, MNRAS, 310, 585
de Zeeuw, P. T., Hoogerwerf, R., de Bruijne, J. H. J., Brown, A. G. A., & Blaauw, A. 1999, AJ, 117, 354
Deacon, N. R., Liu, M. C., Magnier, E. A., et al. 2014, ApJ, 792, 119
Dhital, S., West, A. A., Stassun, K. G., & Bochanski, J. J. 2010, AJ, 139, 2566
Ducourant, C., Teixeira, R., Périé, J. P., et al. 2005, A&A, 438, 769
Esplin, T. L., Luhman, K. L., & Mamajek, E. E. 2014, ApJ, 784, 126
Faherty, J. K., Rice, E. L., Cruz, K. L., Mamajek, E. E., & Núñez, A. 2013, AJ, 145, 2
Festin, L. 1998, MNRAS, 298, L34
Finch, C. T., & Zacharias, N. 2016, AJ, 151, 160
Gagné, J., Burgasser, A. J., Faherty, J. K., et al. 2015a, ApJL, 808, L20
Gagné, J., Faherty, J. K., Cruz, K. L., et al. 2015b, ApJS, 219, 33
Gaia Collaboration, Prusti, T., de Bruijne, J. H. J., et al. 2016, A&A, 595, A1
Gizis, J. E., Faherty, J. K., Liu, M. C., et al. 2012, AJ, 144, 94
Guieu, S., Dougados, C., Monin, J.-L., Magnier, E. A., & Martín, E. L. 2006, A&A, 446, 485
Høg, E., Fabricius, C., Makarov, V. V., et al. 2000, A&A, 355, L27
Kaiser, N., Burgett, W., Chambers, K., et al. 2010, Proc. SPIE, 7733, 12
Kellogg, K., Metchev, S. A., Gagné, J., & Faherty, J. 2016, ApJL, 821, L15
Kenyon, S. J., Gómez, M., & Whitney, B. A. 2008, in Handbook of Star-forming Regions Vol. I, The Northern Sky, ed. B. Reipurth (San Francisco: ASP Mongraph Publications), 405
Kirkpatrick, J. D., Barman, T. S., Burgasser, A. J., et al. 2006, ApJ, 639, 1120
Kirkpatrick, J. D., Cruz, K. L., Barman, T. S., et al. 2008, ApJ, 689, 1295
Kirkpatrick, J. D., Looper, D. L., Burgasser, A. J., et al. 2010, ApJS, 190, 100
Kirkpatrick, J. D., Reid, I. N., Liebert, J., et al. 1999, ApJ, 519, 802
Kouwenhoven, M. B. N., Goodwin, S. P., Parker, R. J., et al. 2010, MNRAS, 404, 1835
Kraus, A. L., & Hillenbrand, L. A. 2009, ApJ, 704, 531
Lafreniere, D., Jayawardhana, R., & van Kerkwijk, M. H. 2008, ApJL, 689, L153
Lawrence, A., Warren, S. J., Almaini, O., et al. 2007, MNRAS, 379, 1599
Lawrence, A., Warren, S. J., Almaini, O., et al. 2012, yCat, II/314, 0
Lawrence, A., Warren, S. J., Almaini, O., et al. 2013, yCat, II/319, 0
Leggett, S. K., Morley, C. V., Marley, M. S., & Saumon, D. 2015, ApJ, 799, 37
Lindegren, L., Lammers, U., Bastian, U., et al. 2016, A&A, 595, A4
Liu, M. C., Dupuy, T. J., & Allers, K. N. 2016, ApJ, 833, 96
Liu, M. C., Dupuy, T. J., & Leggett, S. K. 2010, ApJ, 722, 311
Liu, M. C., Magnier, E. A., Deacon, N. R., et al. 2013, ApJL, 777, L20
Lodieu, N. 2013, MNRAS, 431, 3222
Lodieu, N., Dobbie, P. D., Cross, N. J. G., et al. 2013, MNRAS, 435, 2474
Lodieu, N., Dobbie, P. D., & Hambly, N. C. 2011, A&A, 527, 24
Lodieu, N., Hambly, N. C., & Jameson, R. F. 2006, MNRAS, 373, 95
Lodieu, N., Hambly, N. C., Jameson, R. F., et al. 2007, MNRAS, 374, 372
Lodieu, N., Hambly, N. C., Jameson, R. F., & Hodgkin, S. T. 2008, MNRAS, 383, 1385
Lucas, P. W., Hoare, M. G., Longmore, A., et al. 2012, yCat, II/316
Luhman, K. L. 2006, ApJ, 645, 676
Luhman, K. L. 2014, ApJL, 786, L18
Luhman, K. L., Allen, L. E., Allen, P. R., et al. 2008, ApJ, 675, 1375
Luhman, K. L., & Mamajek, E. E. 2012, ApJ, 758, 31
Luhman, K. L., Mamajek, E. E., Allen, P. R., & Cruz, K. L. 2009, ApJ, 703, 399
Luhman, K. L., Stauffer, J. R., Muench, A. A., et al. 2003, ApJ, 593, 1093
Luhman, K. L., Wilson, J. C., Brandner, W., et al. 2006, ApJ, 649, 894
Martín, E. L., Basri, G., Gallegos, J. E., et al. 1998a, ApJL, 499, L61
Martín, E. L., Basri, G., Zapatero Osorio, M. R., Rebolo, R., & García López, R. J. 1998b, ApJL, 507, L41
Martín, E. L., Brandner, W., Bouvier, J., et al. 2000, ApJ, 543, 299
Martín, E. L., Delfosse, X., & Guieu, S. 2004, AJ, 127, 449
Martín, E. L., Rebolo, R., & Zapatero Osorio, M. R. 1996, ApJ, 469, 706
Mathews, G. S., Williams, J. P., Ménard, F., et al. 2012, ApJ, 745, 23
Melis, C., Reid, M. J., Mioduszewski, A. J., Stauffer, J. R., & Bower, G. C. 2014, Sci, 345, 1029
Monet, D. G., Levine, S. E., Canzian, B., et al. 2003, AJ, 125, 984
Pecaut, M. J., Mamajek, E. E., & Bubar, E. J. 2012, ApJ, 746, 154
Pinfield, D. J., Dobbie, P. D., Jameson, R. F., et al. 2003, MNRAS, 342, 1241
Preibisch, T., & Mamajek, E. 2008, in Handbook of Star-forming Regions, Vol. II, The Southern Sky, ed. B. Reipurth (San Francisco: ASP Mongraph Publications), 235
Preibisch, T., & Zinnecker, H. 1999, AJ, 117, 2381
Quanz, S. P., Goldman, B., Henning, T., et al. 2010, ApJ, 708, 770
Rayner, J. T., Toomey, D. W., Onaka, P. M., et al. 2003, PASP, 115, 362
Rebull, L. M., Padgett, D. L., McCabe, C. E., et al. 2010, ApJS, 186, 259
Riaz, B., Martín, E. L., Petr-Gotzens, M. G., & Monin, J.-L. 2013, A&A, 559, A109
Rizzuto, A. C., Ireland, M. J., & Kraus, A. L. 2015, MNRAS, 448, 2737
Robin, A. C., Reylé, C., Derriere, S., & Picaud, S. 2003, A&A, 409, 523
Roeser, S., Demleitner, M., & Schilbach, E. 2010, AJ, 139, 2440
Sarro, L. M., Bouy, H., Berihuete, A., et al. 2014, A&A, 563, A45
Schlafly, E. F., & Finkbeiner, D. P. 2011, ApJ, 737, 103
Schlafly, E. F., Finkbeiner, D. P., Juric, M., et al. 2012, ApJ, 756, 158
Schlafly, E. F., Green, G., Finkbeiner, D. P., et al. 2014, ApJ, 789, 15
Schmidt, S. J., West, A. A., Hawley, S. L., & Pineda, J. S. 2010, AJ, 139, 1808
Schneider, A. C., Windsor, J., Cushing, M. C., Kirkpatrick, J. D., & Wright, E. L. 2016, ApJL, 822, L1
Skrutskie, M. F., Cutri, R. M., Stiening, R., et al. 2006, AJ, 131, 1163
Slesnick, C. L., Carpenter, J. M., Hillenbrand, L. A., & Mamajek, E. E. 2006, AJ, 132, 2665
Slesnick, C. L., Hillenbrand, L. A., & Carpenter, J. M. 2008, ApJ, 688, 377
Stauffer, J. R., Schild, R., Barrado y Navascués, D., et al. 1998a, ApJ, 504, 805
Stauffer, J. R., Schultz, G., & Kirkpatrick, J. D. 1998b, ApJL, 499, L199
Steele, I. A., & Jameson, R. F. 1995, MNRAS, 272, 630
Stephens, D. C., Leggett, S. K., Cushing, M. C., et al. 2009, ApJ, 702, 154
Todorov, K., Luhman, K. L., & McLeod, K. K. 2010, ApJL, 714, L84
Vacca, W. D., Cushing, M. C., & Rayner, J. T. 2003, PASP, 115, 389
van Leeuwen, F. 2007, A&A, 474, 653
Weights, D. J., Lucas, P. W., Roche, P. F., Pinfield, D. J., & Riddick, F. 2009, MNRAS, 392, 817
Wright, E. L., Eisenhardt, P. R. M., Mainzer, A. K., et al. 2010, AJ, 140, 1868
Zacharias, N., Finch, C. T., Girard, T. M., et al. 2013, AJ, 145, 44
Zacharias, N., Monet, D. G., Levine, S. E., et al. 2005, yCat, I/297, 0
Zapatero Osorio, M. R., Béjar, V. J. S., Martín, E. L., et al. 2014a, A&A, 572, A67
Zapatero Osorio, M. R., Gálvez-Ortiz, M. C., Bihain, G., et al. 2014b, A&A, 568, 77
Zapatero Osorio, M. R., Rebolo, R., Martín, E. L., et al. 1997, ApJL, 491, L81